THE OPTIMIZATION OF GLASS-CERAMIC HEAT TREATMENT SCHEDULES

By

DOUG PARSELL

A DISSERTATION PRESENTED TO THE GRADUATE SCHOOL
OF THE UNIVERSITY OF FLORIDA IN PARTIAL FULFILLMENT
OF THE REQUIREMENTS FOR THE DEGREE OF
DOCTOR OF PHILOSOPHY

UNIVERSITY OF FLORIDA

1993

ACKNOWLEDGMENTS

I would like to thank my family, my friends and my advisors. Without the support of these sources, my time at the University of Florida would not have been the great experience that it was.

TABLE OF CONTENTS

Abstract of Dissertation Presented to the Graduate School
of the University of Florida in Partial Fulfillment of the
Requirements for the Degree of Doctor of Philosophy

THE OPTIMIZATION OF GLASS-CERAMIC HEAT TREATMENT SCHEDULES

By

Doug Parsell

December 1993

Chairman: Dr. Larry L. Hench
Cochairman: Dr. Kenneth J. Anusavice
Major Department: Materials Science and Engineering

The controlled crystallization of glasses to produce glass-ceramic materials has traditionally been accomplished via a two-stage heat treatment schedule consisting of an isothermal nucleation stage followed by an isothermal growth stage. Improvement of this method would allow for the production of superior products using an equivalent processing time or a reduction in the needed processing time to produce these materials. A more refined heat treatment schedule is proposed that does not include isothermal stages but rather is formed from a continuously increasing heating rate which is based on analysis of crystal growth rates as a function of crystal size and temperature. There are two fundamental ideas on which this type of heat treatment schedule is based. First, the nonheat-treated glass contains a distribution of sites which have a varying crystallization potential. This is termed the precrystal site distribution. From this population of sites the glass-ceramic microstructure will evolve. The initial temperature of the heat treatment schedule determines the fraction of the total precrystal population which may be grown to maturity. Second, the relationship between the growth rate of a crystal, the size of the growing crystal, and the temperature should govern the construction

of the heat treatment schedule for the production of glass-ceramic materials. The integration of these two ideas allows for the production of a glass-ceramic material with the desired number of crystals per volume in the shortest amount of processing time. Such a schedule is termed the optimum heat treatment schedule.

CHAPTER 1
INTRODUCTION

The main body of this research is divided into six chapters. The first chapter is an overview of crystal phase nucleation in glasses. The second chapter is an overview of crystal phase growth in glasses. Nucleation and growth are the traditional ways to view the evolution of glass-ceramic microstructures. The third chapter details a thermal analysis method which facilitates the development of efficient heat treatment schedules. The fourth chapter presents the traditional two-stage heat treatment schedules commonly used in the production of glass-ceramics. As an example, the thermal analysis method from chapter three is used to determine the parameters needed for construction of two-stage schedules for a glass-ceramic. The fifth chapter introduces the idea of the precrystal distribution, presents evidence for its significance, and demonstrates its usage. The sixth chapter presents two experimental approaches for determination of an optimum heat treatment schedule and demonstrates both approaches. The seventh chapter consists of the development of a theoretical growth rate equation which is a function of crystal size and temperature, the experimental determination of a growth rate equation, and the mathematical operation which yields the optimum heat treatment schedule for a specific growth-rate equation.

There are several significant rationales for the use of the most efficient heat treatment schedule in the processing of glass-ceramic materials. For reasons of production economics and commercial viability, it is beneficial to produce a material with a needed level of microstructural refinement in the shortest amount of time. For product development reasons, it is beneficial to estimate the potential properties of a given composition. Because of the direct relationship between material properties and material microstructure, in terms of mechanical, optical, or chemical properties, the potential properties of a material cannot be realized until adequate microstructural refinement is achieved. For scientific reasons, the form of the optimum heat treatment schedule is based on the relationships between crystal growth rate, crystal size, and temperature. These relationships form the basis for all nucleation and growth theories.

If the growth rate of crystals from their parent glass were only dependent upon temperature, there would be no need for sophisticated heat treatment schedules. The optimum schedule would consist of a single isothermal stage at the temperature of maximum crystal growth rate. Unfortunately, this is not the situation at hand. It is seen that the size of the growing crystal plays a very significant role in influencing the relationship between crystal growth rate and temperature. The high free energy produced at the glass/crystal interfaceresults in smaller crystal sizes having lower maximum crystal growth temperatures and lower crystal stability temperatures. These relationships are shown schematically in Figure 1.1. The optimum heat treatment schedule would be that

which maintains the temperature which corresponds to the maximum growth rate for the critical sized crystal as the microstructure continues to develop. The critical sized crystal is defined as that smallest (i.e., slowest growing) crystal which needs to be developed to maturity to achieve the desired microstructure. This optimum path is shown as a bold line in Figure 1.1. If the information in Figure 1.1 were readily available for crystallizing glass systems, an optimum heat treatment schedule could be generated through mathematical manipulation of this data. Unfortunately, this data is only obtainable by way of extensive work with SAXS or TEM and may only be attainable with these techniques for certain systems.

An option exists for the determination of the optimum heat treatment schedules which do not require the difficult experimental measurement of the crystal nuclei dimensions as did the previously described approach. This approach is based on the idea that for every temperature there exists a certain number density of sites within the glass which will generate stable crystal growth. For the glasses studied, a lower temperature results in a greater number density of growth sites. These sites of preferred crystallization have been termed precrystal sites and the effective size of these sites corresponds to the size of the crystal which would be needed to achieve stable growth at that particular temperature. Once the precrystal number densities are known as a function of temperature, the heat treatment schedule involves finding the most rapid heating rate at which to crystallize the glass from each of these initial temperatures and maintain the full number of stable crystals as defined by the precrystal information.

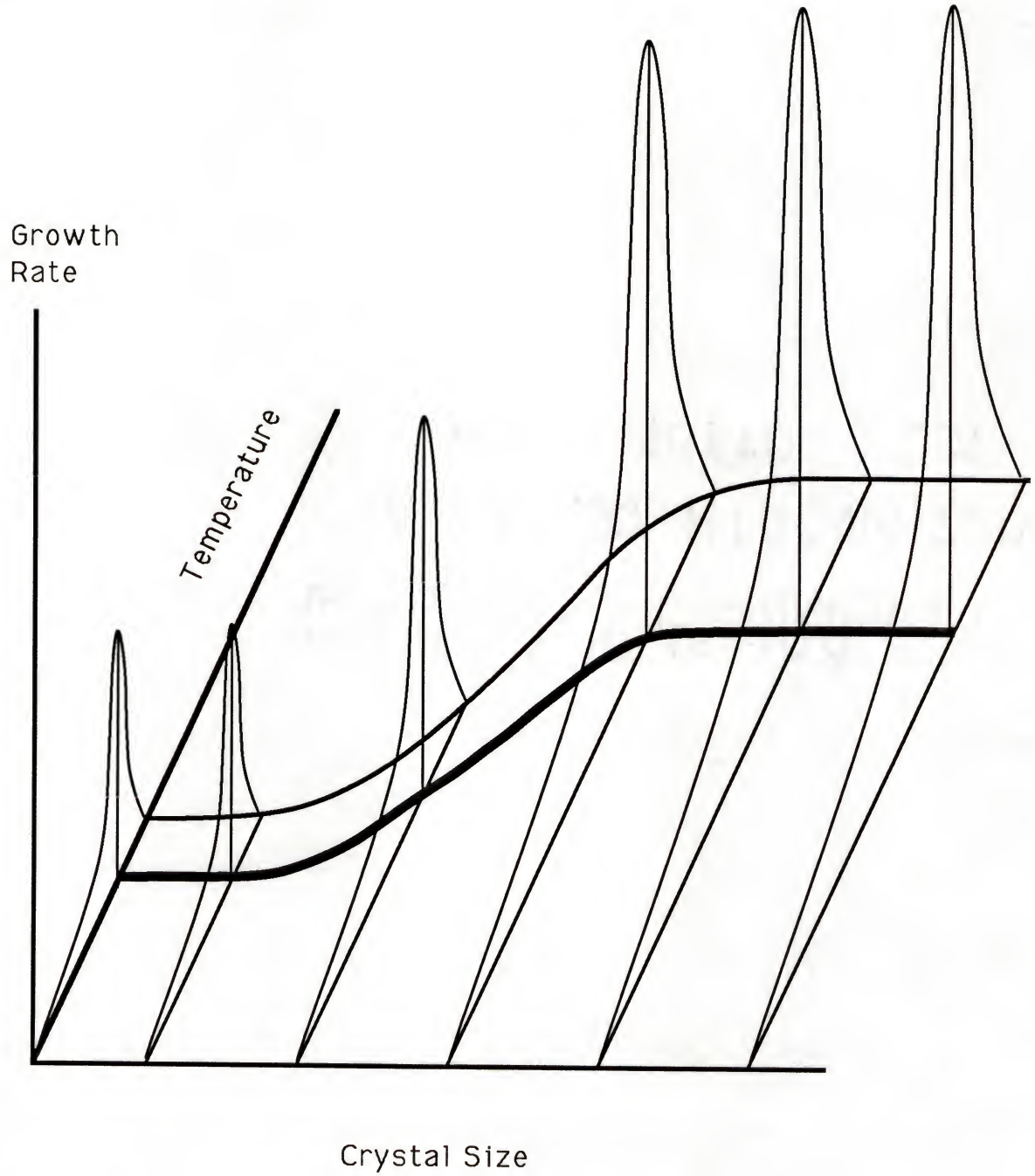

Figure 1.1 : Schematic representation of temperature and crystal size effect on crystal growth rate.

CHAPTER 2
REVIEW OF NUCLEATION AND GROWTH

2.1: Background on Crystal Nucleation

2.1.1: Introduction

Nucleation can be defined as the generation of stable crystalline phases. The process is thermodynamically controlled although significant kinetic factors are also involved.[1] Two examples are given to demonstrate the influence of each of these factors. At a particular temperature, a plot of system free energy (Gibbs free energy) versus composition for certain materials will show a sigmoidal form (Figure 2.1). The compositional region on this plot between the two points of inflection (a and b) is known as the spinodal region. Within this compositional region, any fluctuation in composition reduces the free energy of the system and therefore occurs spontaneously. The microstructure which results from such spinodal decomposition is one of a continually interlocking two-phase morphology. The compositional regions adjacent to the spinodal region and within the two minima of the free energy function (c and d) are the regions of nucleation and growth. In these regions, small fluctuations in composition result in an overall increase in free energy and the regions are therefore unstable. System free energy is minimized by nucleation of a new phase of

composition significantly different from the matrix phase. The new crystalline phase corresponds to that which produces a minimum in the free energy diagram. As this crystalline phase grows, the composition of the matrix phase approachs the composition dictated by the other free energy minima. For a system that is of a composition which corresponds to a free energy minima composition (c or d), crystallization of the matrix phase results in no compositional change of the matrix. For such systems, crystallization may proceed until only a single crystal phase exists. Lithium disilicate is an example of such a system. Therefore, the thermodynamic properties of a system usually dictate the phases which form, the percentage of those phases and the form of those phases which would evolve to minimize the free energy of the system.[2]

Thermodynamics dictates which phases should exist, but does not yield information pertaining to the rates of evolution for these phases. Activation energies for the phase transitions greatly affect the crystallization process. The rate of phase change must, therefore, be analyzed as a kinetic problem. To illustrate this factor, consider the temperature difference between the melting point and the freezing point for a wide variety of materials (Figure 2.2). The temperature difference between melting point and freezing point is direct evidence of an activation energy barrier influencing the phase transition. The additional free energy term associated with the existence of an interface between the newly formed crystalline nuclei and the matrix phase forces crystalline nuclei to be above a critical size before stable growth can be established. The

observed degree of undercooling (melting temperature minus freezing temperature) relates to the statistical probability of forming critical-size nuclei at a significant rate such that the system crystallizes in an experimentally accessible time period. The rate of formation of critical-size nuclei is termed the nucleation rate and is a cornerstone in traditional glass-ceramic processing.

2.1.2: Homogeneous Nucleation

Homogeneous nucleation refers to the generation of a stable, growing crystal which arises spontaneously from a site in the glassy matrix of which has approximately average properties such as density, stress, composition or temperature. In its simplest form, classical nucleation theory attempts to model this process for a system which crystallizes a spherical phase of the same composition as the matrix phase.[3] The classical theory also makes the simplifying assumption that the strain caused by volume changes due to the phase transformation is accommodated by the matrix phase through viscoelastic relaxation at a rate proportional to their occurrence. Other simplifying assumptions are that there is a sharp interface exist between the crystal and the matrix phases and that macroscopic values for surface and volume free energy apply to very small cluster sizes.

Equation 2.1 describes the free energy of a spherical nucleus within a matrix phase.

$$\Delta G_T = \Delta G_V(.75\pi r^3) - \sigma 4\pi r^2 \qquad (2.1)$$

where ΔG_T = total change in the system free energy

ΔG_v = free energy change associated with a new amount of volume

σ = free energy change associated with a new amount of interface

r = radius of new phase

The maximum point in this free energy function corresponds to the smallest nucleus (radius = r_{crit}) which will exhibit stable growth. This is termed the critical nuclei radius. Nuclei above this critical radius will continue to grow while nuclei below this critical radius will melt back into the surrounding matrix phase. The critical radius is easily found be taking the first derivative of equation 2.1 with respect to the radius of a nucleus.

$$r^* = \frac{2\sigma}{\Delta G_v} \qquad (2.2)$$

At small nucleus sizes the free energy of the system is dominated by the interfacial energy term. The surface to volume ratio is reduced as nucleus growth continues and the volume free energy term then becomes dominant. The competition between these two factors results in the maxima observed in the free energy function (Figure 2.3). The probability of forming a radius large enough for thermodynamic stability through random atomic fluctuations for a system in equilibrium is defined by equation 2.3.

$$P_n \propto \exp(-\Delta G_n/K_B T) \qquad (2.3)$$

where P_n = probability of formation of a cluster of n units

ΔG_n = free energy change resulting from formation of a cluster of n units

K_B = Boltzman's constant

Equation 2.3 can be translated into the number of clusters of a given size per mole through multiplication by Avagadro's number (N_A).

$$N^e_n = N_A \exp(-\Delta G_n/K_B T) \qquad (2.4)$$

Volmer and Weber[4] were the first to view the nucleation mechanism in terms of the flux of atomic units across the crystalline/noncrystalline interface. This kinetic approach was further developed by many others such as Farkas[5], Volmer[6], Becker and Doring[7], Zeldovich[8], Frenkel[9-10], and Turnbull and Fisher[11]. Crystalline clusters were assumed to evolve through a series of bimolecular reactions whereby an atomic unit is either added to the cluster or lost from the cluster. The rate of size change caused by these reactions is modeled by a master equation.

$$\frac{dN_{n,t}}{dt} = N_{n-1}K^+_{n-1} - [N_{n,t}K^-_n + N_{n,t}K^+_n] + N_{n+1,t}K^-_{n+1} \qquad (2.5)$$

where N_n = the number of clusters of a size denoted by the subscript (i.e., n-1, n, n+1) at time t

K_n^+ = the rate at which clusters of size n gain one unit at time t

K_n^- = the rate at which clusters of size n lose one unit at time t

Assuming a steady-state cluster size distribution, Becker and Doring[7] derived an expression for the steady-state nucleation rate assuming all clusters were larger than *u* and smaller than *v*.

$$I_s \sum_u^v \frac{1}{N_{e,n} K_{t,n}} = \frac{N_{s,u}}{N_{e,u}} - \frac{N_{s,v+1}}{N_{e,v+1}} = 1 \qquad (2.6)$$

Zeldovich[8] transformed equation 2.6 into a usable form by making several assumptions : (1) the summation term is largest and is dominant near the critical cluster size; (2) the forward growth rate constant is assumed to be that of the critical cluster; (3) the free energy term is replaced by the first two nonzero terms in a Taylor series expansion about that for the critical cluster; (4) the sum is replaced by a continuous function (ie. an integral). Using these approximations the steady-state nucleation rate can be expressed as:

$$I_s = N^e_{n^*} K^+_{n^*} (|\Delta G'|/6\pi K_B T_{n^*})^{1/2} = N^e_{n^*} K^+_{n^*} Z \qquad (2.7)$$

where $N^e_{n^*}$ = the number of equilibrium sized clusters at time t

$K^+_{n^*}$ = the forward rate constant for critical-size clusters

$\Delta G'$ = free energy change for critical cluster

growth

T_{n^*} = temperature of critical cluster growth (°K)

The forward and reverse rate constants are modeled by reaction rate theory.[12] The addition or subtraction of units from a cluster is modeled as involving an intermediate activated energy state. This energy level is higher than that of either the initial or the final state but is the lowest energy route connecting the two.

$$K^+_n = 4\, n^{2/3}\, \gamma \exp[-\delta g_n / 2K_B\, T] \qquad (2.8)$$

$$K^-_n = 4\, (n-1)^{2/3}\, \gamma \exp[+\delta g_{n-1} / 2K_B\, T] \qquad (2.9)$$

where γ = atomic jump frequency

n = number of units capable of crossing an interface

δg_n = free energy change associated with a forward jump

δg_{n-1} = free energy change associated with a backwards jump

Classical nucleation theory assumes that the jump frequency at the crystal interface is comparable to the jump frequency for bulk diffusion.

$$\gamma = \frac{6D}{\lambda^2} \qquad (2.10)$$

where D = self-diffusion coefficient

λ = jump distance

Combining equations 2.7, 2.8, and 2.10, the steady-state nucleation rate for a glass-ceramic system is expressed as equation 2.11. Steady-state nucleation is defined as the production of stable nuclei at a rate (number/time/volume) which is constant as a function of time.

$$I_s = \frac{24\, D\, n^{*2/3}\, N_A}{\lambda^2}\left(\frac{|\Delta G'|}{6\pi K_B T_{n^*}}\right)^{1/2}\exp\left(-\frac{\Delta G_{n^*}}{K_B T}\right) \qquad (2.11)$$

Equation 2.11 can be simplified and written as equation 2.12

$$I_s = A^*\exp(-W/K_B T) \qquad (2.12)$$

where A^* = kinetic prefactor

W = work to form a critical-size nucleus

The exponential portion of equation 2.12 relates to the probability of structural fluctuations resulting in the formation of a critical-size cluster. The nonexponential prefactor portion of equation 2.12 relates to the growth dynamics of the cluster.

2.1.3: Time-Dependent Nucleation

Time-dependent or transient nucleation describes the onset region of nucleation as well as the steady-state region. The transient region is characterized by the nucleation rate increasing from an undetectable rate to the steady-state value. Figure 2.4

shows a typical transition from transient nucleation to steady-state nucleation.

Treating the cluster size function as continuous, Zeldovich[8] showed that the general equation 2.5 could be approximated by an equation typical of diffusion processes.

$$\frac{\delta N_{n,t}}{\delta t} = \frac{\delta}{\delta n}\{K_n^+ N_n^e \frac{\delta}{\delta n}(\frac{N_{n,t}}{N_n^e})\} \qquad (2.13)$$

Most transient nucleation equations are based on analytical solutions to equation 2.13 using various assumptions for describing the rate constants and the free energy of cluster formation. This approach can be expanded to take into consideration pre-existing cluster distributions[13]. Preexisting cluster distributions could form during cooling from the melt or from intentional heterogeneous doping. Kashchiev[14] developed one of the most rigorous solutions to describe transient nucleation. Making the assumption that the forward rate constant does not vary with cluster size and that it has a value equal to that for the critical-size cluster and that the reverse rate constant is small for critical-sized clusters, Kashchiev derived equation 2.14.

$$I_{n^*,t} = I_s[1 + 2\sum_{m=1}^{\infty}(-1)^m \exp(-\frac{m^2 t}{\tau_k})] \qquad (2.14)$$

where I_s = steady-state nucleation rate

τ_k = driving force for forward flux of critical-size nuclei

m = series expansion coefficient

Equation 2.14 has been shown to fit experimental data of time-dependent nucleation.[14] The major problem with use of this equation is the independent measurement of forward and reverse interfacial rate constants as a function of temperature and cluster size. Equation 2.14 could be tested much more critically if these data were derived from an independent source as opposed to manipulation of the`data to fit the equation to the experimental data.

2.1.4: Heterogeneous Nucleation

Glasses can be doped with various species for a variety of reasons. The control of glass color and photosensitivity are two potential results of glass doping. The most common reason for doping is the control of microstructural development through controlled addition of nucleation sites. Because of the monetary demands for shorter processing times, the commercial use of glass-ceramic materials is dominated by systems which are nucleated heterogeneously.

There are several possible reasons for a given species functioning as an effective nucleating agent. Most explanations are based on increasing the probability of nucleation by decreasing the interfacial energy demands which are experienced during the formation of a homogeneous nucleus. Volmer[15] first expressed this concept mathematically by the equation:.

$$A_K^* = A_K\left(\frac{1}{2} - \frac{3}{4}\cos\theta + \frac{1}{4}\cos^3\theta\right) \qquad (2.15)$$

where θ = contact angle for isotropic cap-shaped nuclei

A_k = work of formation for critical spherical nuclei

The importance of similarity in lattice plane spacing was first noted by Turnbull and Vonnegut[16]. They concluded that if there existed a lattice plane spacing, in the nucleating phase that differed less than 10 to 15 percent from the closest matching heterogeneous phase lattice spacing then the heterogeneous phase will act as an effective nucleation site. This criterion was used to explain the effectiveness of platinum to nucleate lithium disilicate since the (111) plane spacing of a platinum crystal differs slightly from the (002) plane spacing of a lithium disilicate crystal by approximately 5 percent.

Gutzow and Toschiev[17] demonstrated a relationship between thermal expansion strains generated during cooling and the promotion of nucleation. due to these strains They concluded that an increase in the difference between the coefficients of thermal expansion for the glass and the heterogeneous phase produced a more effective nucleating agent. A possible explanation for this correlation is that the glassy region (which is surrounding the heterogeneous particle) that was strained during cooling from the melt temperature more closely matches the density of the crystalline phase and therefore experiences less stress upon transformation. Because of the lessened transformation stresses, the new crystalline phase is more stable than a comparably sized homogeneous crystal. An increase in structural defects and higher

energy configurations associated with the strained region can also result in the increased tendency towards stable crystal growth.

It has been shown that nucleation is encouraged through phase separation of the glass. Tomozawa[18] found that P_2O_5 promoted phase separation by an upward shift of the immiscibility boundary. Rindone[19] showed that lithia-rich regions formed around platinum clusters in a lithium disilicate glass. There are certain characteristic features of dopants which promote phase separation. The introduction of another glass-forming phase which cannot be easily incorporated into the preexisting network structure because of a difference in preferred bond angle will tend to separate the network into regions corresponding to the different bond angle species.[20] When the dominant network-forming species has a charge which differs from that of the network-forming dopant species, phase separation is also encouraged.[20] In this case, the different species charges result in noncompatible structural configurations which tend to segregate in order to minimize overall free energy.

2.1.5: Experimental Studies of Glass Nucleation

Certain glass systems are ideal materials for the experimental study of nucleation. Lithium disilicate is an example of such a system. The properties of lithium disilicate which make it a good choice for nucleation experiments are its tendency towards homogeneous bulk nucleation, availability of thermodynamic and

viscosity data, long-range diffusion is not needed for the phase transformation, and growth rates are slow enough that interfacial temperatures approximate bulk temperatures.

A consistent trend emerges when experimental nucleation rate curves are compared to nucleation rate curves derived from the classical nucleation theory (equation 2.11). Good correlation is seen between theory and experiment in terms of the shape of the nucleation curve; however, a major discrepancy is seen in the magnitude of the nucleation rate. The pre-exponential factor (A) generated from the theory is roughly 20 orders of magnitude smaller than that experimentally measured.[21-22]

There have been several possible explanations suggested to account for the large difference in experimentally and theoretically derived preexponential factors. Using a similar approach as Turnbull[23] used for nucleation studies of a metallic system, James[24] proposed a interfacial energy term which has a linear temperature dependence.

$$\sigma(T) = \sigma_o + \sigma_1 T \qquad (2.16)$$

where σ_o = temperature-independent interfacial energy term

σ_1 = temperature-dependent interfacial energy term

James used the theoretically derived preexponential factor and adjusted the interfacial energy term to best fit the experimental

data. Reasonable interfacial energy values are given by equation 2.16 for the temperature range where nucleation occurs. It was also shown that the temperature-dependent interfacial energy term would not significantly effect the classically predicted linear nature of [ln(Iη/T) versus $1/T\Delta G_v^2$]. A possible flaw in the temperature-dependent interfacial energy approach was shown by Hishinuma and Uhlmann.[25] They reported that if the interfacial energy increases with temperature, the critical nucleues radius (equation 2.2) would be reduced to only a few Angstroms. Since this size is less than the lithium disilicate unit cell size, such a critical nucleues is considered unrealistic. Therefore, the concept that a temperature-dependent interfacial energy term can bring the classical theory into accordance with experimental data while maintaining realistic physical parameters is questionable.

An alternative explanation for the large discrepancy in pre-exponential factors is based on the formation of an intermediate metastable phase which precludes the formation and growth of the stable phase.[25] The error due to the use of the wrong free energy data is said to account for the very low value of A. For the classical theory to predict experimental results , it is suggested that the data for the metastable phase be used instead of that of the stable phase. In support of this idea, evidence exists that the growth of lithium disilicate crystals from a glass of the same composition is preceded by the formation of an intermediate lithium metasilicate phase.[26] It is also possible that a significant percentage of the nuclei generated by what has been termed homogeneous nucleation are actually formed at sites in the glass characterized by atypical structural

configurations which facilitate nucleation. This approach does not require the existence of a metastable phase as previously suggested, but the influence on improving the predictions of the classical nucleation theory would be similar.

2.2: Background on Crystal Growth

2.2.1: Introduction

The majority of the research in the field of crystal growth has traditionally been directed towards the growth of crystals from a solution or from a melt. Technologically, these situations are important for the control of solidification and separation processes. Chemicals such as salt, ammonium nitrate, PVC, terephthalic acid and chlorine are produced by such processes. The growth of crystals from a glass closely parallels crystal growth in these solid/liquid systems, under certain conditions. For a crystalline phase of the same composition as its parent glass phase, growth can be modeled equivalently as a solid/liquid system when the solid/liquid system is not limited by the reactant flow rate, by adsorption, dissociation or desorption at the surface, or by the mobility of reactants or products at the surface.[27] As long as incorporation of atomic units into the crystalline structure is the primary rate-limiting step, the two systems (crystal/glass and crystal/liquid) can be modeled similarly.

2.2.2: Growth Kinetics

The rate of continuous growth was first modeled by Wilson[28]

and Frenkel.[29] Assuming that there exist activation energies for atomic movement or rearrangement within the solid, within the glass, and at the interface, the growth rate for continuous growth can be derived from reaction rate theory[30] as follows.

$$V = a\upsilon_i \exp(-\frac{Q_i}{KT})(1 - \exp(-\frac{L\Delta T}{KT_m T}) \qquad (2.17)$$

where a = jump distance

ν_i = atomic vibration frequency

Q_i = activation energy for interfacial transport

ΔT = undercooling = $T_m - T$

T_m = melt temperature

Equation 2.17 represents the upper-end for continuous growth rate predictions because it is based on the assumption that every site on the interface functions as a step site (i.e., an active growth site).[31] Cahn *et al.*[32] demonstrated how the mechanism for growth varied as a function of the crystallization driving force. Equation 2.18 shows the active growth mechanism changing from ledge growth to continuous growth by way of a transitional region which has partial characteristics from both the ledge and the continuous growth mechanisms.

$-\Delta F_v < \sigma\, g/a$	Ledge Growth Mechanism	(2.18a)
$\sigma\, g/a < -\Delta F_v < \pi\, \sigma\, g/a$	Transitional Region	(2.18b)
$-\Delta F_v > \pi\, \sigma\, g/a$	Continuous Growth Mechanism	(2.18c)

where $-\Delta F_v$ = driving force = $L\Delta T/V_m T_o$

σ = interfacial energy at growth surface

a = step height of ledge

L = latent heat of fusion

V_m = molar volume

T_o = melt temperature

$g \approx 1$ for sharp interfaces

$g = \pi x^3 \exp(-\pi x)$ for diffuse interfaces

where $x = \pi h/2$

h = number of atomic layers in transition region

Equation 2.17 models the interface as being atomically sharp. In other words, what can clearly be defined as ordered and what can clearly be defined as amorphous are separated by only one atomic spacing. This assumption was later avoided[32] through the introduction of a term for the interface diffuseness.

The first step towards recognizing the significance of interfacial topography can be associated with the early theories of heterogeneous nucleation.[15] Because it was calculated that nucleation would occur preferentially on a surface through a decrease in the nucleueses total surface free energy as compared to nucleation in the absence of a surface, it was predicted that growth would be encouraged by a rough surface. This idea was formalized by Kossel, Stranski, and Volmer.[33] They showed that the greatest binding energy for addition of new crystalline units occurs at kink sites along a surface ledge. It was also shown that any site along a

surface ledge has a greater binding energy than does a surface site. Figure 2.5 is a schematic of the different types of surface sites. A major problem with the KSV theory is that once the kink sites and the ledge sites are occupied there is no mechanism to resupply the surface with these features. Becker and Doring[7] avoided this problem by modeling the interface as a completely filled surface which progressed by formation of a two-dimensional nucleus. The nucleus grows along its ledge sites until a new atomic layer has formed and then the process starts over again. Application of this approach to real-life materials is difficult because the addition of defects to the model often creates sites which are nonsaturable, and thus the necessary nucleation events are bypassed.[34] A theory proposed by Burton, Cabrera, and Frank[35] suggested a plausible source for renewable ledge sites in real-life materials. They showed how the intersection of a screw dislocation with the crystal surface acts as a continuous generator of surface ledges. Burton, Cabrera, and Frank were also the first to propose a relationship between kink density (i.e., surface roughness) and crystallographic plane bonding forces. This allows an explanation of different growth rates for different crystallographic directions which result in the high-aspect-ratio of macroscopic shapes often seen in crystals.

2.2.3: Interface Roughness

Once a stable phase has been formed, the advancement of the interface constitutes growth. To understand the factors which affect the growth rate, one must first look at the interface. As has been shown, crystal interfaces advance by either a continuous

growth mechanism or by a ledge growth mechanism. Continuous growth is associated with an atomically rough interface where every surface site is considered a potential growth site. Ledge growth, on the other hand, depends on sites of accelerated growth potential due to topographical differences for growth to occur. The first two attempts at a theoretical approach for predicting which growth mechanism will dominate for a given material under given temperature conditions were Cahn's interface diffusiveness theory[32] and Jackson's interface free energy minimization theory.[36]

Cahn *et al.*[32] proposed that the active growth mechanism is determined by the energy required to advance the crystalline interface. The barrier energy to interface motion is proportional to the increase in surface energy experienced as the interface advances. The surface energy cycles from an energetic minima due to the interface surface corresponding to the close-packed unit cell surface to an intermediate maxima when the interface is in transition to the next close-packed surface minima. When the "driving force" is small, growth occurs through a ledge growth mechanism. When it is large, growth occurs through a continuous growth mechanism. Between these two extremes exists a transition region. The extent of the transition region depends on the diffuseness of the interface, in other words, how many atomic spacings of material exist between the matrix phase and the growing phase. This transition region has a level of structural order between those of the two phases. The diffuseness term is expressed by the parameter g. Cahn notes that the dependence of g on n is so sensitive that only direct experimental evaluation should be used.

(2.19)

$G = [\beta (1+ 2g^{1/2}) D L^2 (\Delta T)^2]/[4\pi T^2 RT \sigma V_m g]$ for lateral growth

$G = [\beta D \pi \sigma V_m g]/[a R T^2]$ for transition growth

$G = [\beta D \pi \sigma V_m]/[a R T^2]$ for continuous growth

Using these equations, the growth rate, adjusted for the temperature dependence of the melt viscosity and divided by the undercooling, can be plotted versus degree of undercooling (Figure 2.6).

An alternative theory to predict the dominant state of the interface and therefore the mechanism for crystal growth was presented by Jackson.[36] He determined the roughness of the interface by minimizing the free energy generated due to the addition of new atomic units on the interface. Jackson used a single-layer Bragg-Williams model. Equation 2.20 describes the free energy change accompanying additions of new atomic units.

$$\frac{\Delta F_s}{NkT_E} = \frac{-\Delta H_{fm}\Delta T}{RTT_E} X + \alpha X(1-X) + \frac{T}{T_E}(X\ln X + (1-X)\ln(1-X)) \qquad (2.20)$$

where N = number of sites on the interface

X = fraction of sites which are occupied

$\alpha = (\Delta S_{fm}/R)\varepsilon$

ΔS_{fm} = molar entropy of fusion

ε = number of nearest-neighbor sites in a layer parallel to the surface divided by the total number of nearest neighbors

Equation 2.20 is plotted in terms of the fraction of occupied surface sites for various alpha values in Figure 2.7. The alpha term is a relative predictor of the ease of rearrangement to form the crystalline phase. Alpha equals the product of the heat of fusion and the ratio of the number of parallel bonds between the bulk and the interface divided by the product of the melt temperature and Boltzman's constant. It can be seen from Figure 2.7 that dual free energy minima occur at a high and low volume fraction of occupied sites for high alpha cases. The dual minima predict a surface which is either close to fully occupied or nearly empty. This is representative of a ledge growth mechanism. For low alpha cases, a single free energy minima exists at half of the filled sites and half of the empty sites. This is representative of a continuous growth mechanism.

From Jackson's theory, an alpha of 2.0 is the value which separates normal growth from ledge growth. Therefore, for materials with entropies of fusion less than 2R all of their interfaces should be rough on an atomic scale. Growth should occur with equal velocity in all directions. Materials with entropies of fusion greater than 2R should have interfaces which are smooth and faceted. Significant growth rate anisotropy would also be expected for the higher entropy of fusion materials.

There are two main simplifying assumptions on which Jackson's theory is based: 1) the interface is only two atomic units thick and 2) only interactions between nearest neighbors are accounted for. Despite these assumptions, the theory correctly predicts the experimentally observed growth mechanism for a wide

range of materials, especially when alpha values are either less than 1.0 or greater than 4.0.[37] As would be expected, the theory is most accurate for cases of very high or very low entropies of fusion.

Jackson's model assumes that the two bulk phases are in equilibrium. Mutaftschiev[38] approaches the problem in the same manner as Jackson, except that he assumes that a driving force exists at the interface. Mataftschiev also predicted a smooth interface when F, synonymous with Jackson's alpha term, is large and a rough interface when F is small. Because the Mataftschiev theory considers the effect of the chemical potential driving force it is predicted that for any material a transition from a smooth interface to a rough interface could be achieved given a sufficient driving force. These conclusions are in agreement with those of Cahn.

Bennema and Gilmer[39] expanded upon the work of Jackson, Mataftschiev, and Hartman and Perdock[40] to define the set of conditions for rough versus smooth interfaces. In this work, beta is proportional to the chemical potential between the phases and alpha is proportional to energy gained as a result of interfacial roughening. A plot of log (beta) versus alpha defines the two growth fields (Figure 2.8). The plot shows the expected relations: large driving forces and large roughening energy gains promote rough interfaces while small driving forces and small roughening energy gains promote smooth interfaces.

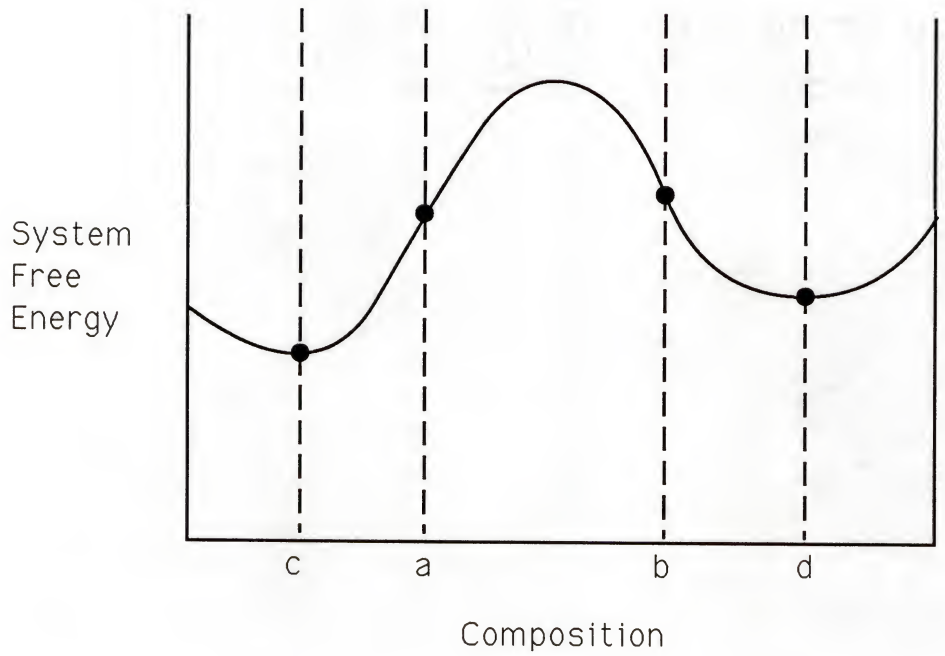

Figure 2.1 : Schematic free energy diagram of a material which exhibits a sigmoidal response in free energy to variation in composition. The compositions range between c and a and between b and d can lower their free energies through a process of nucleation and growth. Compositions between a and b can lower their free energies through a process of spinodal decomposition.

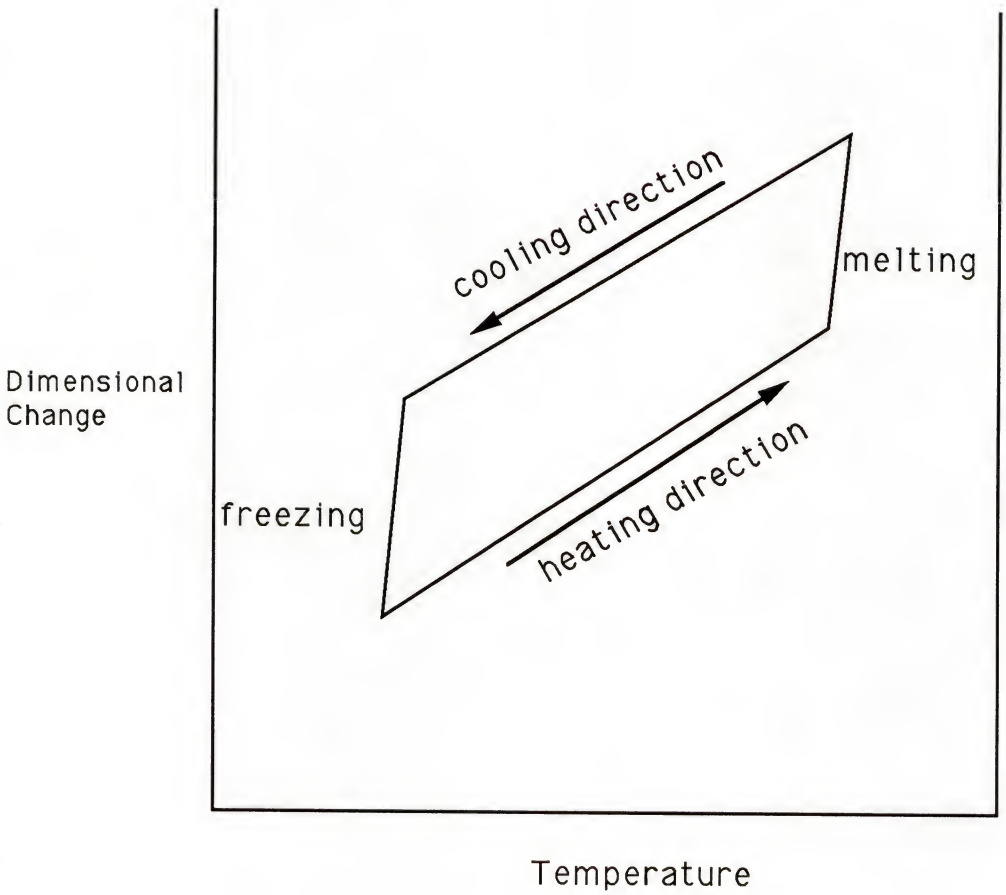

Figure 2.2 : Typical dilatometer output which demonstrates the hysteresis between melting points and freezing points due to the energy barrier for initiation of new phase sites upon freezing.

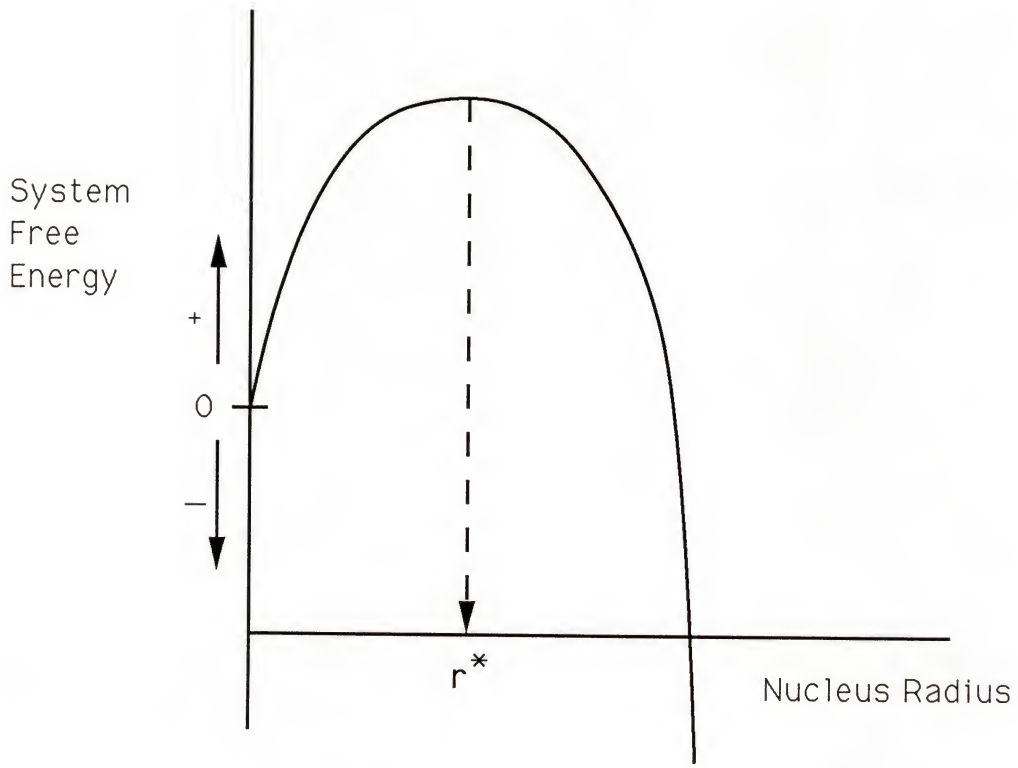

Figure 2.3 : Schematic drawing of the relationship between free energy and nuclei size. The maxima of the curve corresponds to the size of the critical nucleus (r*). Above this size, stable growth is thermodynamically predicted.

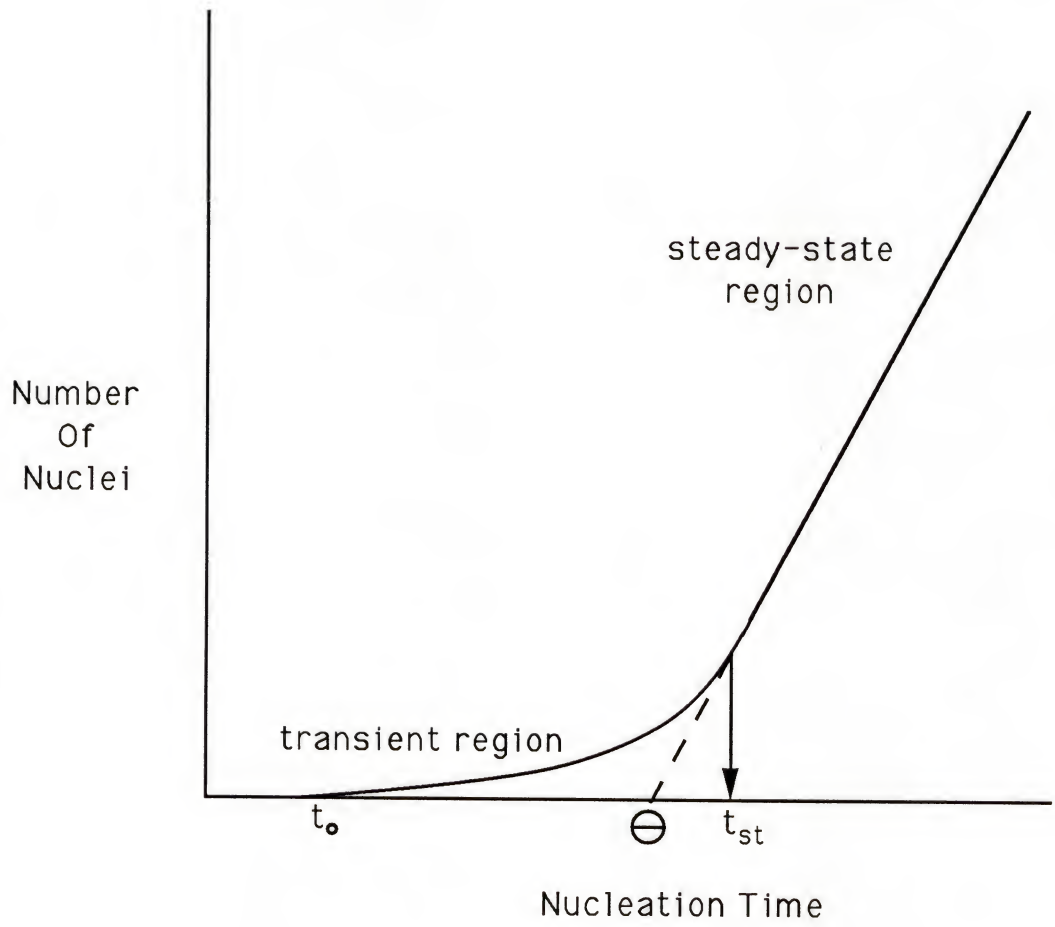

Figure 2.4 : The diagram shows the characteristic features of time-dependent nucleation. The nucleation rate initially increases during the transient phase and eventually reaches a constant rate during the steady-state phase.

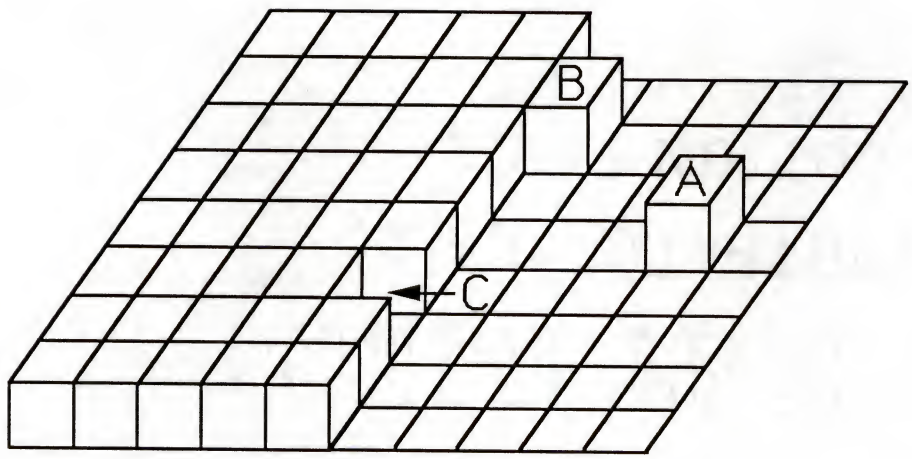

Figure 2.5 : Schematic of possible growth sites from the KSV model; A: surface site, B: ledge site, and C: kink site.

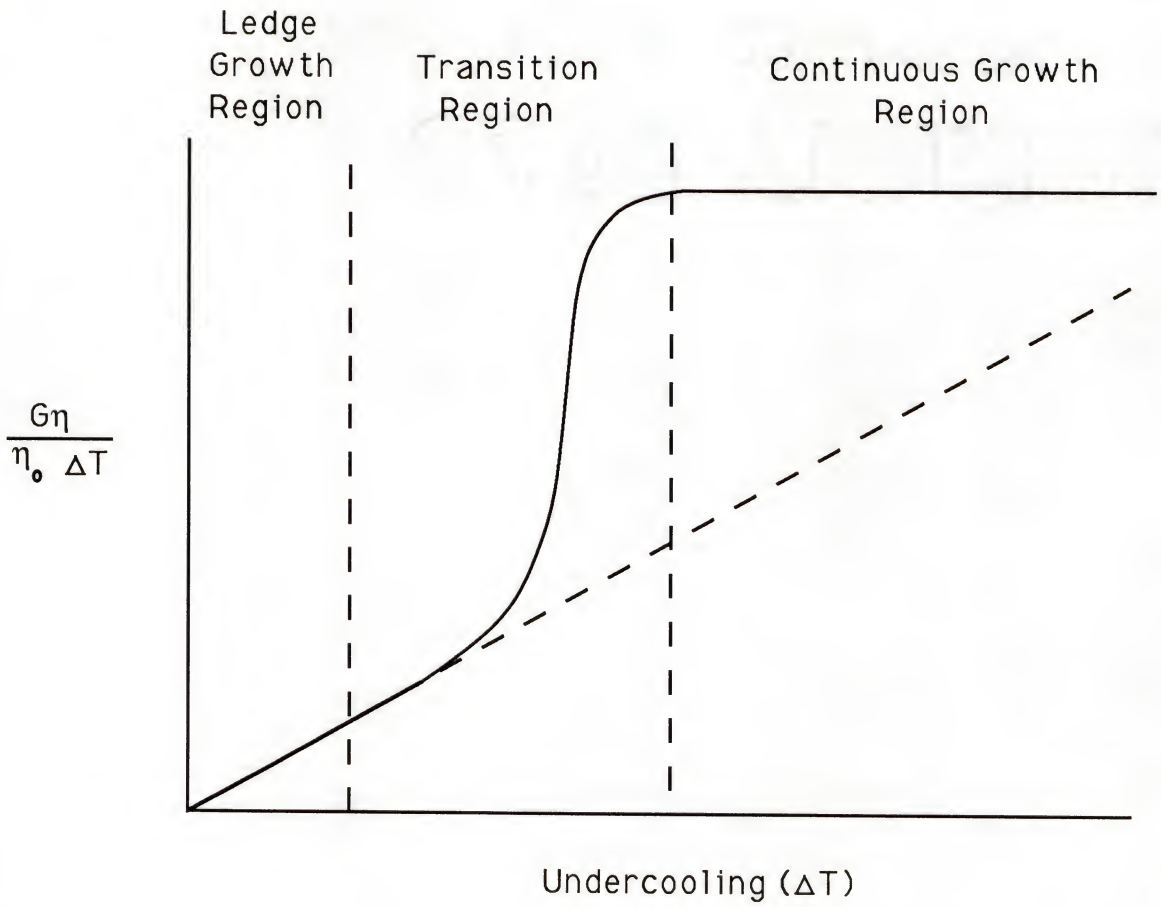

Figure 2.6 : Growth relationship as calculated by Cahn.[25]
As the degree of undercooling increases, crystal growth morphology shifts from ledge growth to a transition region to continuous growth.

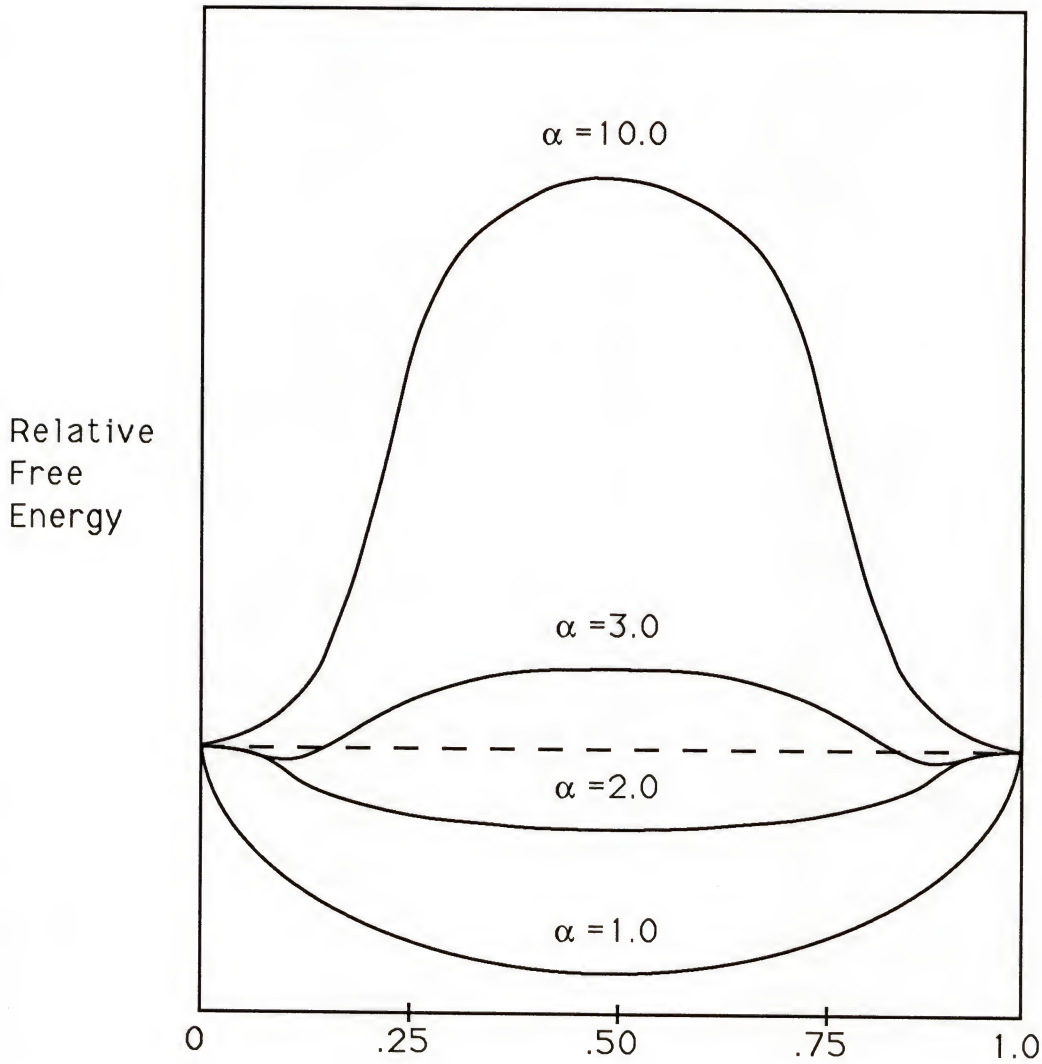

Figure 2.7 : Graphical depiction of Jackson's equation which predicts the topography of the growth surface by the system's alpha value. Alpha values which produce curves with central maxima predict a ledge growth mechanism while alpha values which produce curves without central maxima predict a continuous growth mechanism.

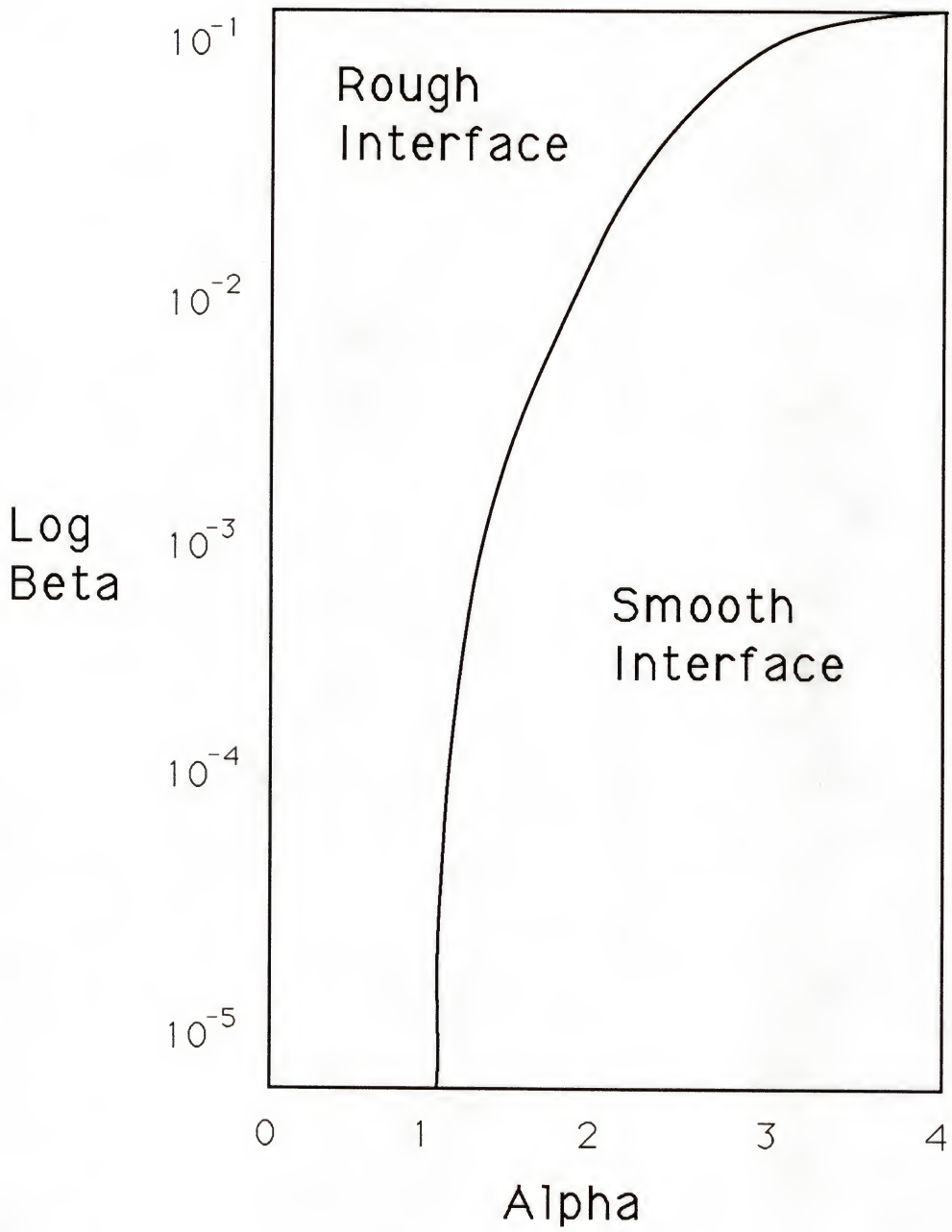

Figure 2.8 : Predicted regions of rough versus smooth growth interfaces.

CHAPTER 3
THERMAL ANALYSIS METHOD

3.1: Introduction

When attempting to determine the effectiveness of a given heat treatment schedule on the development of the crystal microstructure there are several different experimental techniques which can be used to yield the needed microstructural information (number of crystals per glass volume or number of crystals per glass area). The most traditional method involves performing the heat treatment with a conventional oven on a bulk piece of material. After the heat treatment, the crystallized material is cut cross-sectionally with a slow speed diamond saw, polished through 1 μm grit size abrasive, etched with dilute HF, sputter-coated with Au/Pd if necessary for improved image resolution, and photographed with an optical microscope. The effectiveness of the prior heat treatment schedule is determined by counting the number of crystals per area as recorded by the optical micrographs. A slight modification of this procedure involves the use of thermal analysis equipment for their ability to execute the desired heat treatment schedule accurately (± approximately 0.5°C). When using the thermal analysis equipment in place of a conventional heat treatment oven, sample size will be reduced to small monoliths or fairly large grained powders, as

limited by the sample pan size for the particular thermal analysis equipment.

Assuming that a large enough cross-sectional area was sampled to ensure representative data of the entire body, the optical microscopy method yields the best possible data. The data is the most representative because it is a direct measurement of the microstructural feature in question, namely, the crystal population density. The most significant problem with this method is the amount of time required to execute the procedure. The time required to obtain this data could potentially become the bottleneck in the material optimization project, especially when a project requires a broad range of compositions, heterogeneous additions, and heat treatment schedules.

An alternative method for measuring the effectiveness of heat treatment schedules is one which is based on thermal analysis techniques. The main advantage of this method is the relative speed at which heat treatment schedule efficiencies can be evaluated. The main disadvantage of this method is that the method indirectly measures the crystal population density and is therefore less accurate and yields only relative crystal density values as compared to the more time consuming direct method. The thermal analysis method is based on the fact that as the number of growing crystals, per volume of glass, increases from one sample to another, because of the modification of the applied heat treatment schedule, the peak in the exotherm detected as a result of these growing crystals will occur sooner and with greater magnitude. It should therefore be possible to correlate these peak characteristics with the

effectiveness of any prior heat treatments given the material. The method involves the use of either differential scanning calorimetry (DSC) or differential thermal analysis (DTA) to act as the heat treatment oven and to measure the crystallization exotherm. Once the sample has passed through the desired heat treatment schedule and reached a temperature where crystallization will proceed at a rate rapid enough to produce detectable exothermic activity, the sample is held isothermally or at a constant heating rate and the exothermic peak is recorded. Ray and Day[41-42] first proposed the relationship between exotherm peak height and crystal population density. Marotta, *et al.*[43] first proposed the relationship between time to exotherm maximum and crystal number density. Weinberg[44] mathematically validated these relationships between exotherm peak characteristics and crystal number density. The determination as to which piece of equipment should be used (DSC or DTA) is based on the maximum temperature (i.e., the isothermal temperature) which will be experienced during the heat treatment. If this maximum temperature is below approximately 700°C, DSC can be used. DTA is used for compositions which requires higher temperatures. The disadvantage of using the DTA is a reduced signal sensitivity as compared to that possible with the DSC. The greater temperature sensitivity and lower temperature limitations for the DSC are associated with the use of silver in their thermocouple/heat sink construction.

3.2: Materials and Methods

In an effort to understand the significance of the experimental parameters on the exothermic peak, a computer model was made to simulate the crystallization of the glass during the isothermal exotherm measurement phase of the thermal analysis method. The variable experimental parameters which were investigated include population density of growing crystal sites, sample particle size, isothermal temperature at which the exotherm is measured, and lag time between the onset of surface crystallization and the onset of bulk crystallization. The model operated under the assumption that since the measured thermal signal is approximately equal to the summation of each individual thermal signal emitted by each particle in the sample pan, the simulation can model the thermal response of a single glass particle and then multiply this response by the number of particles in the sample to simulate the total thermal response. The model also makes the assumption that the sample particles are glass spheres. The necessary input data was the initial nuclei density, the particle size, and the isothermal temperature. The initial nuclei density is the parameter which represents the effectiveness of the prior heat treatment. The particle size will determine not only the surface to volume ratio but also the number of particles contained in each simulated sample pan (total sample weight was constant). The isothermal temperature affects the rate of crystallization.

The computer program was based on dividing the available glass volume in the spherical particle into a number of volume

elements equal to the number of initial nuclei and placing a crystal of zero diameter in the center of each glass volume element. Crystallization begins on the outer surface of the glass sphere and grows inward forming a thickening crystalline shell around the particle. This is termed surface crystallization. Bulk crystallization also occurs at the internal sites in the form of expanding crystalline spheres. Under normal processing conditions, surface crystallization will always precede bulk crystallization. The program predicted the thermal energy produced by the phase transformation by calculating the volume of glass converted to crystal phase as a function of time. For each iteration of the program, the various crystal fronts grow at the expense of the available glass phase. When growing crystalline fronts impinge upon one another, crystallization ceases at that location. The simulation takes into consideration impingements between both bulk and bulk crystal fronts and surface and bulk crystal fronts. The isothermal temperature that was used in the program will dictate the amount of growth per time interval. Each iteration of the program represents an interval of time. The total volume of glass transformed to crystalline phase as a function of time can now be converted to thermal energy emitted as a function of time. The final predicted signal corresponding to that measured by the real-world thermal analysis equipment, is calculated by multiplying the volume transformed per time by the heat of transformation for the crystallization process by the number of particle in the sample pan. A schematic of the program logic is shown in Figure 3.1. A copy of the thermal analysis simulation program is listed in Appendix A.

3.3: Results and Discussion

3.3.1: Variation of Simulated Experimental Parameters

For any simulation effort to be useful it must act as a good predictor of the real-world event. As a first test for the thermal analysis simulation program, the program was used to simulate the thermal outputs when each of the experimental parameters was varied and the remaining parameters were held constant. Figure 3.2 shows the simulated response for variation in the nuclei population density. Figure 3.3 shows the simulated response for variation in particle size. Figure 3.4 shows the simulated response for variation in isothermal temperature. For all of these simulations, unless otherwise stated, the nuclei number density was held constant at $1x10^{-3}/\mu m^3$, the particle size was held constant at a diameter of 200 μm diameter, and the isothermal temperature was held constant at 600°C. Results from simulations of variations in lag time between initiation of surface crystallization and bulk crystallization are not shown because the present work did not involve such variations. However, possible future work dealing with variations in firing atmosphere, or surface finish and/or cleanliness would make such simulations pertinent.

The simulations involving variation in nuclei population density (Figure 3.2) show a logical response. As the nuclei density increases, the exotherm peak height increases and the time to exotherm maximum decreases. It is reassuring to note that the area beneath all of the curves is equal. This is an expected result because

the area under the curve represents the total heat evolved. In each case, independent of the number of crystals, the total crystal volume for the 200 μm diameter particle is transformed, so it is expected that equal amounts of energy would be released for each nuclei number density case. The major effect shown in Figure 3.3 is the competition between surface crystallization and bulk crystallization. The heat generated from surface crystallization will be at a maximum initially, and subsequently decreases as the crystallizing surface area decreases with the progression of the shell-like crystal front into the particle interior. The component of the simulated thermal analysis signal which comes from surface crystallization will therefore be at a maximum initially and will decrease as time increases. On the other hand, the simulated thermal analysis signal arising from bulk crystallization will initially be zero and then it will increase as the surface area of the internal spheres increase. The total simulated signal is the summation of the signal generated by the surface component and the bulk component. It is seen that as the particle size increases, the total signal evolves from one which is dominated by the surface crystallization component to one which is dominated by the bulk crystallization component. Complete crystal impingement results in the termination of all thermal output. This occurs simultaneously for all particle sizes. This is an expected result because the time interval until impingement occurs is dependent upon the distance between bulk crystal centers which is a function of nuclei density not crystal size. Because this is logically expected and is observed in the simulation results, further validity is given to the simulation

program as being a good predictor of the actual thermal analysis technique.

3.3.2: Comparison of Model Predictions with Experimentally Generated Data

To test the accuracy of the computer model in predicting the response of the thermal analysis method to changes in experimental parameters, data predicted from the model was compared directly to experimentally derived data. The experimental parameters which were investigated were particle size, isothermal temperature, and nuclei population density. For each case, the parameter of interest was varied while the remaining parameters were held constant. For the effect of variation in isothermal temperature, a conversion was made between temperature and crystal growth rate to facilitate comparison. The experimental data used to predict crystal growth rates as a function of temperature is shown in Figure 3.5. This data were collected by measuring the advance of the surface crystalline layer into the interior as a function of time and temperature. The measurements were made by taking optical micrographs of cross-sectional pieces of the heat treated glass, with special attention being given to assure that the plane cut by the cross-section through the glass body intersected the surface of the glass body perpendicularly.

The comparisons between model data and experimental data for variations in particle size, isothermal temperature, and nuclei population density are shown in Figs. 3.6, 3.7, and 3.8, respectively. For all cases, the abscissa shows the variation in the experimental parameter while the ordinate shows the corresponding response in

the exothermic crystallization peak. The response in the exothermic peak was characterized in terms of its measured time to reach its exothermic maximum from the onset of the isothermal temperature condition. It was observed that there was nearly no effect induced through variation in the particle sizes, for the range of sizes used (diameters of 15μm to 60μm). A decrease in isothermal temperature or nuclei population density was found to increase the time to when the exotherm maximum. For all three cases the computer model predicted the experimental response sufficiently such that the model can be used with confidence to understand the relationships between the experimental parameters and the exothermic peak response.

The most important model predicted relationships between the experimental parameters and the time to the exotherm maximum are shown in Figure 3.9. The relationship between an increase in nuclei population density and a corresponding decrease in the time to reach the exotherm maximum is confirmed. It can also be seen that as the isothermal temperature is decreased, the amount of change in the time to reach the exotherm maximum that occurs due to a set amount of change in the nuclei population density increases. In other words, the sensitivity of the thermal analysis technique to detect small changes in the effectiveness of nuclei generating heat treatments is increased by lowering the isothermal temperature used. A third conclusion is that the thermal analysis technique decreases in sensitivity as the nuclei population density increases. Potentially, this would limit the use of this technique to roughly (and quickly) determining an appropriate heat treatment schedule.

Further refinement would require more traditional (and time consuming) methods.

3.4: Conclusions

Thermal analysis techniques are a significant asset towards the development of glass-ceramic heat treatment schedules. Modeling and experimental validation of the relationships between effectiveness of heat treatment schedules and exothermic peak characteristics have been demonstrated. It is concluded that this novel technique offers a significant time savings over traditional methods and sufficient sensitivity for initial determination of a heat treatment schedule. It is estimated that use of this technique would yeild time savings of approximately 50% as compared to traditional quantitative stereology methods.

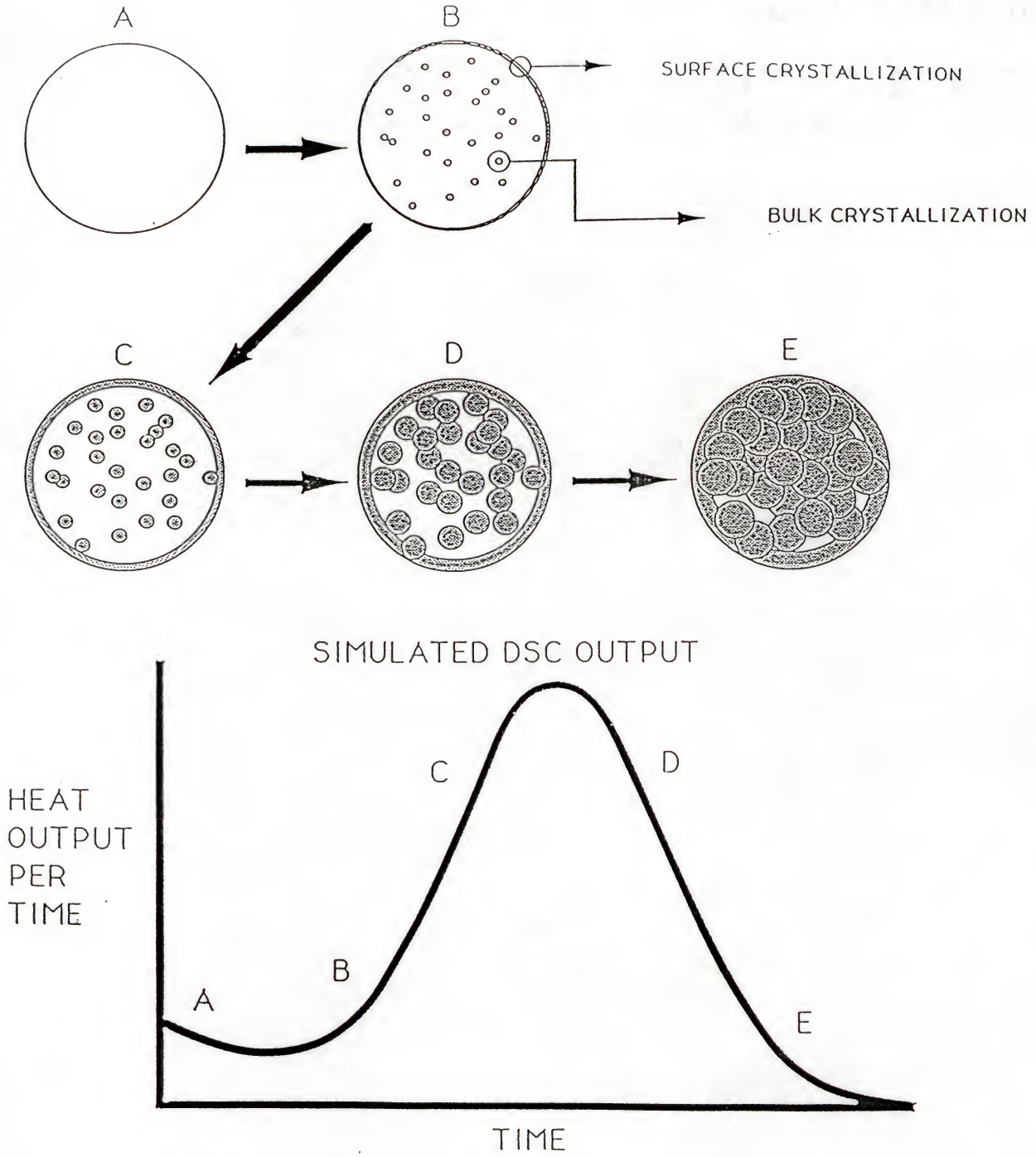

Figure 3.1 : The above schematic illustration is of the computer model method for simulating the thermal analysis output generated during material crystallization.

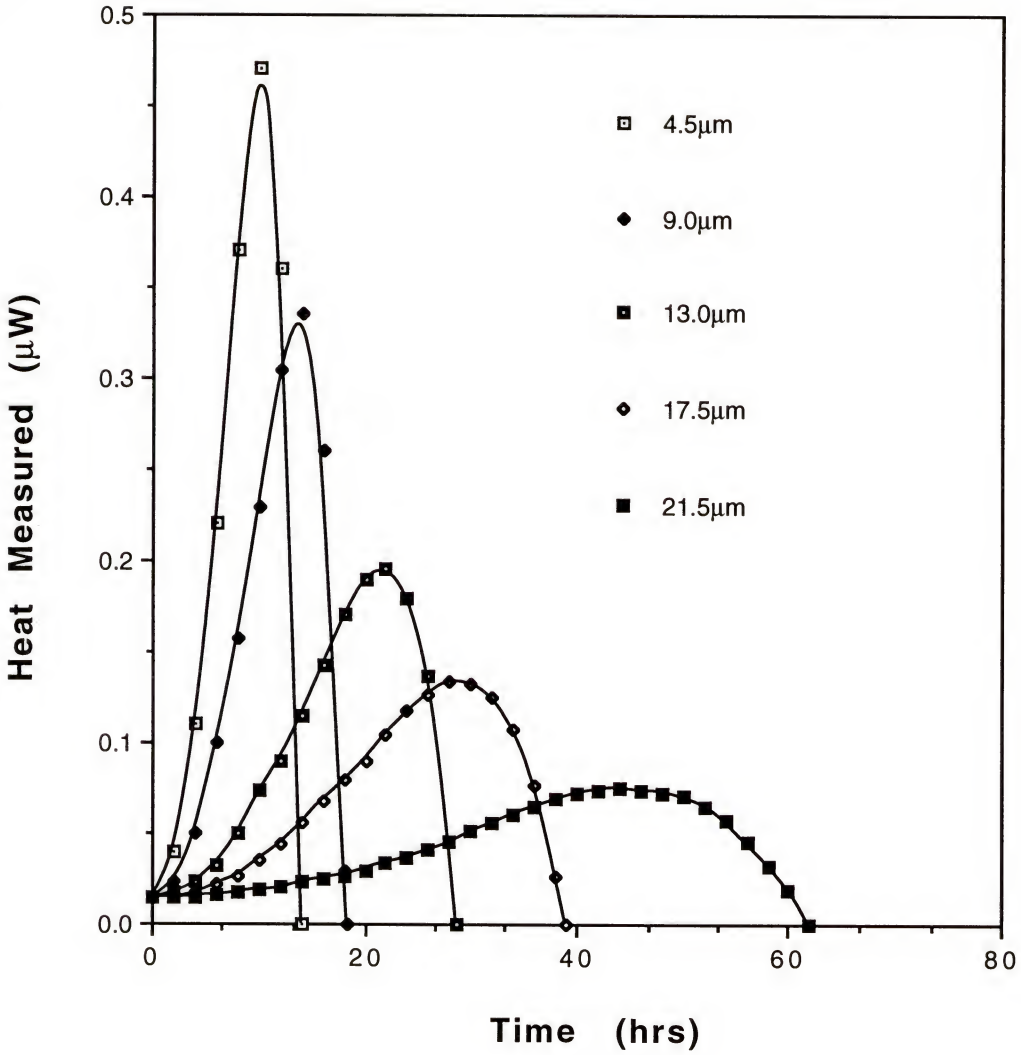

Figure 3.2 : Computer model simulated thermal outputs for variations in the nuclei density. The data is displayed in terms of the grain size of the final microstructure.

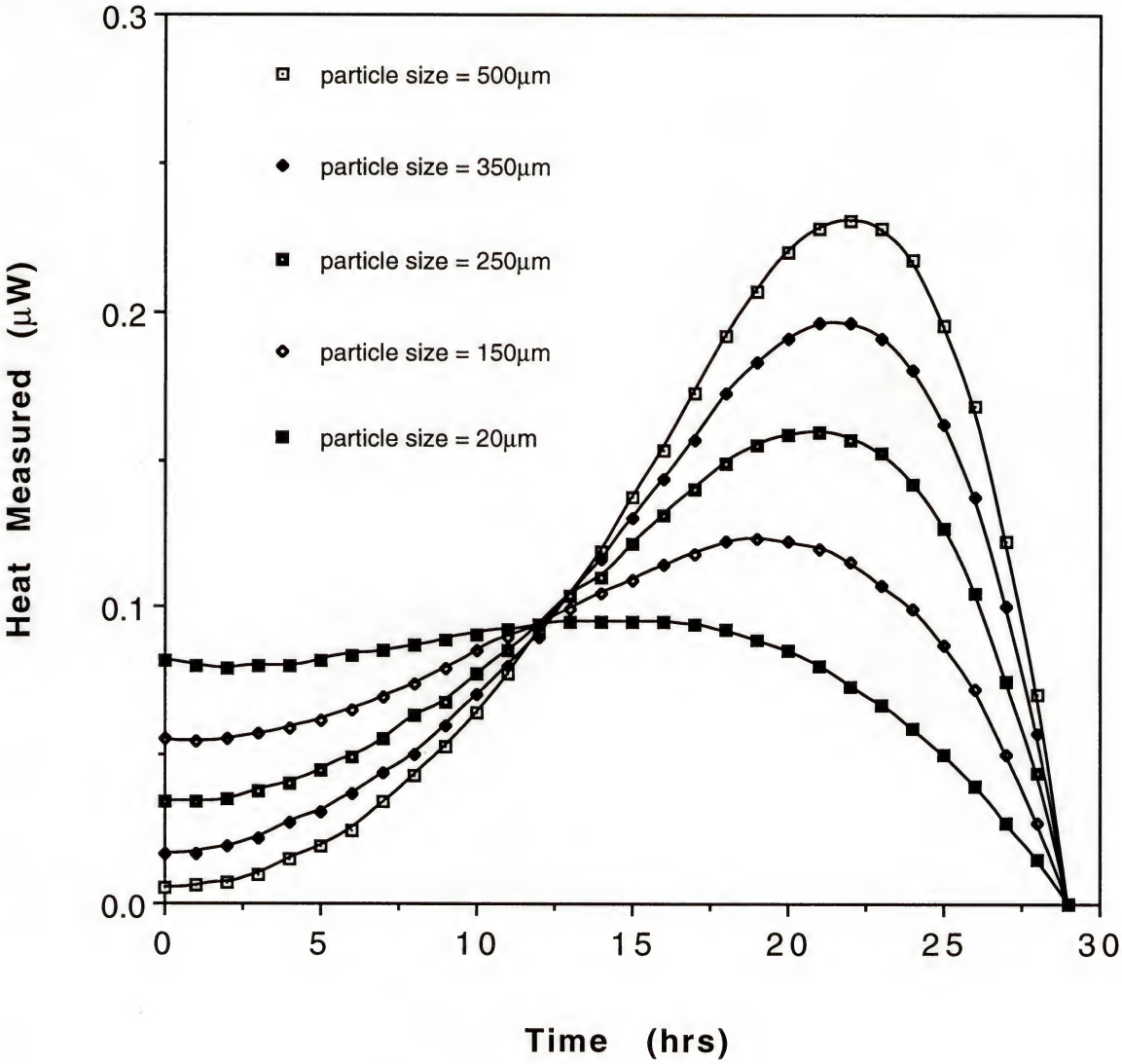

Figure 3.3 : Computer model simulated thermal outputs for variations in particle size.

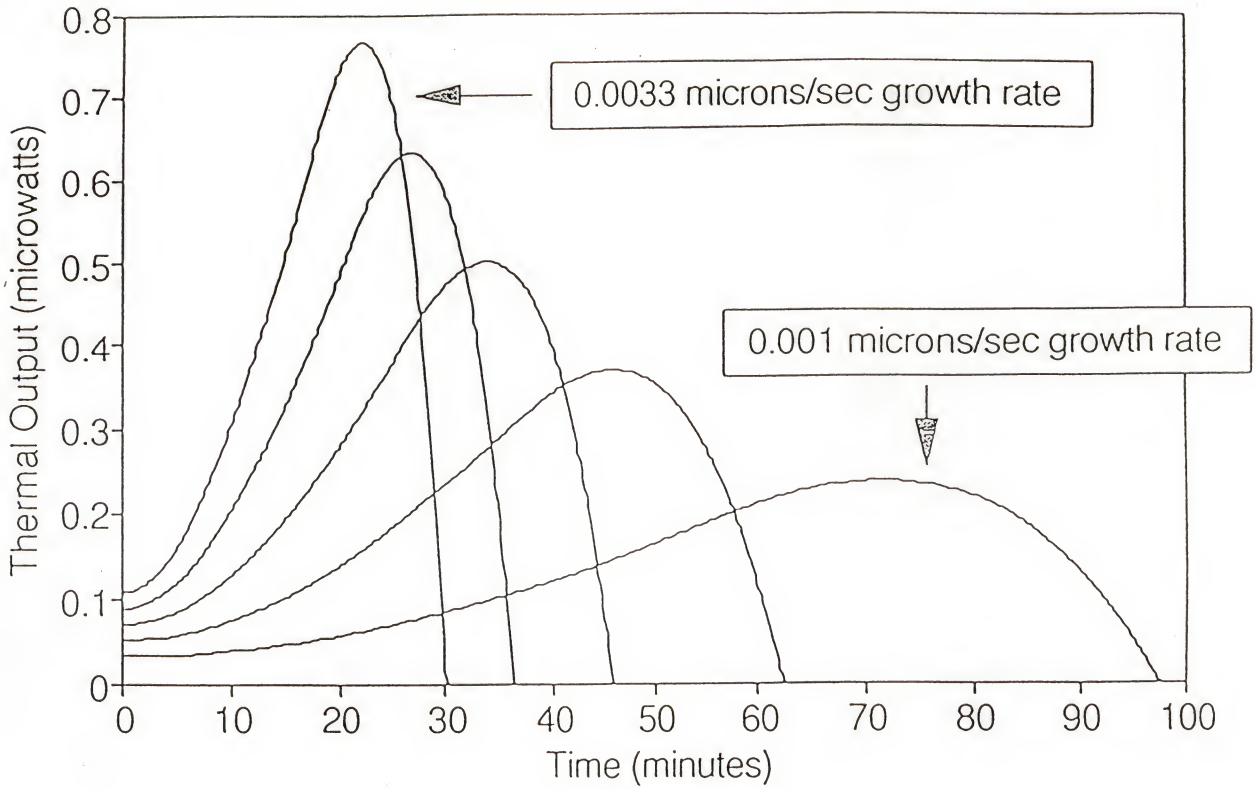

Figure 3.4 : Computer model predicted thermal output for variations in isothermal temperature.

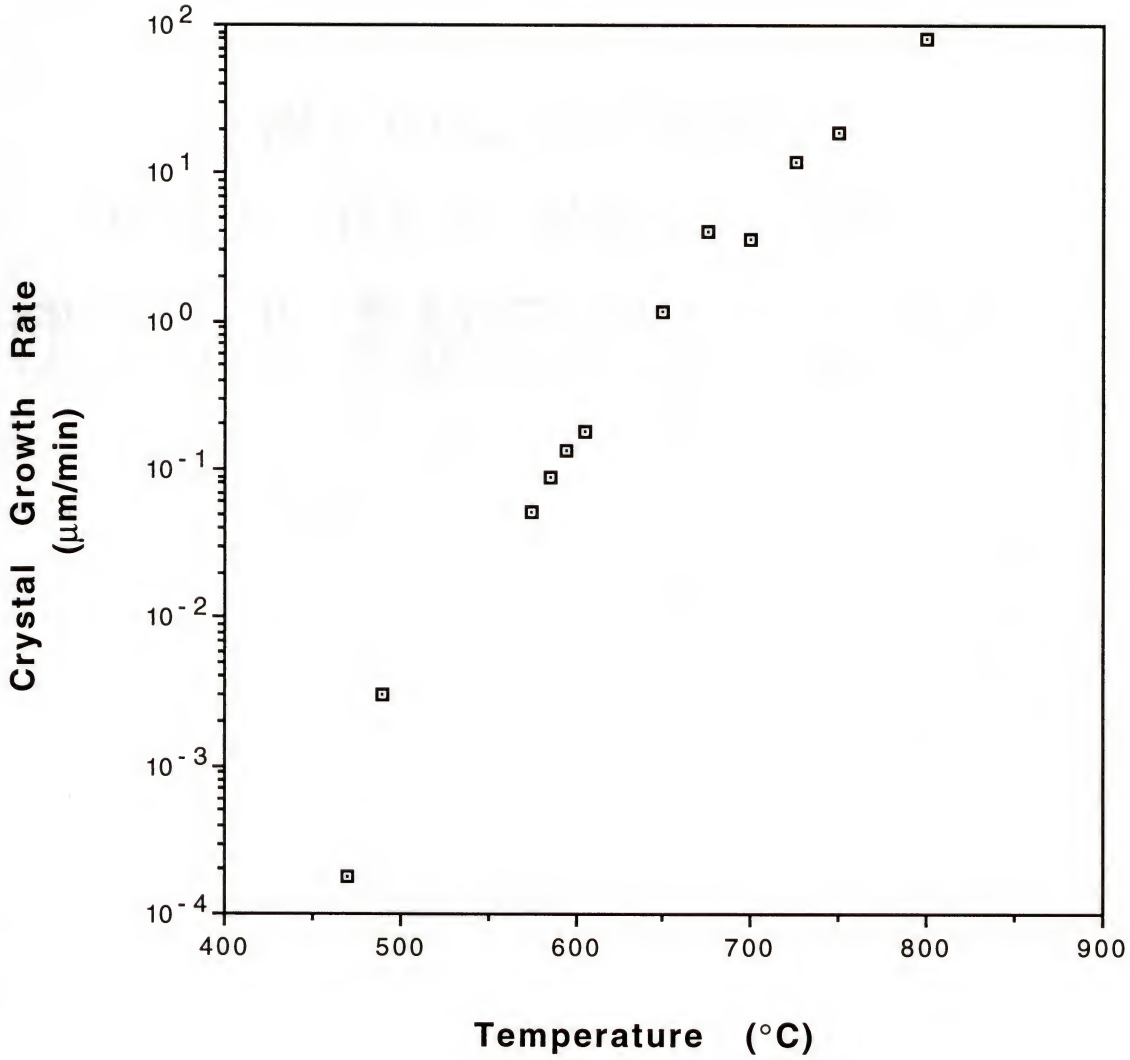

Figure 3.5 : Growth rate of bulk-sized lithium disilicate crystals as a function of temperature

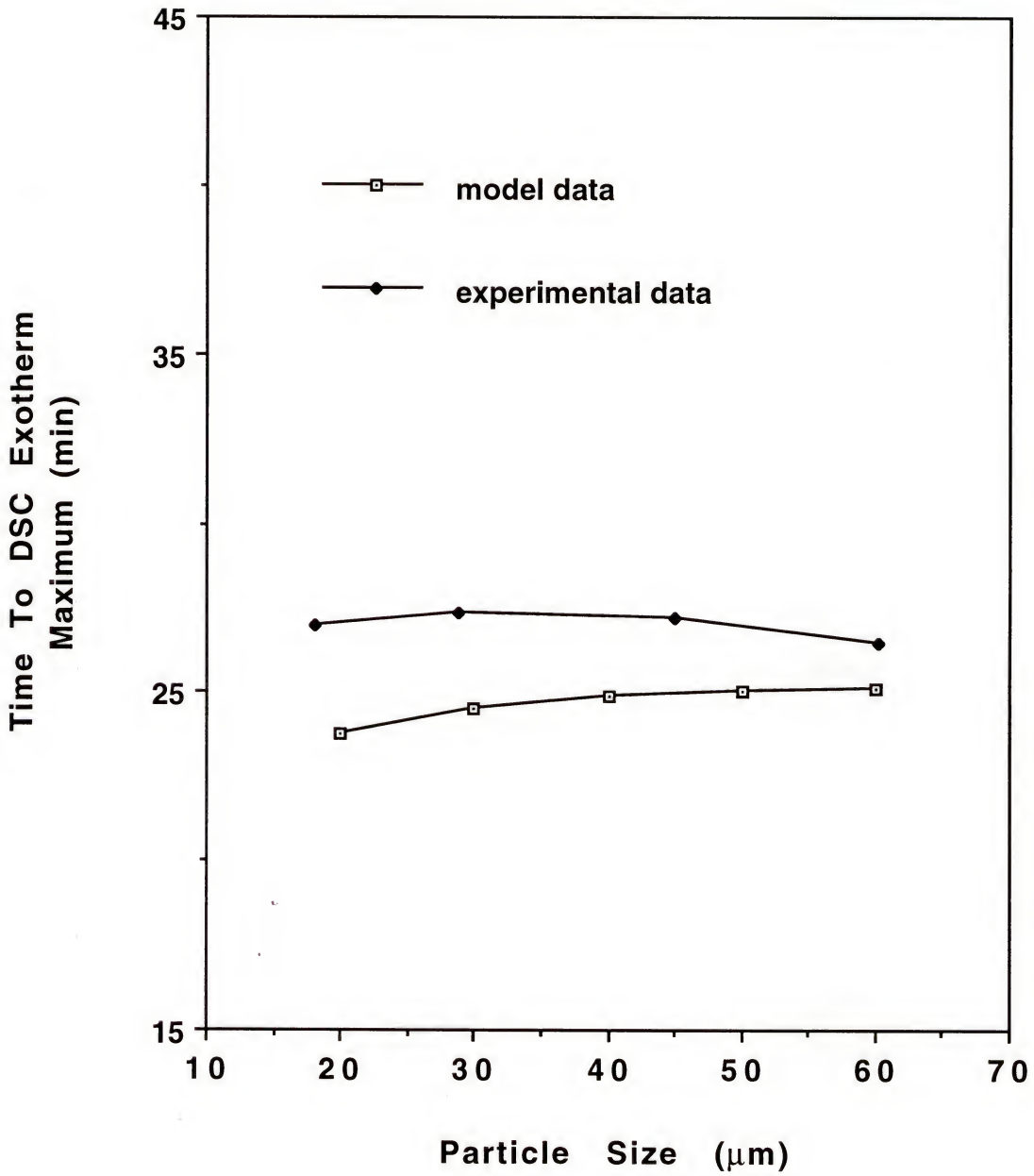

Figure 3.6 : Comparison of model predicted time to exotherm maximum to experimentally measured time to exotherm maximum for variations in particle size

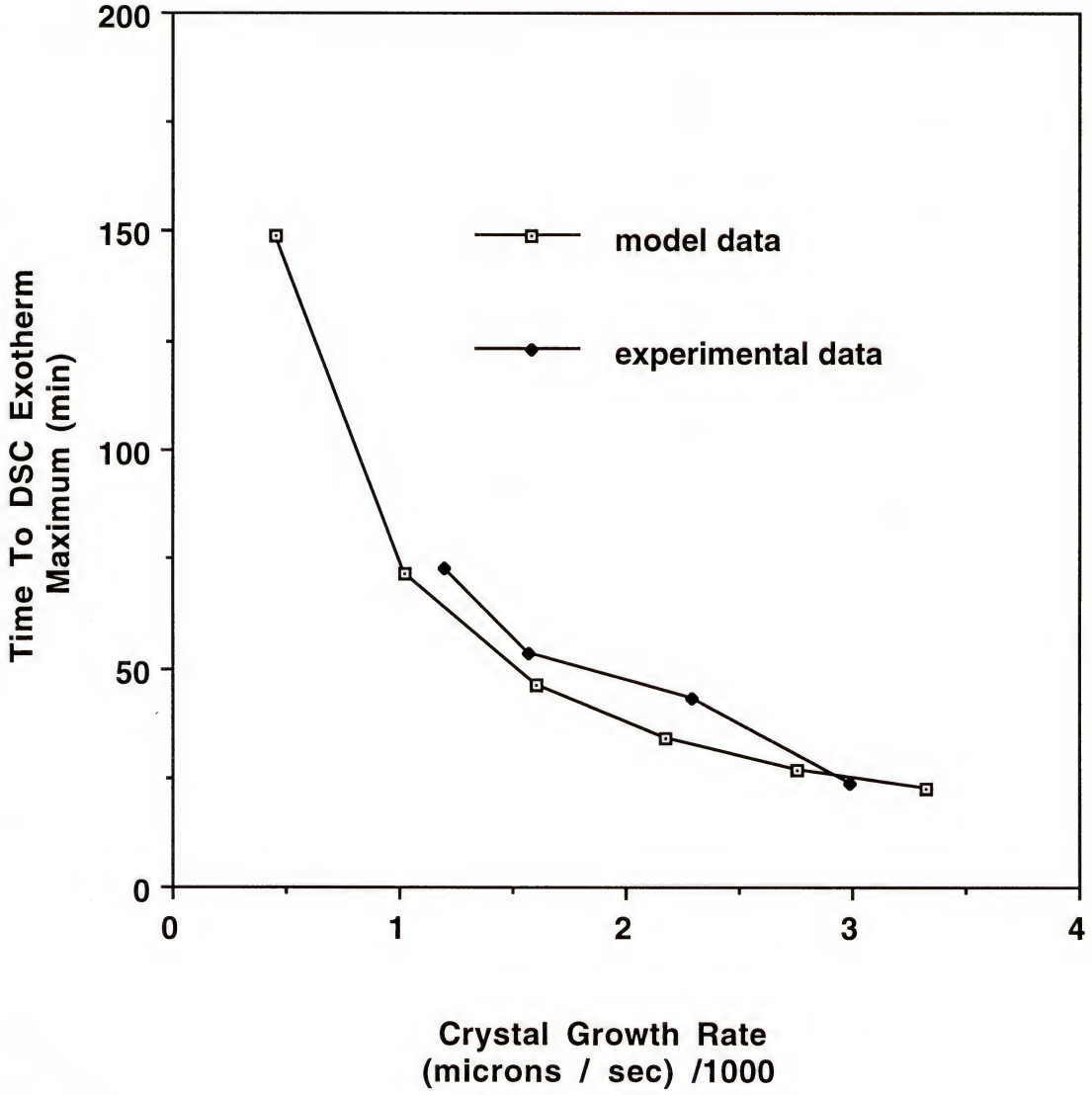

Figure 3.7 : Comparison of model predicted time to exotherm maximum to experimentally measured time to exotherm maximum for variations in isothermal temperature

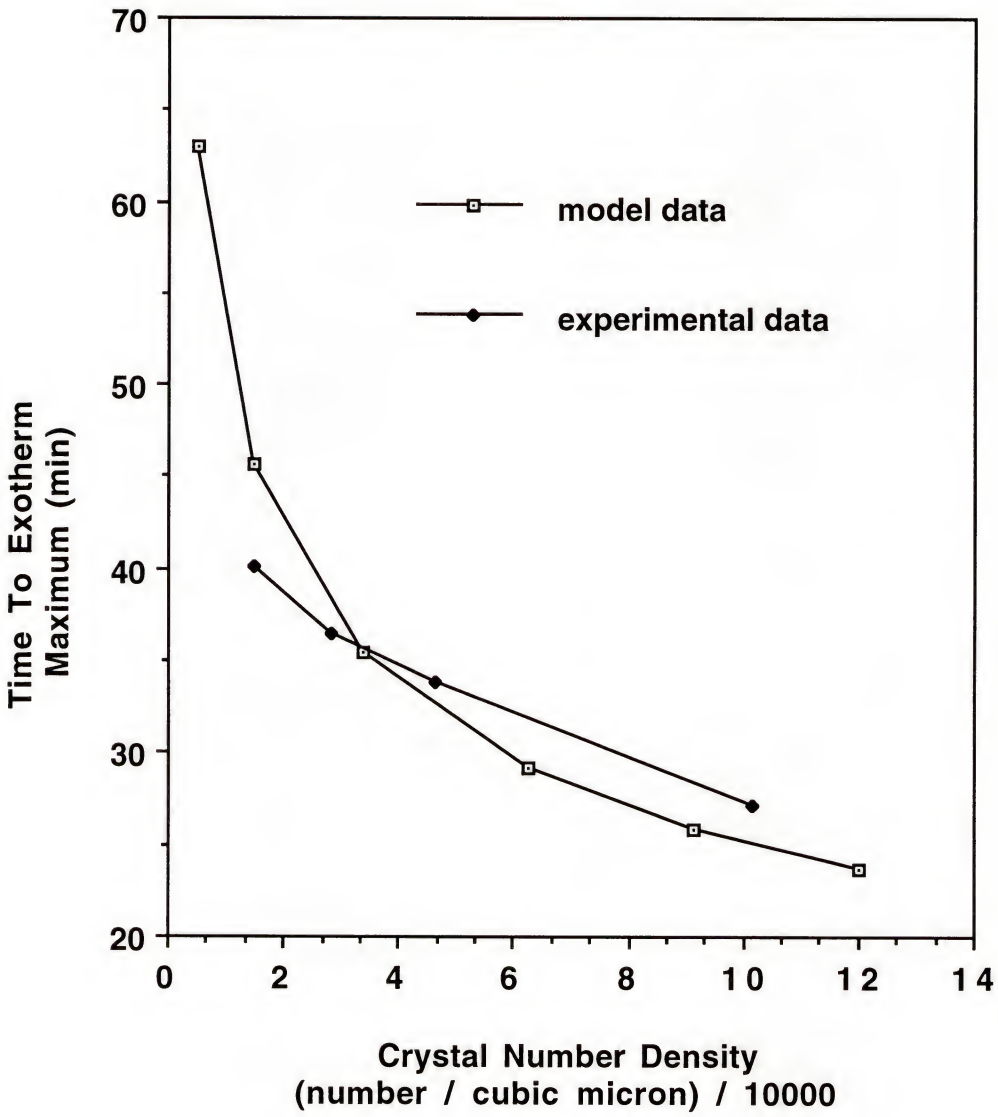

Figure 3.8 : Comparison of model predicted time to exotherm maximum and experimentally measured time to exotherm maximum for variations in sample nuclei density

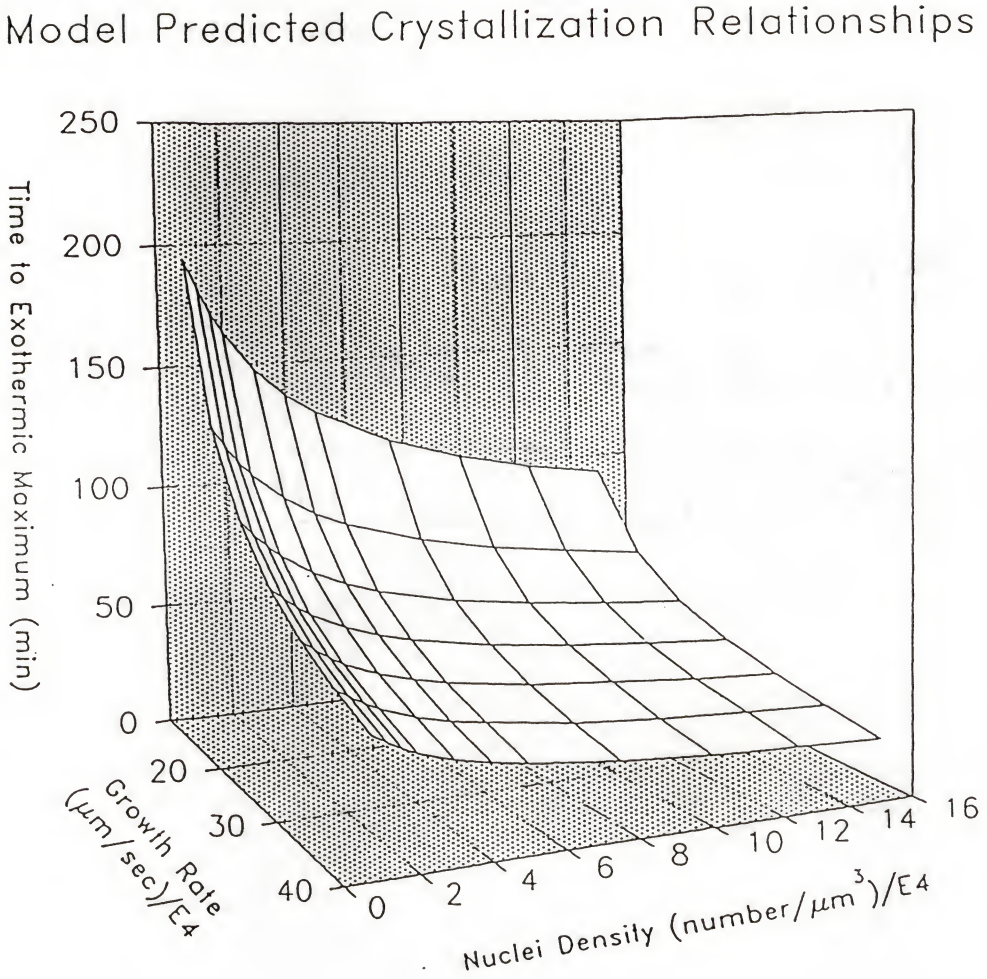

Figure 3.9 : Crystallization simulation output; effect on time to exotherm maximum by variation of growth rate (ie. isothermal temperature) and nuclei density.

CHAPTER 4
TRADITIONAL TWO-STAGE PROCESSING OF GLASS-CERAMICS

4.1: Introduction

4.1.1: The Two-Stage Method for Determination of Nucleation Rate Curves

The processing of glass-ceramic materials has classically been viewed as a two-stage event consisting of nucleation and growth stages. In most systems, devitrification is not the difficult stage in the processing sequence and therefore the bulk of the scientific attention has been centered on the kinetics of nucleation as a function of temperature. The nucleation kinetics for glass-ceramic systems are described by nucleation rate curves. The most common method for generation of nucleation rate curves is the two-stage method. The first step in this method is the production of a matrix of nucleated samples by heat treating at varying heat treatment temperatures and heat treatment times. This matrix of samples is then given a second heat treatment of sufficient time and temperature that the nuclei generated in the previous heat treatment are grown to microscopically observable size. Samples are then cut cross-sectionally and the newly exposed surface is polished and etched as necessary. A cross-sectional surface is preferred so that surface crystallization can easily be differentiated from bulk crystallization. Standard stereological

measurements are then made on each sample. From these data (number of nuclei per area), nucleation rate as a function of temperature can then be calculated.

There exist two main problems with the two-stage method for determination of nucleation rate curves. Firstly, the technique is very labor intensive and time consuming. For the study of a single glass composition, the time demands of this technique may be acceptable. For most industrial applications, however, many system parameters need to be varied in order to optimize the material in terms of product performance as a function of total processing costs. Such parameters include glass composition, nucleating agent composition and nucleating agent concentration. For situations with a large number of compositions, the two-stage method constitutes a significant investment in labor and time.

The second drawback to the two-stage method is that the measured nuclei density is not the true nuclei density but only the small fraction of the original nuclei population which survived the rapid heating rate from the nucleation temperature region to the secondary growth region. Therefore, the evaluation as to overall effectiveness of the nucleation heat treatment will be based on the effectiveness of the heat treatment to generate large nuclei which can withstand the rapid heating rate. Because the rate of heating from the nucleation temperature to the growth temperature influences the predicted effectiveness of the nucleation heat treatment, the general use of this method is questionable. The effect of heating rate on the resulting crystal population is discussed and evaluated in greater detail later in this work.

4.1.2: Two-Stage Heat Treatment Schedules Produced from Curves

Nucleation rate curves and growth rate curves are the necessary sources of information for the generation of traditional two-stage heat treatments. Figure 4.1 shows the typical presentation of these curves and the heat treatment schedule derived from them. Temperature is plotted along the abscissa while the vertical axis is both nucleation rate and growth rate. The most important features on these curves are the maximum in the nucleation rate curve and the amount of overlap between the two curves at this point. If, for a given system, a significant growth rate is present at the temperature which corresponds to the maximum nucleation rate, the best nucleation temperature to use may be one which is shifted to lower temperatures. The decrease in nucleation temperature is thought to be necessary to prevent significant growth of nuclei during the nucleation stage. This premature growth is undesirable because it is thought to result in generation of a nonuniform final microstructure.[45] Ideally, there will be sufficient separation between the two curves to allow for the use of the maximum nucleation rate temperature.

4.1.3: Reasons for Acceptance of Traditional Two-Stage Heat Treatment Schedules

The two-stage heat treatment schedules traditionally used for the processing of glass-ceramic materials are at least partly a result of the simplified view of the nucleation and crystallization process presented by nucleation rate curves and growth rate curves. Depiction of the phase transformation from glass to crystal as

occurring in two separate steps, nucleation then growth, is not an accurate representation of the actual mechanics of the phase transformation. To develop more effective heat treatment schedules, the assumptions that the two-stage heat treatment schedules are based upon must be replaced by a more realistic view of the phase transformation process.

Another reason for the acceptance of the traditional two-stage heat treatment schedule is the simple oven control needed to execute the schedule. A two-temperature zone oven with a conveyer system for moving the material from one zone to the next is sufficient for production. Not until recently did the advent of multi-step proportional band temperature controllers permit execution of complex heat treatment schedules.

The third reason for the acceptance of the traditional two-stage heat treatment is that they work. The motto "if it isn't broke, don't fix it," appears to carry significant weight in the commercial world. Two-stage heat treatment schedules produce fine microstructures within tolerable amounts of production time. As was previously mentioned, commercial production of glass-ceramic materials is dominated by heterogeneously nucleated materials. These are the best systems for maintaining large crystal populations under conditions of non-ideal heating rates.

4.2: Methods and Results

4.2.1: Determination of Traditional Nucleation Temperature for Lithium Disilicate

As has been previously mentioned, lithium disilicate is a

commonly used glass for the study of nucleation and crystallization. Thus, there exists many published studies which measure the nucleation rate as a function of heat treatment temperature.[46-51] The optimum temperature for nucleation given in the literature was found to range between 455°C and 470°C. This existing literature permits a further test of the thermal analysis method through comparison. If the thermal analysis method predicts an optimum nucleation temperature within this range, then the method can be considered usable for the determination of heat treatment schedules for other systems.

A Seiko DSC220C was used to both heat treat the glass and to measure the exothermic energy generated by the crystallization of the glass. Lithium disilicate glass was ground with a mortar and pestle and sieved. Particle sizes between 200 μm and 500 μm were used. Preoxidized stainless steel sample pans were filled with 16.0 mg of glass particles. The samples were rapidly (20°C/min) heated to a nucleation temperature, held at this temperature for 1 hour, heated at 10°C/min to the isothermal temperature (610°C) and held until the sample had completely crystallized. The exothermic activity caused by crystallization was measured and recorded during this isothermal period. A range of nucleation temperatures were used. To test the reproducibility of the thermal analysis method, six samples were run for each nucleation temperature investigated. The average standard deviation was found to be 1.1 minutes, while the time difference between an effectively nucleated sample and an uneffectively nucleated sample was greater than 15 minutes. The method is deemed acceptable because the standard deviation of the

data is significantly less (more than an order of magnitude) than the change in the data associated with detection of improved nucleation efficiency.

Figure 4.2 shows the exothermic activity recorded for a series of samples, each of which was held at a different nucleation temperature. Figure 4.3 shows the measured time to the exotherm maximum as a function of the nucleation temperature that the sample was held at previously. From this data the best nucleation temperatures for a 1 hour nucleation time are between 460°C and 485°C. The nucleation temperature which corresponded to the shortest time to the exothermic maximum was 467°C. This temperature is within the range of temperatures cited as producing the maximum nucleation rate.

To further validate the technique, micrographs were made from the heat treated sample particle and crystal number densities were measured. This was accomplished by securing the crystallized particles to a metal stud with a polymer resin. Careful polishing using a hand lapper results in polished cross-sections of the particles. Micrographs were made of surfaces by using the same techniques of etching, coating, and photographing as has been previously detailed. A typical micrograph of a fully crystallized lithium disilicate sample is shown in Figure 4.4. Figure 4.5 shows the resulting data. Since the optimum nucleation temperature will produce the largest number of crystals per volume, the optimum nucleation temperature is predicted to be approximately 467°C. The exact match with the optimum nucleation temperature predicted by the thermal analysis technique is seen as fortuitous. However, the

microstructural data clearly supports the belief that the thermal analysis technique is a reliable method for assessing the effectiveness of heat treatment schedules. It should be noted, as was previously mentioned, the thermal analysis technique appears to lack the sensitivity required to measure small changes in the crystal number density when this value is large. This can be seen in that the microstructural data shows a sharper maxima than is observed from the thermal analysis data.

4.2.2: Determination of the Two-Stage Heat Treatment Schedule for LACSP by the Thermal Analysis Method

The information necessary to construct a two-stage heat treatment schedule includes nucleation temperature, nucleation time, heating rate between the nucleation temperature and the growth temperature, growth temperature, and growth time. All of these parameters can be ascertained through the use of the thermal analysis technique. A glass composition of 30.2 Li_2O, 2.5 Al_2O_3, 6.0 CaO, 60.3 SiO_2, and 1.0 P_2O_5 (mol%) was used in this investigation because of its potential use as a dental restorative material. Glass particle sizes were approximately 400μm in diameter. A Seiko TG/DTA320 was used to heat treat the glass as well as to measure the exothermic activity due to crystallization. The use of the DTA was necessary due to the high crystallization temperatures for this system (>700°C). The glass particles were held in open platinum pans during the analysis. The nucleation temperature was determined in the same manner as for the lithium disilicate glass. As with the lithium disilicate, a nucleation time of 1 hour was used. Unlike the disilicate, however, the LACSP glass was held at an

isothermal temperature of 715°C. The time to the exotherm maximum as a function of nucleation temperature is shown in Figure 4.6. The data shows the best nucleation temperature to occur between 500°C and 510°C. A value of 505°C will be used as the nucleation temperature.

Next, the most efficient time period to hold the sample at the nucleation temperature must be determined. Samples were held at 505°C for a series of times and then heated at 10°C/min to the isothermal temperature for measurement of the crystallization exotherm. The results of this series of experiments are shown in Figure 4.7. The data shows an initial steep decrease in the measured time to the exotherm maximum with increases in the nucleation time. At longer nucleation times, however, the rate of decrease in the time to the exotherm maximum decreases until a steady-state condition is reached in approximately 10 hours. From this data it was concluded that a 3-hour nucleation time would be sufficient without being too time consuming.

The next schedule parameter to be determined is the rate used to heat the sample from the nucleation temperature to the growth temperature. This is a parameter whose significance has traditionally been overlooked. To investigate this parameter, samples were held for 3 hours at 505°C and then heated at a series of heating rates to the isothermal temperature. To ensure that the various heating rates did not affect the exothermic peak characteristics, all the samples were heated at the same rate (5°C/min) once they had reached a temperature 15°C below the isothermal temperature. The resulting data are shown in Figure 4.8.

This data clearly show the strong effect that heating rate has in determining the percentage of the initial nuclei population which will contribute to the final microstructure. It is seen that the more rapid the heating rate, the fewer nuclei will survive. From these data, it was judged that 2°C/min would be a sufficiently slow heating rate. Therefore, a sufficient two-stage heat treatment schedule for the LACSP glass is 3 hours at 505°C followed by heating at a rate of 2 °C/min until the desired crystal volume fraction is achieved. Given these heat treatment parameters, it was found that a sample will reach full crystallinity by the time the sample temperature reaches approximately 675°C.

4.3: Discussion

In viewing the data of heating rate versus time to the exotherm maximum, the concern arose that the sharp decrease in time to the exotherm maximum associated with the slowest heating rate used (0.5°C/min) resulted from pregrowth of the nuclei population as opposed to an increase in the nuclei number density. It is possible that the time to the exotherm maximum could be decreased by either an increase in the number of nuclei or by an increase in the total surface area of a constant number of nuclei. In other words, the thermal analysis technique is sensitive only to changes in total crystalline surface area and is insensitive as to the source of these changes. In order to determine if the slow heating rate produced a shorter time to the exotherm maximum than that which would be due to only the increase in the nuclei number

density, the previously described computer model (Chapter 3) was used as a predictor which is unaffected by any possible crystal pregrowth. The crystal densities (number of crystals per material volume) of the crystallized sample paricles were measured by the micrographic technique described previously. This data was plotted against the sample heating rate. The computer model was used to predict the crystal density required to produce the time to exotherm maximum which was observed experimentally for each different heating rate. This data was plotted as the model calculated crystal density versus the experimental heating rate. These two plots were then superimposed upon one another to produce Figure 4.9. The figure shows a correlation between the experimental data and the model data which is good enough to conclude that if crystal pregrowth was occurring in the slow heating rate samples, it was not occurring to a degree which would affect the measured time to the exotherm maximum.

4.4: Conclusions

It has been demonstrated that the thermal analysis method can be used to determine the most effective nucleation temperature and to construct a traditional two-stage, glass-ceramic heat treatment schedule. Further confidence in the thermal analysis method was established through agreement with values for the optimum lithium disilicate nucleation temperature as determined by traditional methods.

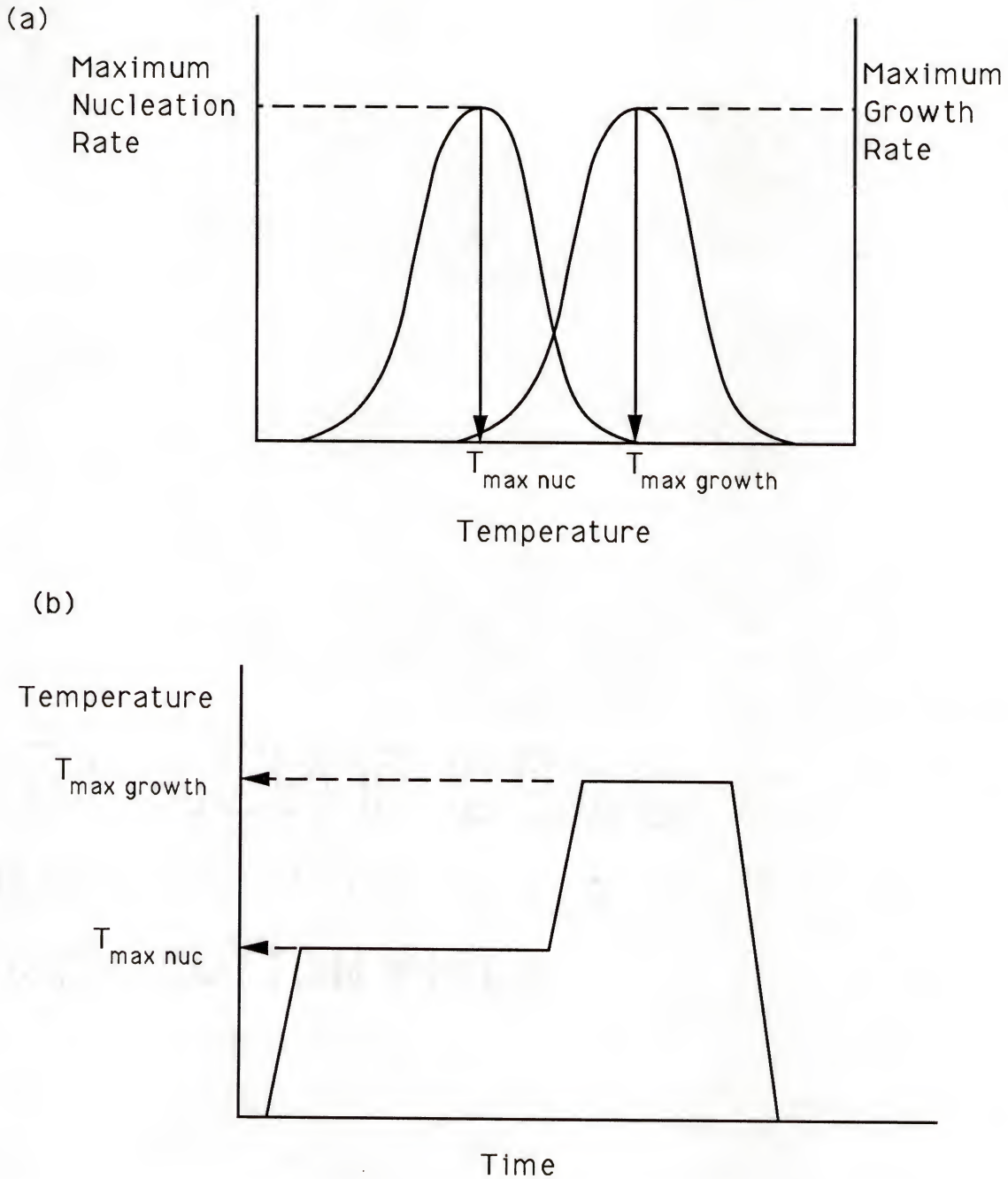

Figure 4.1 : Schematic drawing of traditional two-stage heat treatment approach; (a): nucleation and growth rate curves derived from two-stage method, (b): two-stage heat treatment schedule derived from rate curves.

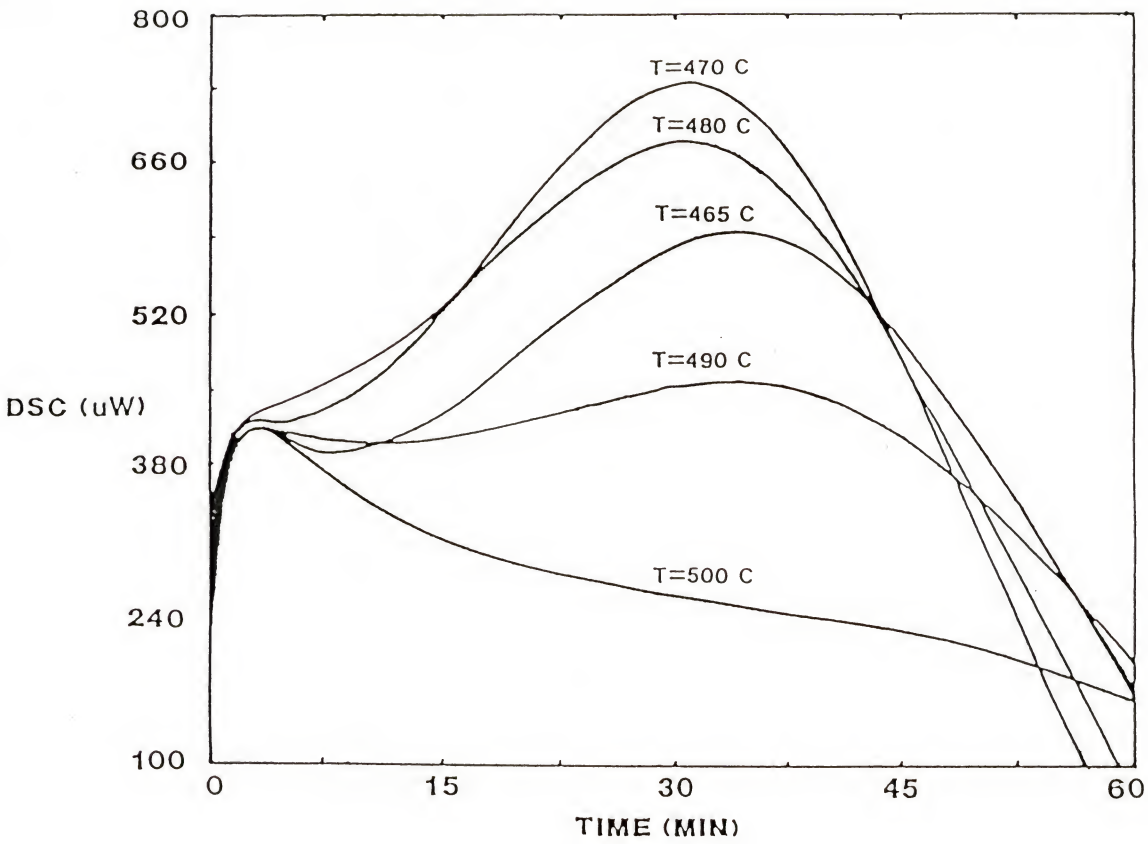

Figure 4.2 : Differential scanning calorimeter measured outputs for lithium disilicate nucleated for 1.0 hrs at a series of temperatures. The isothermal temperature used was 600°C and the particle size used was 200 μm diameter.

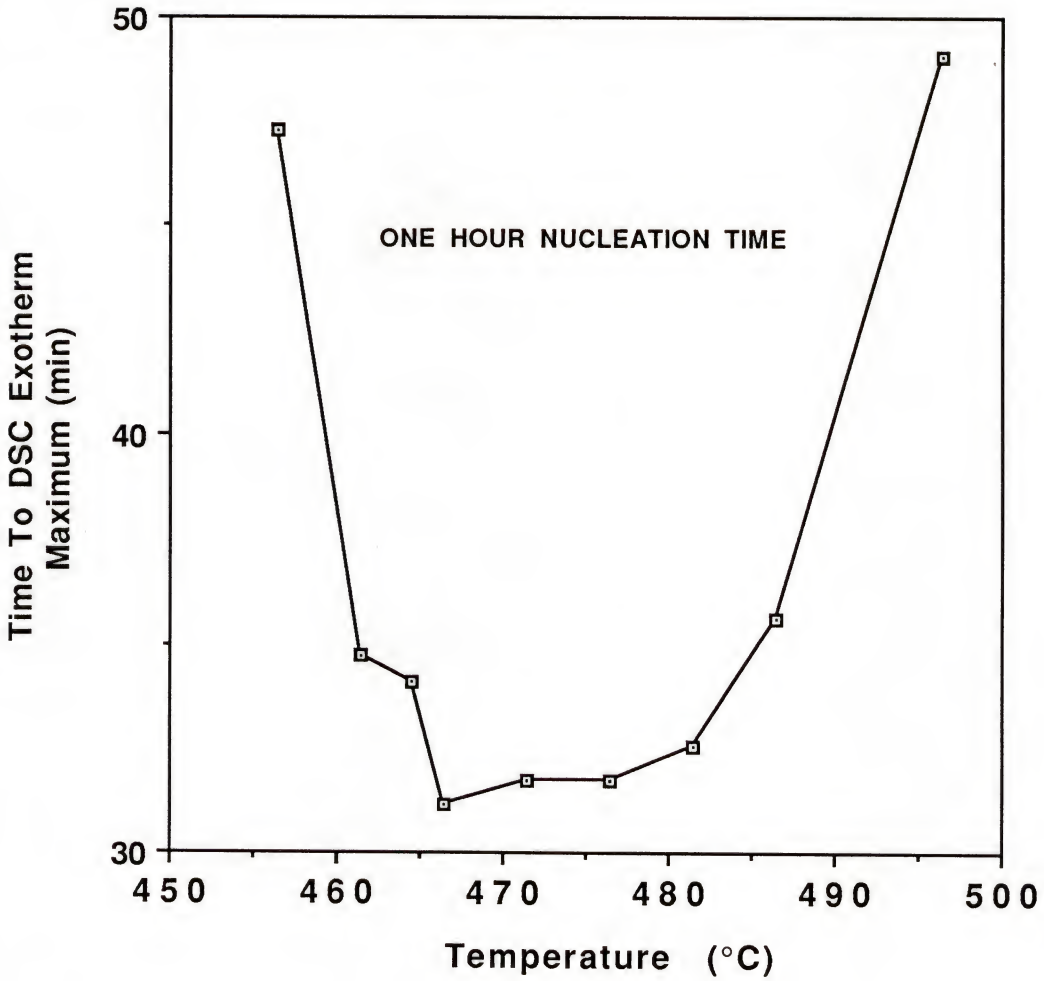

Figure 4.3 : Thermal analysis method (DSC) for determination of optimum nucleation temperature for lithium disilicate.

Figure 4.4 : Typical optical micrograph of a fully crystallized lithium disilicate sample (400x). Sample was cut cross-sectionally, polished through 1 μm grit alumina, etched with dilute HF and sputter-coated with Au/Pd.

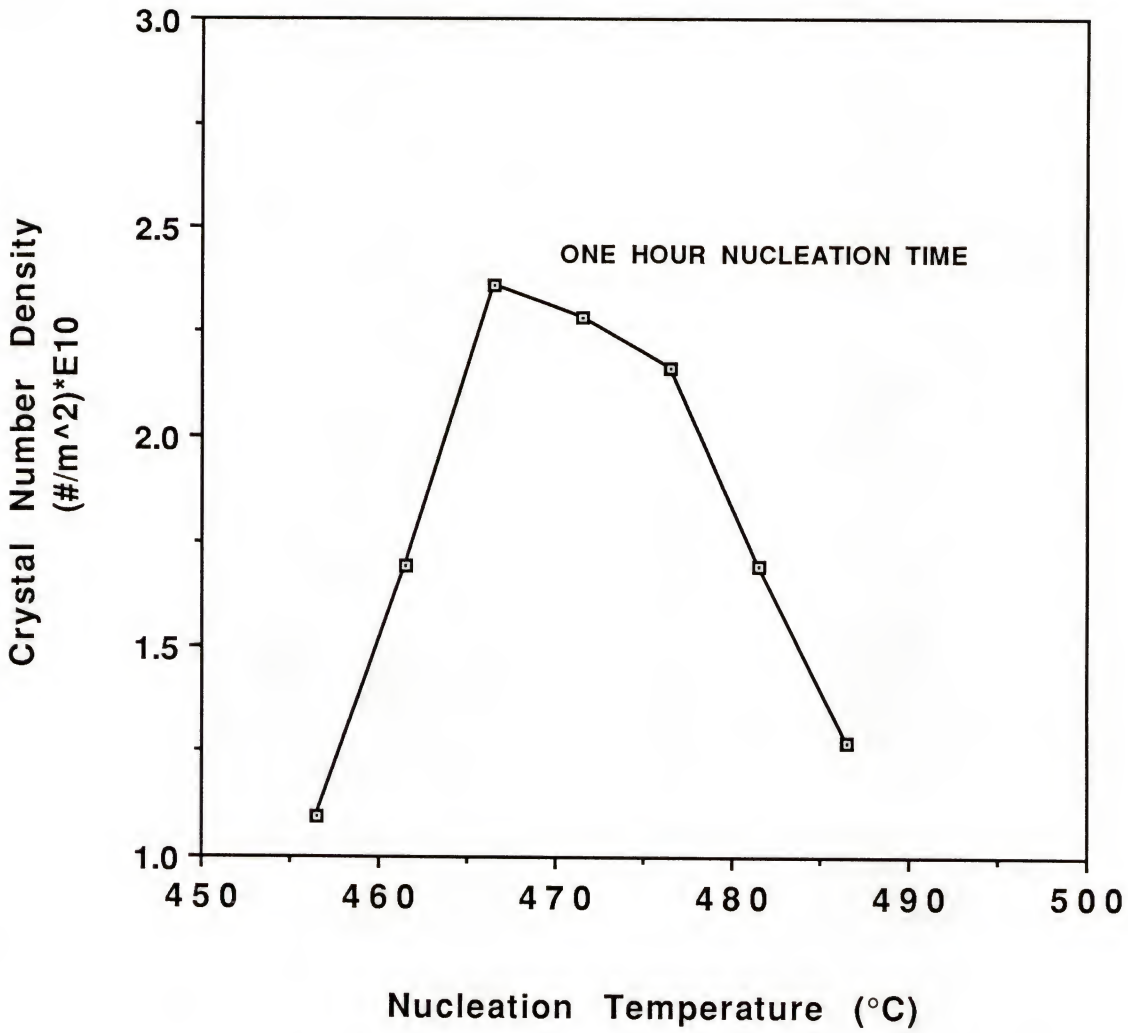

Figure 4.5 : Crystal number density measured optically for a series of nucleation temperatures.

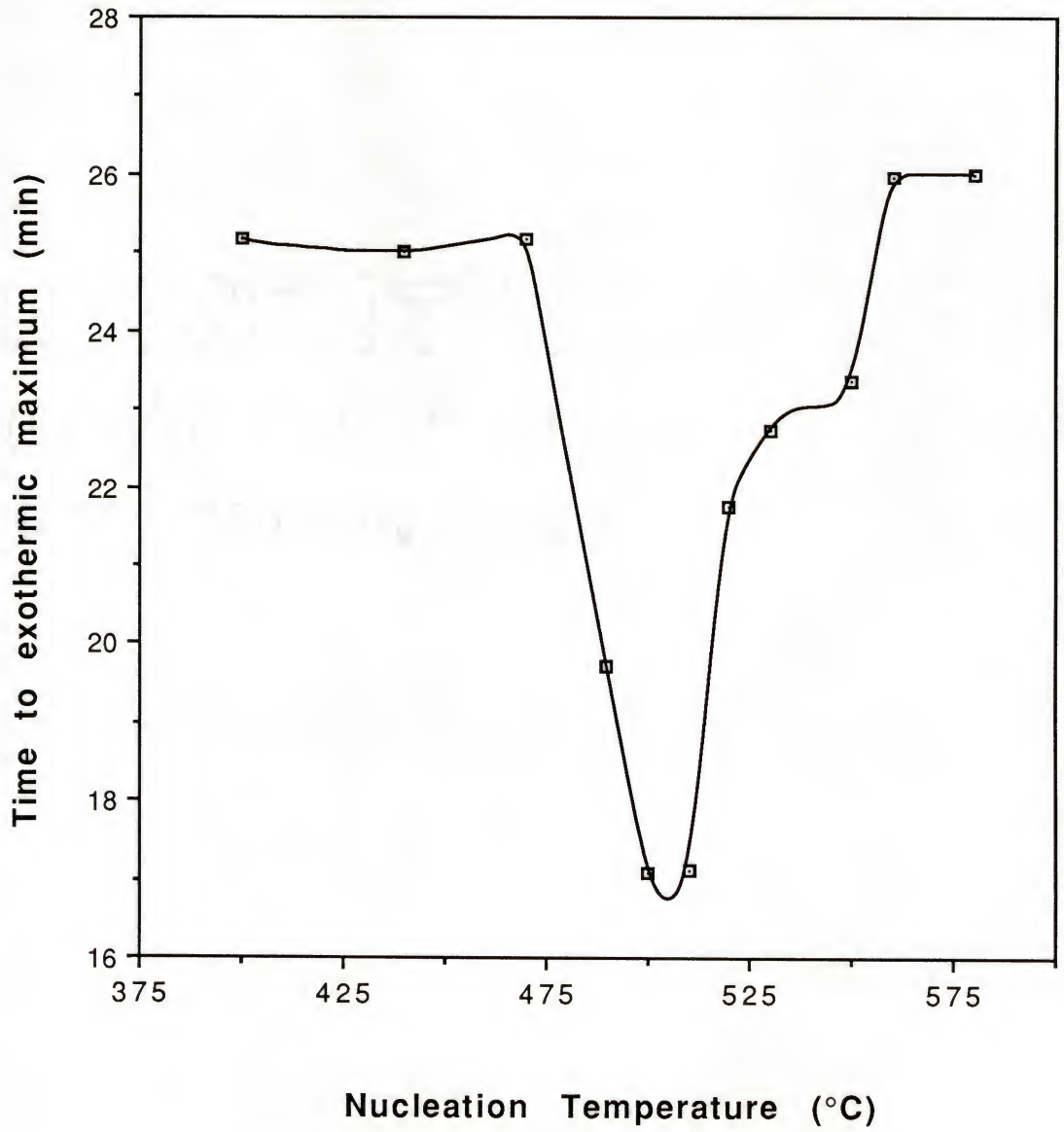

Figure 4.6 : Determination of optimum nucleation temperature for LACSP using thermal analysis (DTA).

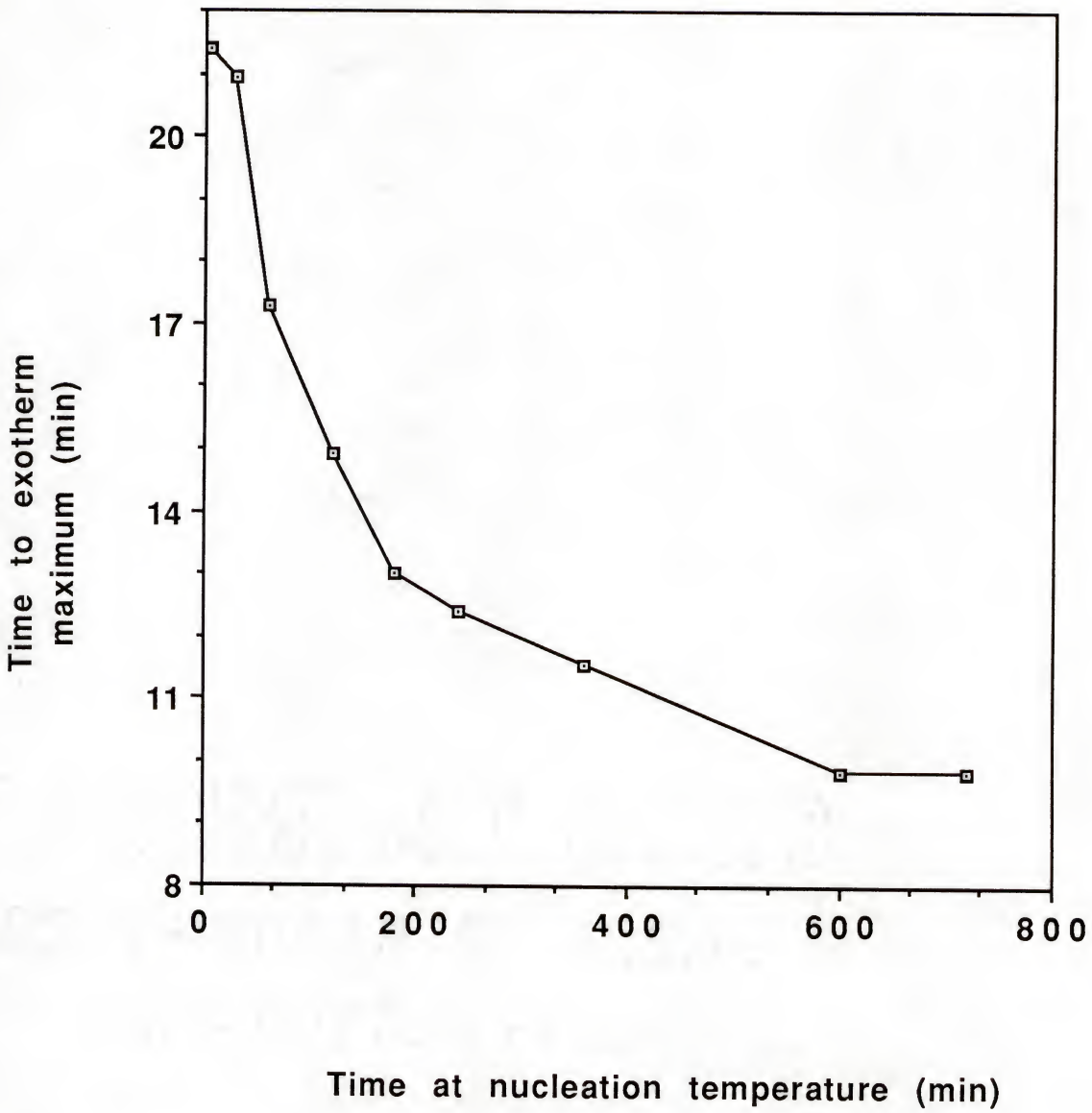

Figure 4.7 : Effect of nucleation time on the time to exotherm maximum. A nucleation temperature of 505°C was used.

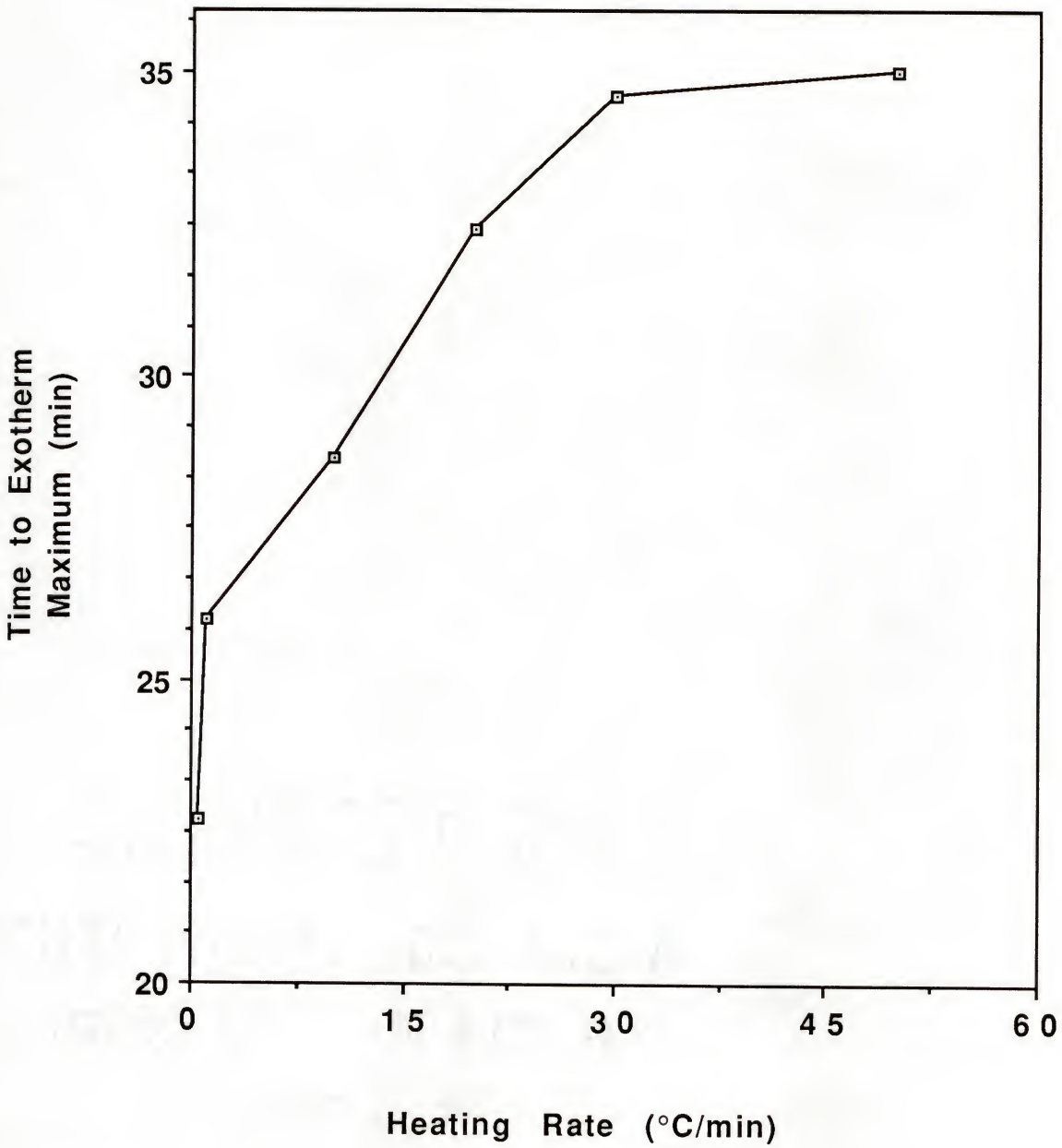

Figure 4.8 : Effect of heating rate on time to exotherm maximum for LACSP as measured by DTA.

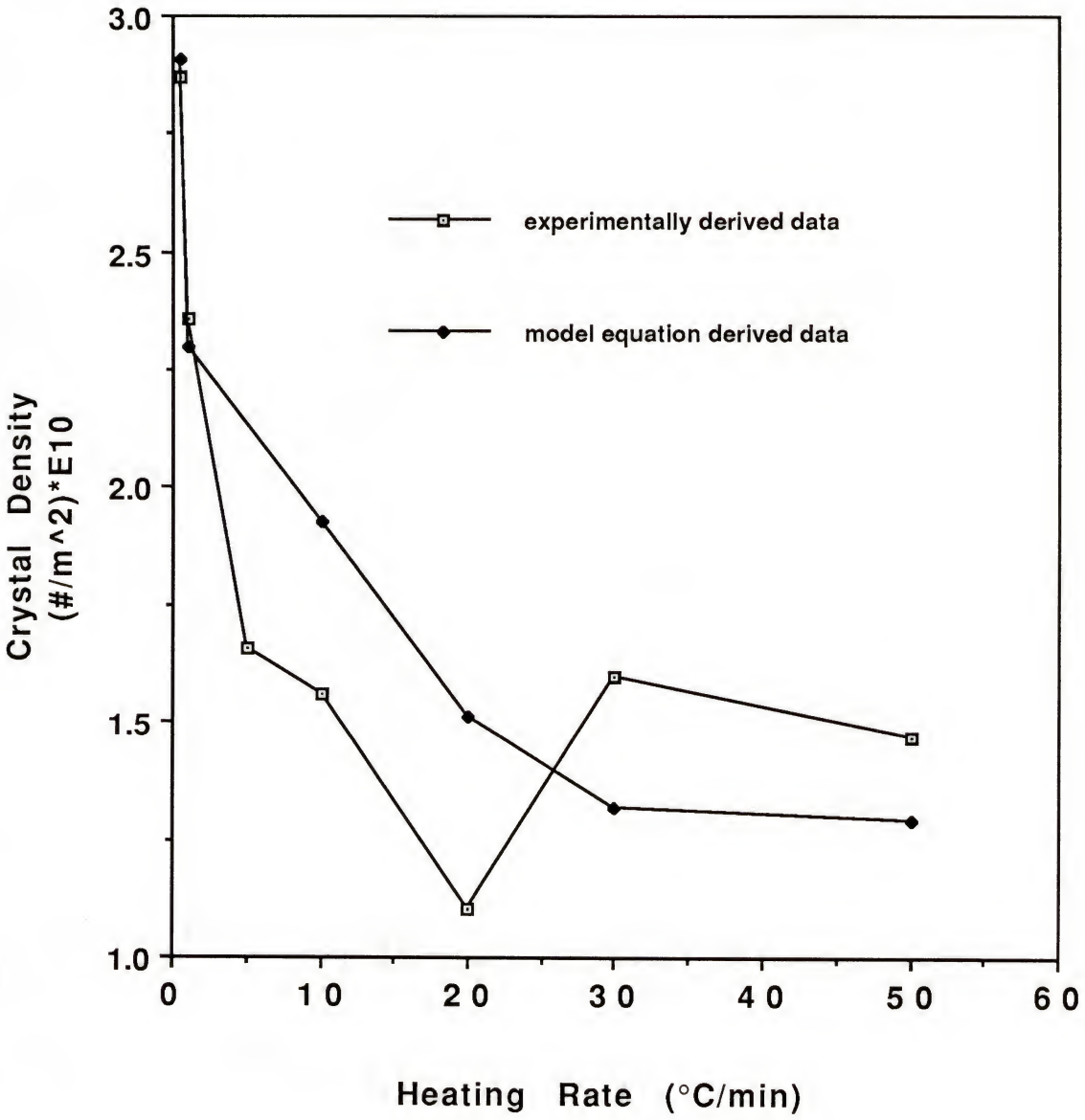

Figure 4.9 : Comparison of model data and experimental data for heating rate effects on crystal density.

CHAPTER 5
A NOVEL VIEW OF NUCLEATION AND CRYSTALLIZATION
THE PRECRYSTAL CONCEPT

5.1: Introduction

This chapter has three objectives. The first objective is to introduce the concepts of a precrystal site distribution within the glass. The second objective is to present evidence which supports the precrystal site approach for the development of glass-ceramic microstructures. The third objective is to demonstrate the generation of precrystal site density maps and their usage for microstructural development of certain glass-ceramics.

5.2: Objective One : The Precrystal Approach

Inherent in the development of optimum heat treatment schedules is the idea that for a given temperature there exists a set number of sites in the glass where crystallization will occur at a certain temperature. These sites have been termed precrystals. The size of the precrystal correlates to the size of the smallest crystal which will exhibit stable growth at the temperature which the precrystal site catalyzed crystal growth. The temperature/critical size relationship is governed by equation 5.1.

$$r^* = 2\sigma/(\Delta G_v - \Delta G_s) \qquad (5.1)$$

where σ = temperature-dependent interfacial free energy

ΔG_v = temperature-dependent volume free energy

ΔG_s = temperature-dependent strain free energy

The development of the optimum heat treatment schedule should begin with the microstructure of the desired final product. From this information the required number of crystals per volume is known. Now consider the glass prior to heat treatment. Within the glassy network is a distribution of sites of varying crystal growth potential. Sites which would preferentially exhibit stable growth at higher temperatures are represented as precrystals of larger size. In other words, because of something atypical about a given location in the glass, crystal growth will occur there as if a crystal of a certain size already existed at that location. Such atypical sites which are equivalent in growth potential to large crystals (large precrystals) might be generated by low surface energy heterogeneities (nucleates, impurities, internal bubbles, concentration gradients, etc.) or by stress fields in the glass which compensate for the volume change associated with the phase transformation. Sites which are equivalent in growth potential to smaller crystals (small precrystals) might be generated by a statistically high population of strained atomic bonds in a certain glass volume or possibly a region of high free volume. In order to know the optimum initial temperature of the heat treatment, the

smallest sized precrystal needed for complete growth should be determined. To find this critical size, the distribution of precrystal sizes could be integrated from the maximum precrystal size towards the minimum precrystal size. The lower limit on the integration which is needed to yield the predetermined number of nuclei per volume corresponds to the critical sized precrystal. The optimum heat treatment schedule should be designed to maximize the growth rate of the smallest of the crystals which must be grown to a mature microstructural state. The finer the desired final microstructure, the more precrystal sites that will be needed. This is shown schematically in Figure 5.1.

The form of an optimum heat treatment schedule is one of a smoothly increasing slope. The size of the smallest precrystal which is needed to produce the desired microstructure determines the initial temperature at which to begin the optimum heat treatment schedule. The smaller the needed precrystal, the lower the temperature which must initiate the optimum heat treatment. For a small nucleus (small precrystal size), both the temperature for stability and the temperature for the maximum growth rate are low. The corresponding growth rate is, therefore, low. These conditions produce a region of small positive slope on the optimum heat treatment schedule at that low temperature. On the other hand, for large crystals the temperature for the maximum growth rate and the corresponding growth rate are both high. These conditions produce a region of large positive slope on the optimum heat treatment schedule at that high temperature. Figure 5.2 depicts this concept graphically.

5.3: Objective Two : Experimental Support of Precrystal Approach

5.3.1: Crystal Size Histogram

The notion of precrystal distributions existing in the unheat-treated glass and controlling the crystallization process suggests that the crystallization process depends primarily on nonhomogeneous nucleation sites. For the lithium disilicate system, this is contrary to the results of previously published studies.[52-54] It is traditionally believed that homogeneous nucleation dominates the crystallization of this system. To investigate the significance of homogeneous nucleation versus precrystal site nucleation, lithium disilicate samples were given isothermal heat treatments at a temperature (470°C) known to be in the traditional nucleation region.

The crystal size distribution which results from this heat treatment can be related to the dominant nucleation mechanism. If homogeneous nucleation was contributing significantly to the crystallization of lithium disilicate the observed size distribution should cover a broad range of sizes. Aside from the largest crystals, which are related to heterogeneous nucleation from controlled impurity sites, the frequency of crystals in each size group should be approximately equal if homogeneous nucleation is active. Such a microstructure would result from continuous homogeneous nucleation during the heat treatment since all of the heat treatment occurred in the nucleation temperature range. The only foreseeable decrease in frequency would be for the smaller sized crystals. This

would be due to the decrease in available (uncrystallized) glass as crystallization proceeds. The decrease in crystal frequency as a function of size should be directly proportional to the volume fraction crystallized at the time of nucleation.

If fewer small sized crystals are observed than can be explained by the decrease in available glass, the notion of precrystal sites dominating the development of the glass-ceramic microstructure is a possible alternative approach. If the vast majority of growth sites which result in mature crystals originate from sites inherent in the glass, the entire nuclei population begins growing at the onset of the heat treatment. There should exist a broad range of growth rates amongst the crystals due to a range of growing crystal sizes, but no significant number of new nuclei should develop outside of this initial population. The initial lower boundary of the active precrystal distribution will depend upon the isothermal temperature. The smallest active precrystal site is equivalent to the critical size crystal which is just thermodynamically stable at that temperature. The assumption is made that the temperatures used for the heat treatment are low enough such that the growth rate difference between the extremes in the crystal size distribution allows for the smaller growth sites to grow to observable size before the larger (faster growing) crystals dominate the microstructure and consume all the available glass. If this assumption is valid, then there should exist a crystal size below which no crystals exist. Figure 5.3 depicts this concept schematically.

To test this idea, air cooled lithium disilicate glass droplets

were heat treated isothermally at 470°C until the microstructure was partially crystallized (60%). The sample was not heat treated to 100% crystallization to facilitate more accurate measurement of crystal sizes. The samples were cut cross-sectionally, polished through 1 μm-grit alumina, etched with a 5% HF solution, sputter coated with Au-Pd alloy, and photographed via an SEM. The crystal size data collected from these micrographs is shown in histogram form in Figure 5.4. It is important to note that the resolution of the SEM instrument is far above that which is needed to image the smallest crystal size recorded. This means that the lack of smaller sized crystals is actually a material property and not an artifact of the imaging instrument. The shape of the histogram does not show the uniform size distribution which would be expected from a continuously operating homogeneous nucleation mechanism. The histogram shape is similar to that which is predicted if the precrystal site approach was dominant. Therefore, this data tends to support the idea of a set precrystal population that controls the developed microstructure as opposed to viewpoint of a traditional homogeneous nucleation mechanism.

5.3.2: Comparison Between a Simulation of Homogeneous Nucleation and Experimental Data

To explore further the viability of the precrystal viewpoint, a computer model was developed to simulate the evolution of a glass-ceramic microstructure assuming that the material obeyed the guidelines for classical homogeneous nucleation. The simulation program is listed in Appendix B. The model can be compared to experimentally measured data and conclusions can be drawn as to

the validity of the homogeneous nucleation approach for this material.

The experimental data were generated using a series of lithium disilicate (glass) discs which were all cut from the same glass rod. These discs were heat treated isothermally at 470°C and periodically individual discs were removed from the oven in order to evaluate the effect of time at temperature for the evolving microstructure. The heat treatment temperature of 470°C was selected because previous work has shown it to be close to the temperature associated with what is traditionally termed the maximum nucleation rate. After removal, the discs were allowed to cool rapidly in air. Cross-sectional micrographs were made from the discs after polishing through 1 μm alumina abrasive and etching with 5% HF. The standard stereological method of counting the number of points on a micrograph where intersecting lines from a superimposed transparent grid coincide with the location of the crystalline phase was used to determine experimental volume fraction crystallized.[55] The number of crystals observed per micrograph were used to calculate the crystal population density data. Six counts of the number of homogeneous crystals per area and six stereological measurements of the volume fraction crystallized were made for each experimental time at 470°C .

For the experimentally collected data, it was important to discriminate between spherulitic crystals which were nucleated at sites typically considered homogeneous sites versus crystals which began to grow from the surface of pre-existing lithium disilicate crystals. It is proposed that a precrystal site which is smaller than

the critical precrystal size for the temperature of the heat treatment could become active because of the presence of the glass/crystal interface from a growing adjacent crystal. For a crystal to be created in such a manner, the maximum growth direction for the new crystal should be close to perpendicular to the maximum growth direction for the parent crystal. All of the experimental data collected for this test of the homogeneous nucleation theory was based on crystal counts of homogeneous crystals. Crystals which showed evidence of growth originating from the surface of another crystal were not counted.

The computer model uses a steady-state nucleation rate which is constant with respect to the amount of available, uncrystallized glass. Therefore, as the volume fraction of glass crystallized increases, the corresponding nucleation rate decreases for a nucleation rate which is defined in terms of the number of nuclei generated for the time per total material volume. The initial steady-state nucleation rate used was taken from experimental data generated by optically counting the number of crystals per cross-sectional area on lithium disilicate samples heat treated for a series of times at a temperature of 470°C. The location of nucleation events is assumed in the simulation program to be completely random. This is consistent with a system which is nucleating homogeneously. The nucleation rate is used to generate a given number of growing crystals per volume for each iteration of the program. Each iteration of the program represents a set amount of time. These nucleated sites are then simulated to grow at a constant growth rate which has been ascribed to be that seen

experimentally for bulk sized crystals at 470°C. As new growth sites are generated for each program iteration, the pre-existing crystals grow a set amount. The overlap from adjacent growing crystals is taken into consideration by using Avarami's equation for the growth of a system of randomly located spheres.[56] The program counts a simulated crystal when that crystal grows to a diameter greater than 1 μm. The 1 μm size limit represents the approximate minimum crystal size which was reliably observed during the experimental portion of this work. The experimental observations were made using an optical microscope at 400X magnification.

Comparisons were made between the experimentally generated data and the homogeneous nucleation simulated data by way of crystal volume fraction versus time at 470°C (Figure 5.5) and crystal population density versus time at 470°C (Figure 5.6). Points representing plus and minus one standard deviation of the experimental data are shown in Figures 5.5 and 5.6. The maximum crystal volume fraction used for the experimental samples was approximately 20%. For samples with greater than this percent crystallization, differentiation between homogeneously nucleated crystals and those nucleated from pre-existing crystal surfaces is uncertain. The model simulated crystal volume fraction is seen to match well with the experimentally measured values. This is a good indication that the parameters used in the simulation are reasonable in comparison to the actual experiment.

Comparison of the experimental and simulated crystal population densities shows an equivalent initial linear portion and largely dissimilar saturation values. The simulation based on

homogeneous nucleation conditions predicts a saturation value almost twice as large as the experimentally measured value. Not only is the magnitude of the saturation different between the simulation and the experiment, but the abruptness of the transition differs as well. The simulation predicts a transition to saturation by way of a gradual flattening out of the curve. The experimentally measured transition occurred much more abruptly than that predicted by the simulation.

Differences between the simulation and experimental data point toward a mechanism dominating the lithium disilicate system which does not follow the same guidelines as a homogeneously nucleated system would. However, the observed experimental data could be explained by the precrystal site distribution approach hypothesized previously. The precrystal theory also can account for the observed histograph data.

5.3.3: Cooling Rate Effects on Crystal Population Density

A third test was developed to evaluate further the credibility of the precrystal theory. According to traditional homogeneous nucleation theory, a sample cooled slowly from the melting temperature to below the glass transition temperature should develop a higher crystal population density, upon further heat treatment, than an equivalent sample which was cooled rapidly. This is because the slowly cooled sample spends a significantly longer time within the temperature region where nucleation is thought to occur rapidly. These nucleation sites initiated during cooling are responsible for the finer microstructure produced when the slowly

cooled sample is subsequently heat treated.

On the other hand, according to the precrystal theory, a sample cooled rapidly should freeze-in a larger population of defect structures than a sample cooled more slowly. Since at elevated temperatures the strained configurations will more readily transform to the lower energy crystalline structure, the higher population of strained sites should generate a higher population of precrystal sites. Therefore, from this theory, the more rapidly cooled samples will develop a finer microstructure than the slowly cooled samples. Because the homogeneous nucleation theory and the precrystal theory predict opposing results as a function of the cooling rate of the sample, this test should help tell which mechanism is more significant in the lithium disilicate system.

For both sample groups, lithium disilicate frit was melted at 1300°C for 24 hours and cast at 1350°C. For the fast cooled samples, the glass was cast onto a chilled metal block and another chilled metal block was immediately placed on top of the glass. Thermal shock usually occurred, but most of the resulting pieces were large enough to be useful. For the slowly cooled samples, the glass was cast into a metal mold. The mold was inside an oven and both the mold and the oven were equilibrated at a constant temperature of 600°C. Once the molten glass was cast into the hot mold, the oven was closed and cooled at a rate of 2°C/min to room temperature. Fast and slow cooled samples were then heat treated at 470°C for a series of times up to a maximum heat treatment time of 509 hours. Microstructural data was recorded in terms of the number of observable crystals per cross-sectional area. The

micrographs were made using the same techniques described previously; cut, polish, etch with dilute HF, sputter-coat with Au/Pd (optional step), photograph at 400X magnification. Six stereological measurements were made for each time for each cooling rate. The mean of the data, plus one standard deviation, and minus one standard deviation are shown in Figure 5.7.

The data in Figure 5.7 clearly shows the effect of cooling rate on the subsequent development of the crystalline microstructure. The fast cooled material developed crystals at a more rapid rate and saturated at a greater magnitude than did the slower cooled material. This data supports the idea that the precrystal theory has a greater application to the development of lithium disilicate microstructure than does the homogeneous nucleation theory. Applying the precrystal theory to explain the observed data, the increased number of crystals that developed for the more rapidly cooled sample during the earlier portion of the experiment can be attributed to larger defects or strained regions in the glass surrounding foreign particles due to thermal contraction mismatches. The faster cooled material does not allow for as much viscous rearrangements of the glass structure to accommodate these strains produced by the coefficient mismatches. These regions would most likely represent precrystals of rather large sizes and would therefore develop into observable crystals relatively early during the isothermal heat treatment. The continued larger number of crystals seen at the longer isothermal times associated with the faster cooled material can be attributed to the effect of the increased cooling rate on the number density of strained defect

structures in the glass. Such precrystal sites would tend to be associated with smaller sized precrystals and would therefore not produce observable crystals until later in the isothermal heat treatment. The saturation value for the crystal population density was greater for the faster cooled material compared to the slower cooled material. This shows that the increase in the cooling rate produced a glass with a larger total population of precrystal sites. It is interesting to note that both glasses (fast cooled and slow cooled) reached their respected population density saturation values at approximately the same time. This is predicted by the precrystal theory because even though the variation in cooling rate changes the population distribution of precrystal sites, it is the isothermal temperature which determines the smallest precrystal site which will eventually grow to a mature crystal. Therefore the time required for this smallest size to become observable is not influenced by the change in the precrystal distribution, only the number of these eventual crystals is changed.

5.3.4: Raman and FTIR Spectroscopy of Fast and Slow Cooled Samples

During the previous discussion, the effect of an increased cooling rate on the precrystal distribution was attributed to an increase in the strained defect structures in the glass. In an attempt to support this concept, Fourier transform infrared spectroscopy (FTIR) and Raman spectroscopy were used to investigate if the cooling rate variations used in the experiment significantly affected the amount of strained bonds in the glass structure. Sample material was used which had been produced simultaneously with that

material which was used to generate the crystal population density versus time data.

Infrared spectroscopy is based on the absorbence of photons due to their coupling with dipoles, in the sample material, associated with atom vibrations.[57] The change in intensity of the photon source, measured in transmission or in reflectance, as a function of frequency, characterizes the bonds present in the sample material. Photons for FTIR are generated from a polychromatic light at infrared wavelengths.

The FTIR spectra generated by the fast cooled and the slowly cooled samples differed substantially in the location of the peak associated with the vibration of the three dimensional silicate structure (Figure 5.8). The location of this peak is in the range of 1060 - 1190 cm^{-1}.[58] Galeener[58] associates this peak with the high frequency, out-of-phase, bending or asymmetric stretching motion of the silicon and oxygen atoms. The oxygen atom is thought to vibrate along a path parallel to a line which would connect the two adjacent silicon atoms (Figure 5.9). This high frequency oscillation is thought to occur when the angle between silica tetrahedra exceeds 112°.[59] The fast cooled sample generated this peak at a wavenumber 30 cm^{-1} higher than did the slow cooled sample for this atomic motion. The higher wavenumber is associated with, on average, a higher bond strain. An increased bond strain results from atoms being located with increasing displacement from their preferred, lower energy locations.

Raman spectroscopy is based on the frequency shift of scattered light, relative to the incident light frequency, caused by

its coupling to vibrational modes in the material through the nonlinear polarizability associated with these modes.[60] The incident light is typically in the visible spectrum and is generated by a narrow-band laser source.

Raman spectroscopy was performed on the fast and slow cooled lithium disilicate samples (Figures 5.10 and 5.11). The initial reason for using of Raman spectroscopy was to measure the alteration in the three-member defect ring structures as a result of the increased cooling rate. In silica, the three-member ring structure produces a Raman peak at a wavenumber of 600 cm^{-1}. These structures were not detected in the spectra. The reason for their absence are that the high concentration of alkali atoms prevented their formation or the broad, lithia-related Raman peak at 600 cm^{-1} overshadowed what peak may exist.

The spectrum obtained from the slow cooled lithium disilicate sample shows a sharp peak at 520 cm^{-1}. This peak is not present in the fast cooled sample. A Raman spectrum for 100% crystallized lithium disilicate is shown in Figure 5.12. The crystalline phase in this sample was confirmed to be lithium disilicate by x-ray diffraction. The peak associated with the crystallized lithium disilicate phase occurs over a range of frequencies from 480 cm^{-1} to 600 cm^{-1} and is centered at 550 cm^{-1}. The peak in the slowly cooled lithium disilicate was assigned to the crystalline lithium disilicate phase. The 30 cm^{-1} deviation between the peak centers for the slow cooled glass and the crystalline phase can be attributed to the very small size and number of the crystals in the glass. In the crystalline sample, the spectra were generated from all orientations

of the crystalline phase while only a limited number of orientations would be detected for the glass sample. The shift in the crystallization peak is thought to be a result of the difference in the number of crystal orientations sampled for the two materials. Optical micrographs of the slowly cooled sample were made to see if the crystals were observable. No evidence of crystallization could be seen optically. Therefore, it is concluded that the size of the crystals is below approximately 1 μm.

5.3.5: Density Measurements of Fast Cooled Glass, Slow Cooled Glass, and Crystallized Glass

To better correlate the effect of the different glass cooling rates on the crystallization of the glass, density measurements were made on the two glasses and the crystallized glass. Archimedes' method was used for the density determination of the glasses. This method involved weighting the samples in air and while suspended in water. The difference between the two measurements is equivalent to the force buoying the water suspended sample which is proportional to the volume of the sample. Helium pycnometry on a finely powdered sample was used for the density determination of the crystalline phase. This technique was necessary because of internal void space within the bulk piece of crystallized glass. Helium pycnometry is based on the pressure change in a closed cell generated by an unknown volume of material when a known pressure of helium gas is introduced into the same closed cell. As was expected, the density of the fast cooled sample (2.31 g/cm^3) was found to be less than that of the slowly cooled sample (2.37 g/cm^3). The density of the crystalline phase was found

to be 2.45 g/cm^3.

5.3.6: Interpretation of Fast Cooled and Slow Cooled Results

From this data it is possible that the increased bond strain observed in the FTIR spectrum of the fast cooled sample is a result of a certain fraction of atoms being located in atomic positions farther away from their equilibrium positions than in the slowly cooled sample. This would explain the lower density but would not explain the increased tendency towards crystallization. Rather, because the glass density would be even further away from the density of the crystalline phase, crystallization of the fast cooled glass should be retarded because of the increased strain due to the larger volume change generated upon crystallization. This was not observed experimentally.

The observed FTIR peak shift might also be attributed to the addition of the crystalline phase's bond vibrations to the spectrum of the slowly cooled glass. A FTIR spectrum from the crystalline lithium disilicate phase is shown in Figure 5.13. It can be seen that if the FTIR spectrum from the slowly cooled sample was being influenced by the signal generated from lithium disilicate crystals, there should be evidence of this influence in the form of sharp peaks at wavenumbers such as 770 cm^{-1} and 640 cm^{-1}. Because no peaks are seen at these wavenumbers and, in fact, no difference is seen between the slow and fast cooled glasses at these wavenumbers, the shift in the peak located at 1100 cm^{-1} is not thought to be caused by the influence of lithium disilicate crystals in the slowly cooled glass.

A third possibility is that the lower density of the fast cooled sample is a result of an increased amount of free volume within the glass structure.[61] The free volume can be thought of as pockets of low density, possibly even voids, within a matrix of average (ie. equilibrium) density. The atomic groups bordering the free volume regions would have atypical vibrational responses and would therefore result in a shifted FTIR peak. These same groups would also have a greater degree of freedom (rotational and translational) as compared to equivalent groups with an average density environment. The free volume of boardering groups could be thought of as existing in a lower viscosity environment and therefore their likelihood of transition to the crystalline phase would be increased. The free volume theory is the only approach which can explain both the increased crystal population density seen experimentally and the shifted FTIR peak.

5.4 : Objective Three : Experimental Generation of Precrystal Distribution Maps

5.4.1: Introduction

It is desirable to have a map of the precrystal density as a function of precrystal size for developing a heat treatment schedule for a given glass. Precrystal maps were generated for bulk crystallization lithium disilicate and bulk crystallization lithium disilicate with heterogeneous additions.

5.4.2: Materials and Methods

The lithium disilicate glass (33.3 mole percent Li_2O , 66.4

mole percent SiO_2) was supplied by Specialty Glass Inc., Oldsmar, Florida. The glass was received in the form of ground frit. The glass was assayed for purity and compositional accuracy by Corning Glassworks Laboratories, Corning, New York. The results are shown in Table 5.1.

To produce the glasses which had additional heterogeneous agents incorporated in the glass, the lithium disilicate frit was ball milled for approximately 10 hours with the appropriate additions (Pt, Ce, Fe and Ag). All of the heterogeneous agents were added to the glass as nitrides or chlorides. The uniformity in appearance on both a macroscopic level and on a microscopic level suggests adequate mixing of the heterogeneous agents was achieved .

All glasses were melted in a platinum crucible covered with a platinum lid. According to James,[62] the amount of platinum that the glass inadvertently obtains from the crucible during melting is insignificant. Individual batches weighed 100 grams. The glass was melted in an electric furnace under in an air atmosphere for eight hours at 1300°C and then cast at a temperature of 1325°C. The glass was cast onto a chilled steel block. Each sample was in the form of a small semi-spherical button weighing approximately 2.0 grams. The chilled steel and the small sample size were both for the purpose of achieving rapid cooling rates. The rapid cooling rate was necessary to prevent significant amounts of crystal growth during the cooling from melt temperatures. X-ray diffraction analysis of the quenched glass samples revealed no detectable crystalline phases. X-ray parameters of 1000 counts per second at a scan rate of 6°/min were used.

Samples were given isothermal heat treatments in a laboratory box oven at a series of temperatures. The duration of each heat treatment was that which was necessary to obtain 100% crystallization. Heat treatment times varied from several minutes for the highest temperatures used up to several weeks for the lowest temperatures used.

After crystallization was complete, cross-sectional specimens were cut from each sample with a diamond blade saw. The pieces were mounted on polishing stubs with a dental resin. The samples were polished through 0.5-μm grit size alumina. The polished surfaces were etched for approximately 3 seconds with 5% hydrofluoric acid. A series of optical micrographs was taken from each sample so crystals could be counted and crystal densities for each heat treatment could be established.

5.4.3: Results and Discussion

In following the described procedure, data are collected which tells of the total number of stable sites for a given temperature. It is important to note, however, that these measured values are the summations of the number of precrystals which are just stable at the given temperature (critical sized precrystals) and all of the precrystals which have critical sizes associated with higher temperatures than the given temperature being used. To map the density of precrystal sites as a function of their size and/or temperature of critical stability, this original data must be converted to that which represents the number of crystals uniquely for each size as opposed to a summed value. The original data

(density of crystals observed versus isothermal heat treatment temperature) for the pure lithium disilicate glass is shown in Figure 5.14.

A unique precrystal distribution is one in which the number of precrystal sites plotted for a temperature of stability is the number of sites unique for that temperature, as opposed to the measured data which is a summation of the number of sites of that size plus all sites larger than that size. There are two viable methods for converting the measured data displayed in Figure 5.14 to that which represents a unique precrystal size distribution. The two methods differ in that one is a discrete method which assumes that the temperatures at which crystal densities were measured (x-axis data in Figure 5.14) corresponds to all of the possible precrystal sizes that exist in the glass. The other is a continuous method which assumes an infinite number of different precrystal sizes that exist in the glass. The discrete method is the simpler method and involves subtracting the previous precrystal density value from the next precrystal density value of a higher temperature (i.e., larger precrystal size). This method assumes that the difference between precrystal densities for two successive temperatures at which precrystal measurements were made is representative of precrystal sites associated solely with the lower temperature. This method is expected to overestimate the actual precrystal density value for any of the measured temperatures.

The continuous method assumes a continuum of precrystal sizes which corresponds to a continuum of critical temperatures. As diagrammed in Figure 5.15, the experimentally measured data can be

thought of as the integral of the function representative of the unique precrystal distribution. Therefore, to generate the unique precrystal distribution, the first derivative of the experimentally measured precrystal function must be taken in terms of temperature. A simplifying assumption is that the measured function is assumed to be linear between successive temperatures. The continuous precrystal value is taken as the slope (Δcrystal number density/Δstability temperature) of the experimental data. The calculated unique precrystal value is assigned a size which corresponds to the average of the pair of measured temperatures used. Figure 5.16 shows the results of both the discrete and the continuous method.

The true precrystal density curve should be somewhere between that which is predicted by the continuous method and that which is predicted by the discrete method. Approximate calculations show that if the precrystal sizes were limited to those which represented integral numbers of lithium disilicate unit cells, then for the range in critical crystal sizes seen for the experimentally investigated temperature range (470°C to 600°C) there would exist only six discrete precrystal sizes and therefore only six discrete precrystal densities. This is not what is observed experimentally. It is more reasonable to view the distribution of precrystals as discrete but with a very large number of possible precrystal sizes because of an almost infinite number of possible precrystal environments. For example, a precrystal of a certain size could result from a higher than usual density fluctuation in a glass region. The same environment with the addition of a strained atomic

configuration, a local strain or a foreign particle some distance away, would result in a precrystal site of a slightly larger size. The almost infinite variety of environments creates such a large number of discrete conditions as to appear continuous. For this reason the continuous method is assumed to be the closest to reality and will be used to represent the precrystal density distribution as needed for further investigation.

Precrystal density maps can be used to identify the influence of heterogeneous phases on the crystallization of the glass. Both the magnitude of the heterogeneous effect and the relative size of the heterogeneous phase particles can be determined from the precrystal map. The determination of the size is termed relative because an actual particle size is not determined but rather the effective size of the heterogeneous particle, i.e., the size of a crystal which would promote growth at the same maximum temperature as the heterogeneous particle. Information on the size and the population density are critical for the design of an efficient heat treatment schedule. Such a schedule would take full advantage of the fast growth potential of the heterogeneous sites while not wasting additional processing time on the minor microstructural improvements that additional homogeneous sites would provide. Precrystal maps were made using a variety of heterogeneous additions to the base lithium disilicate glass. The heterogeneous additions used were 0.01 mol% $PtCl_3$, 0.3 wt% CeO_2, 0.24 wt% $AgNO_3$, and 0.3 wt% $FeCl_3$. The precrystal maps for the Pt containing glass, the Ag containing glass, the Ce containing glass, the Fe containing glass and the unaltered lithium disilicate glass are shown in Figure

5.17. From these data it can be concluded that only Ag and Pt provide preferred growth sites for lithium disilicate because only Ag and Pt additions yeilded higher crystal populations than crystallization of the unaltered lithium disilicate glass. The Pt sites have a larger effective size than the Ag sites but are fewer in number. The Ag sites initiate stable growth below 600°C.

5.4.4: Conclusion

The generation of a precrystal map for a given glass system is a relatively time consuming process, but its application towards the development of effective heat treatment schedules is significant. A precrystal distribution plot of systems containing heterogeneous phases is also very useful for the determination of the initial heat treatment temperature which most efficiently uses these sites. It should be noted that precrystal distribution plots of a given composition cannot be used generally for that composition because of the influence of thermal history of the glass on the precrystal distribution, as was demonstrated in Section 5.3.3.

5.5: Conclusions

The viewpoint that the final glass-ceramic microstructure originates from elements within the glass matrix which are not homogeneous has been termed the precrystal approach. It has been demonstrated that non-homogeneous elements in the glass mainly determine the number of nuclei and the initial temperature for stability of the nuclei population. Precrystal plots of these potential

growth sites can be constructed. Such plots provide the initial information needed to develop optimum heat treatment schedules for glass-ceramic production.

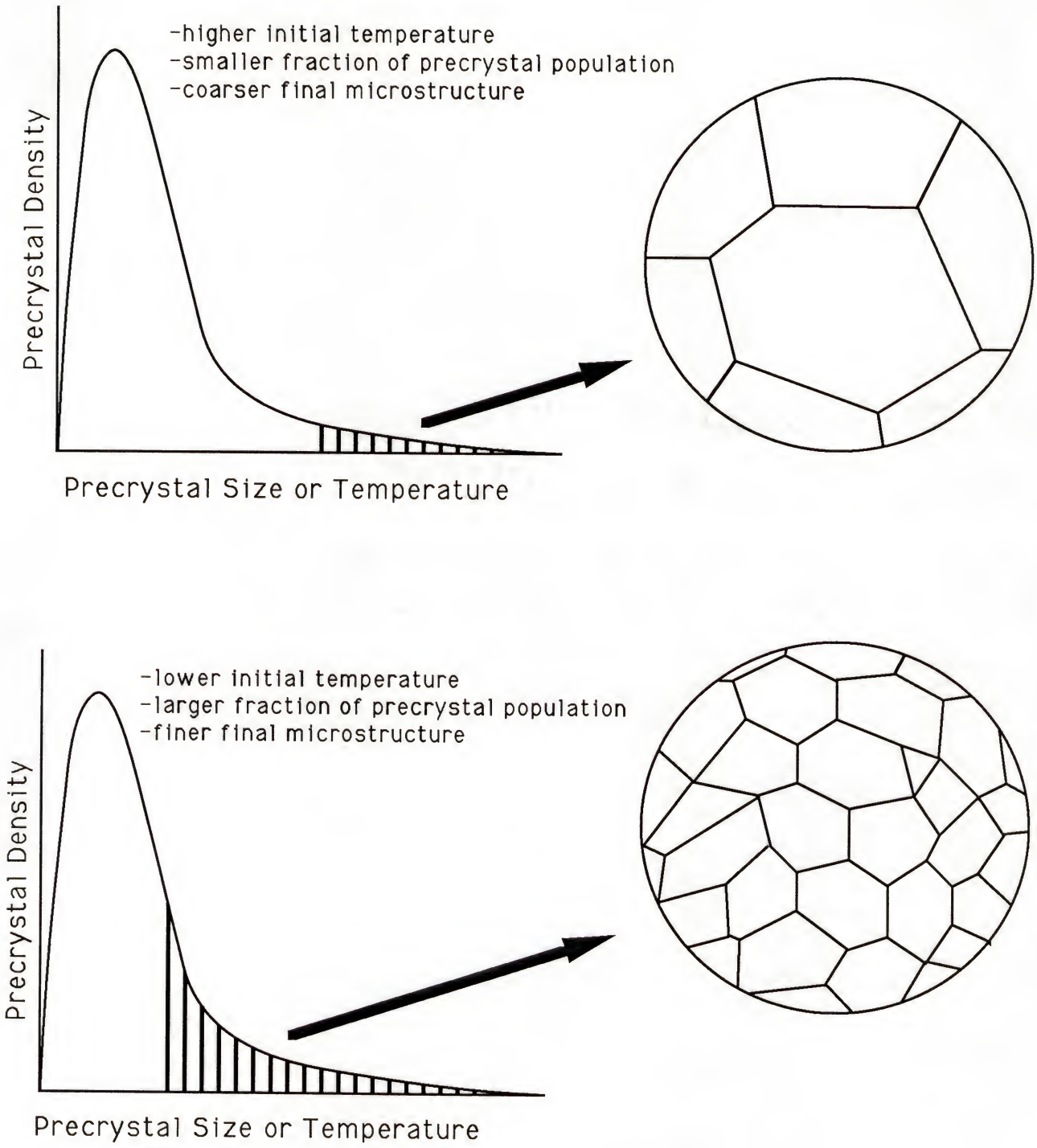

Figure 5.1 : Illustration of the relationship between initial heat treatment temperature and the crystal population density of the final material. The precrystal distribution is the controlling factor in this relationship.

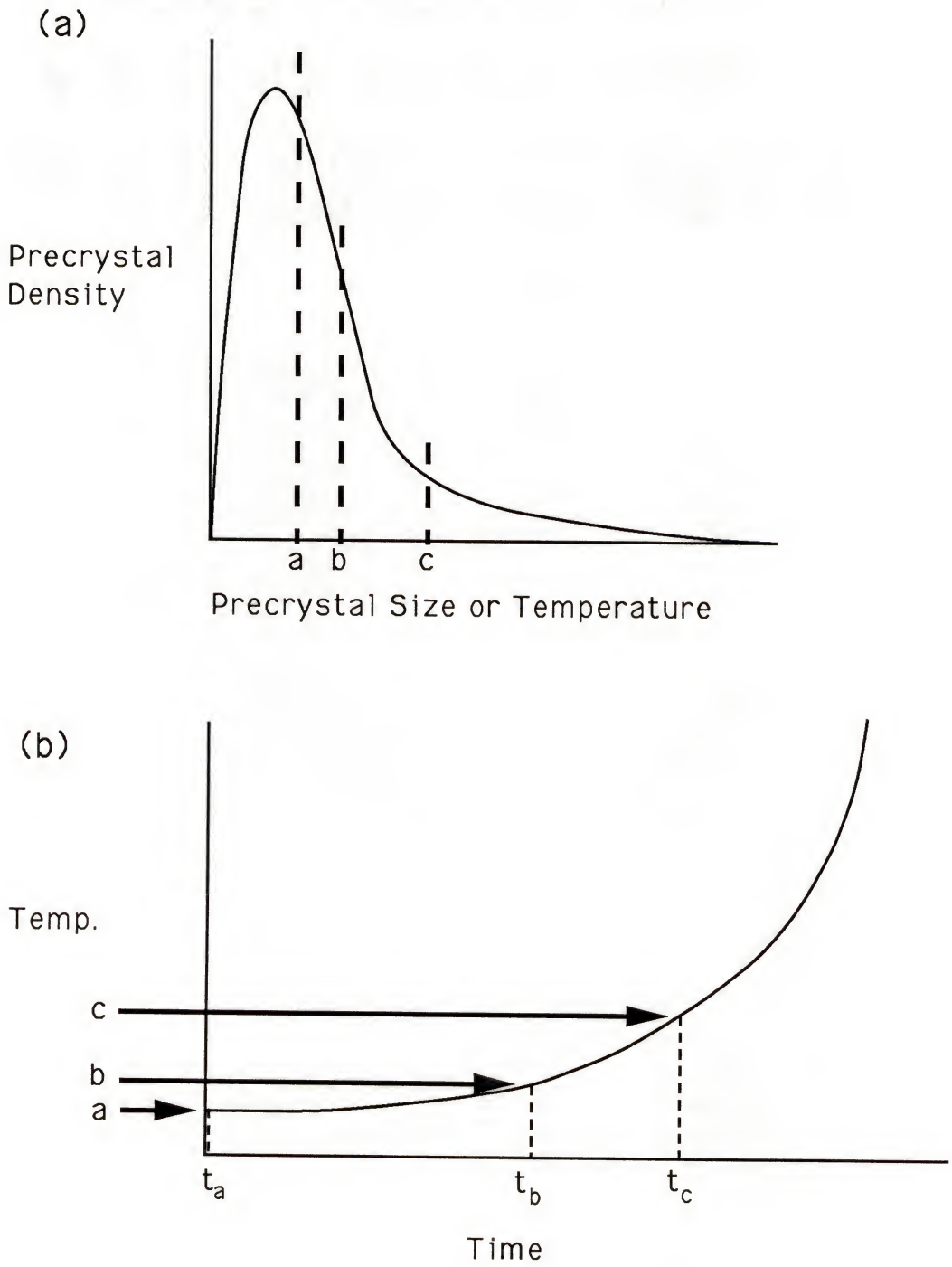

Figure 5.2 : Schematic illustration of the relationship between the smallest precrystal size to be developed and the time needed for the heat treatment: (a) precrystal distribution, (b) heat treatment schedule with corresponding initial temperatures and times.

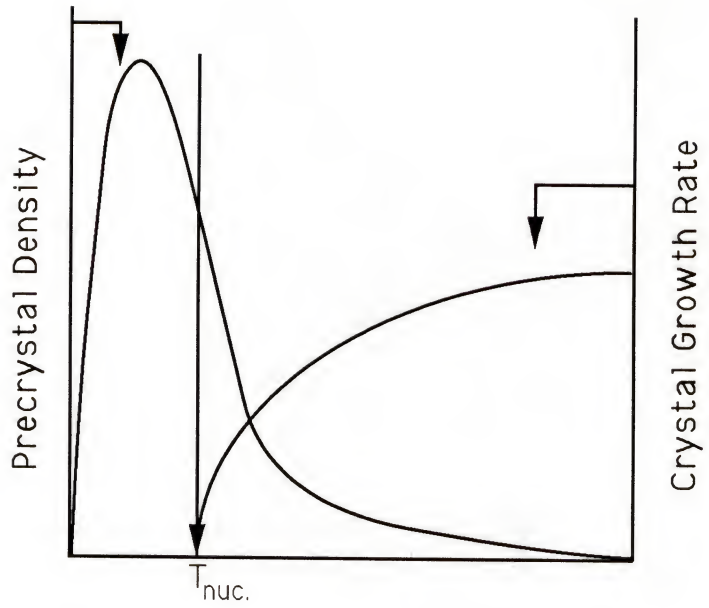

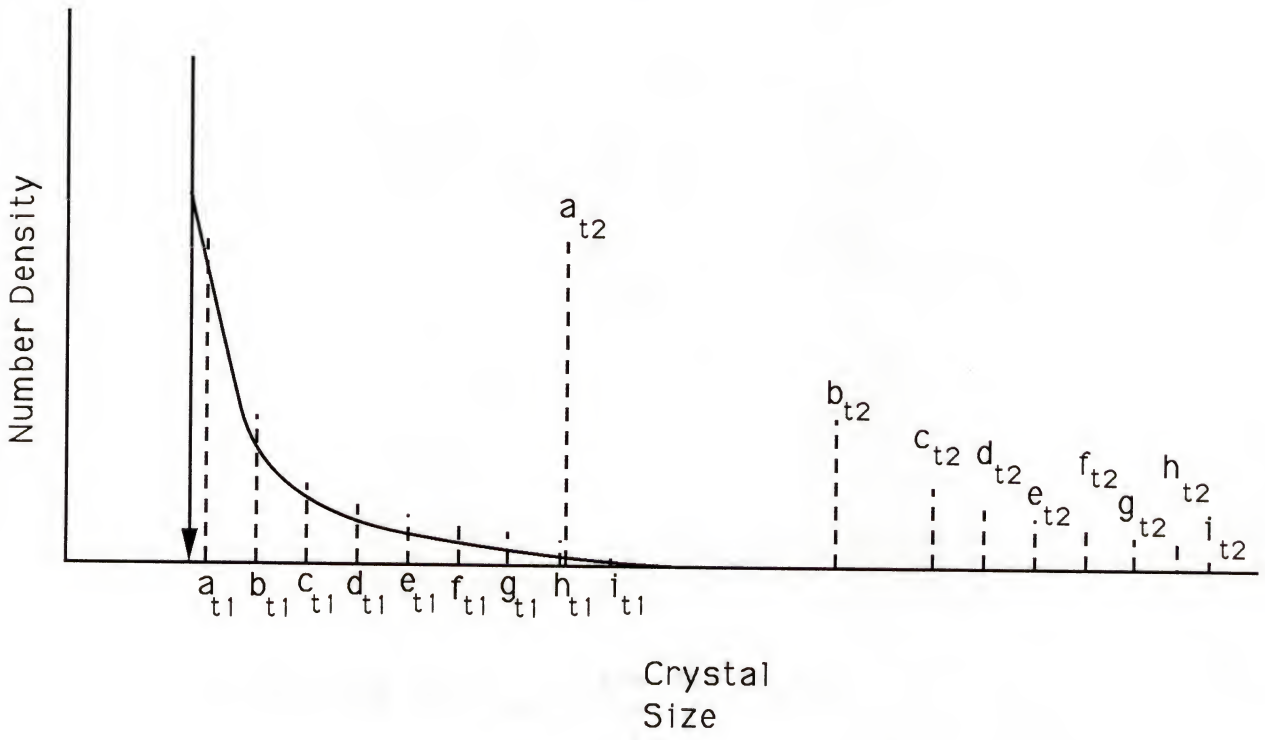

Figure 5.3 : Effect of size dependent growth rate and initial temperature on the macroscopic size of the resulting crystals

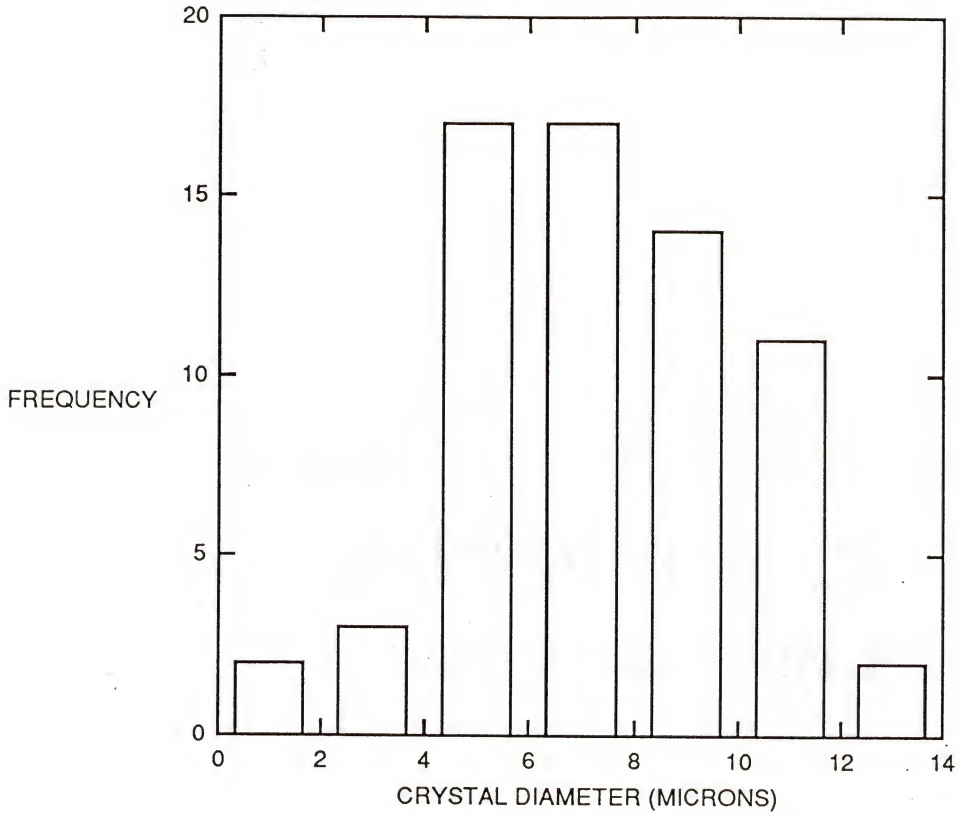

Figure 5.4 : Histogram of the size distribution of lithium disilicate crystals resulting from an extended isothermal heat treatment at the glass nucleation temperature (470°C).

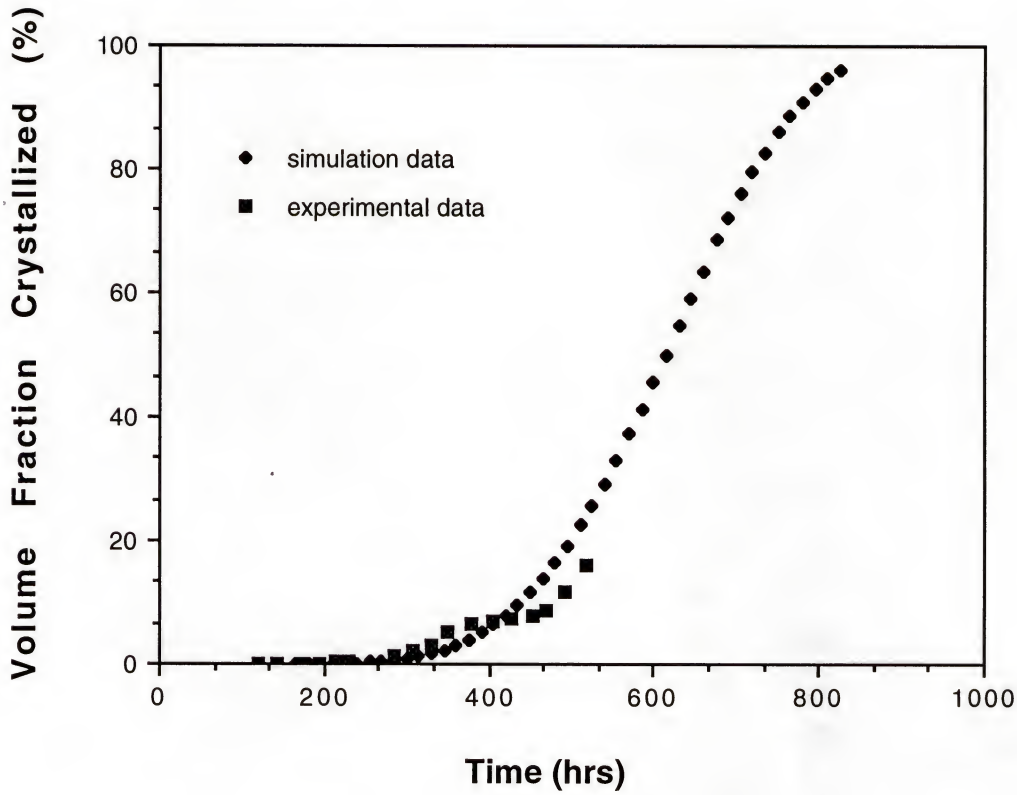

Figure 5.5 : Volume fraction crystallized for lithium disilicate at 470°C as a function of heat treatment time. The plot is a comparison of experimentally collected data and data from the homogeneous nucleation model.

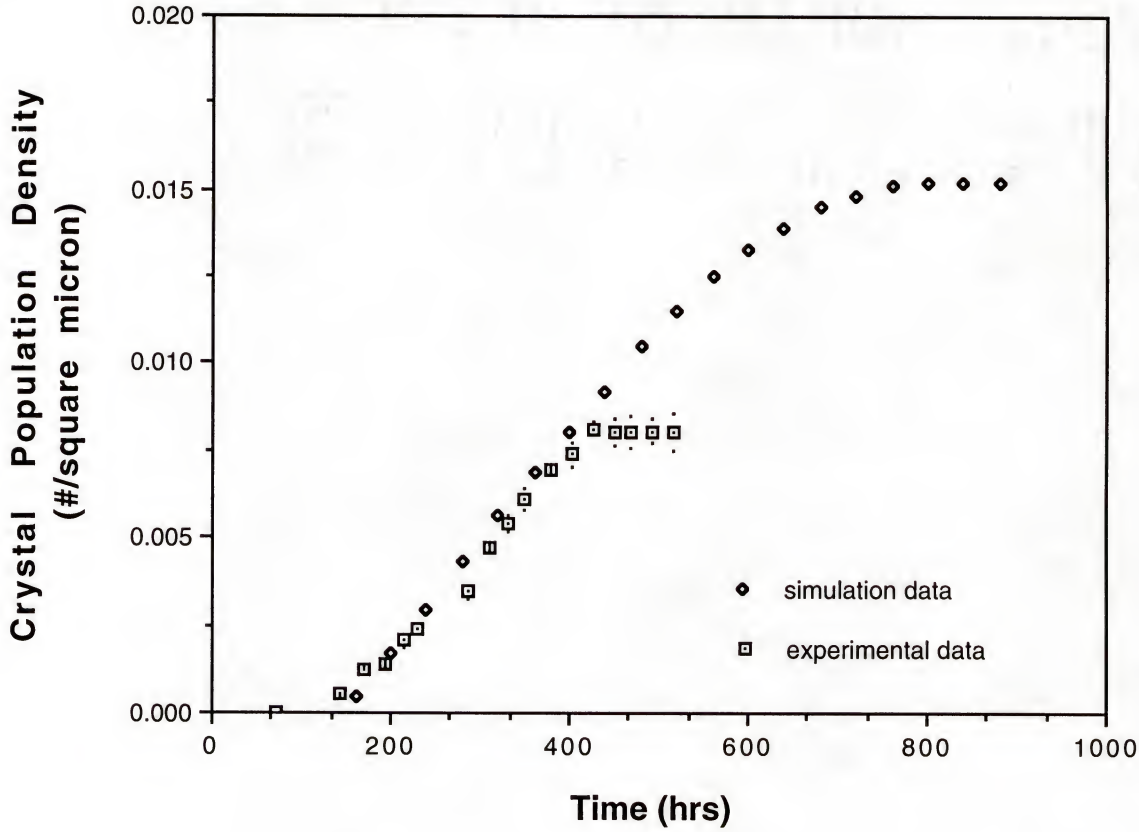

Figure 5.6 : Crystal population density for lithium disilicate at 470°C as a function of heat treatment time. A comparison of experimentally collected data and data from the homogeneous nucleation model.

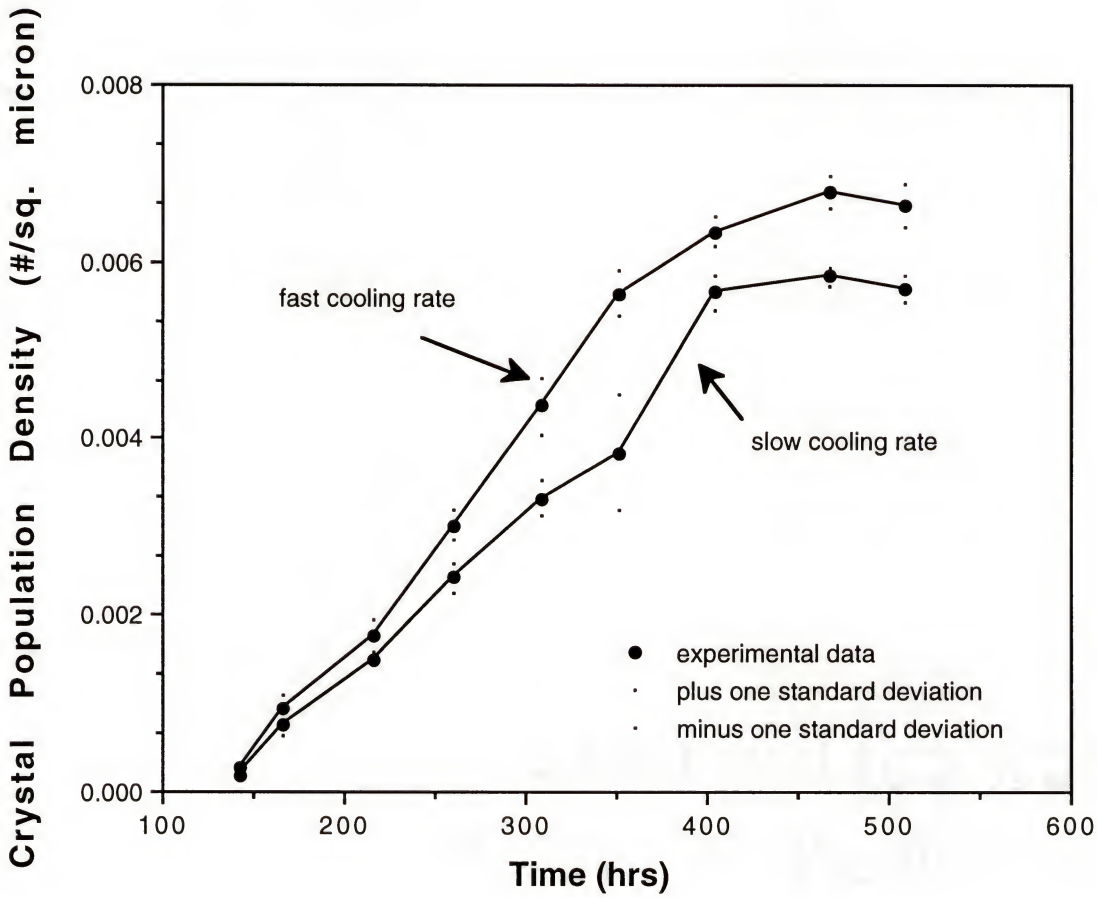

Figure 5.7 : Graph of the population density of lithium disilicate crystals optically observable as a function of time for fast and slow cooled samples. The heat treatment temperature used was 470°C.

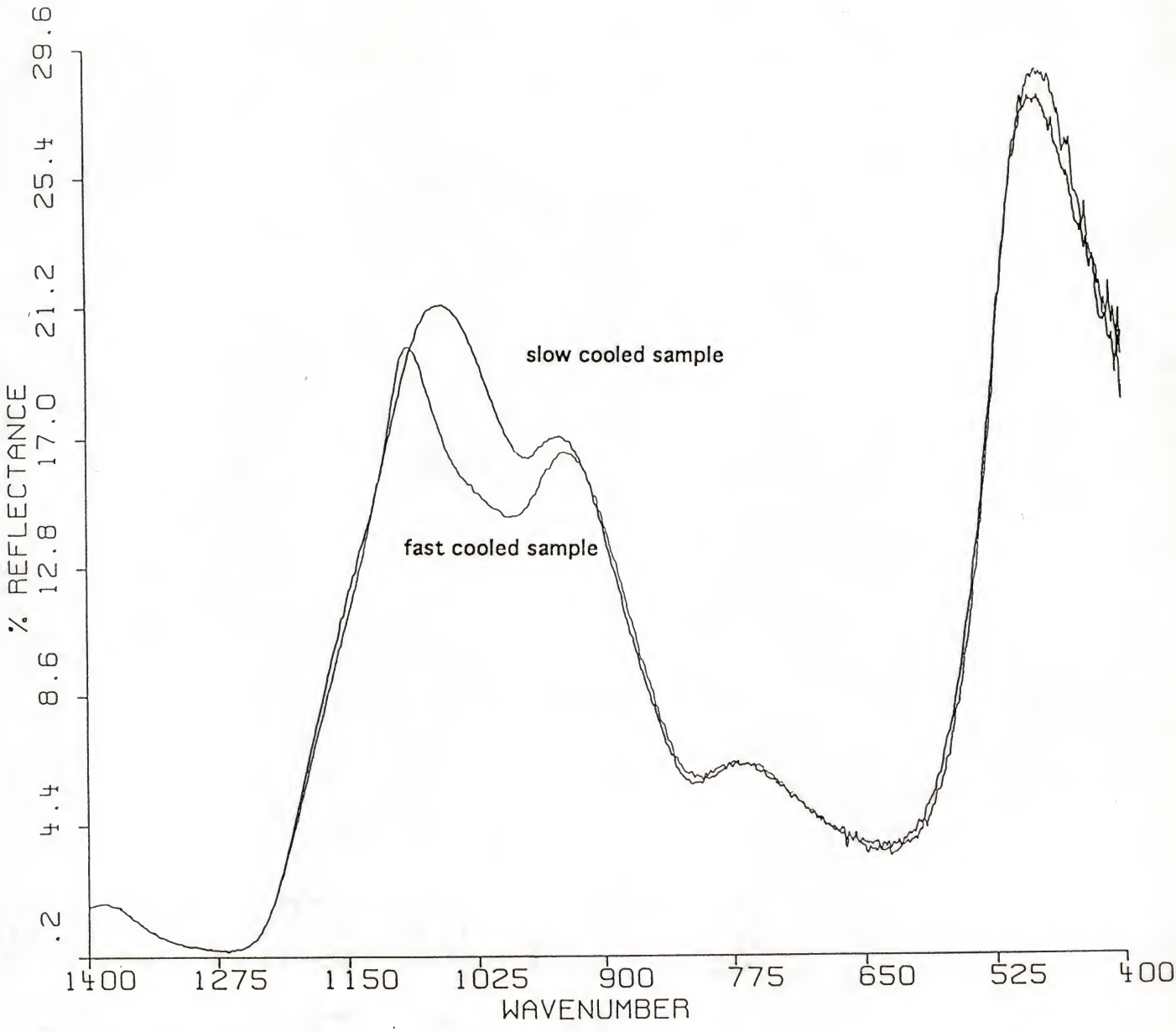

Figure 5.8 : FTIR spectrum from lithium disilicate samples which differ in their cooling rates from the melt temperature. An accelerated cooling rate shifted the peak located at 1050 wavenumber to 1085 wavenumber.

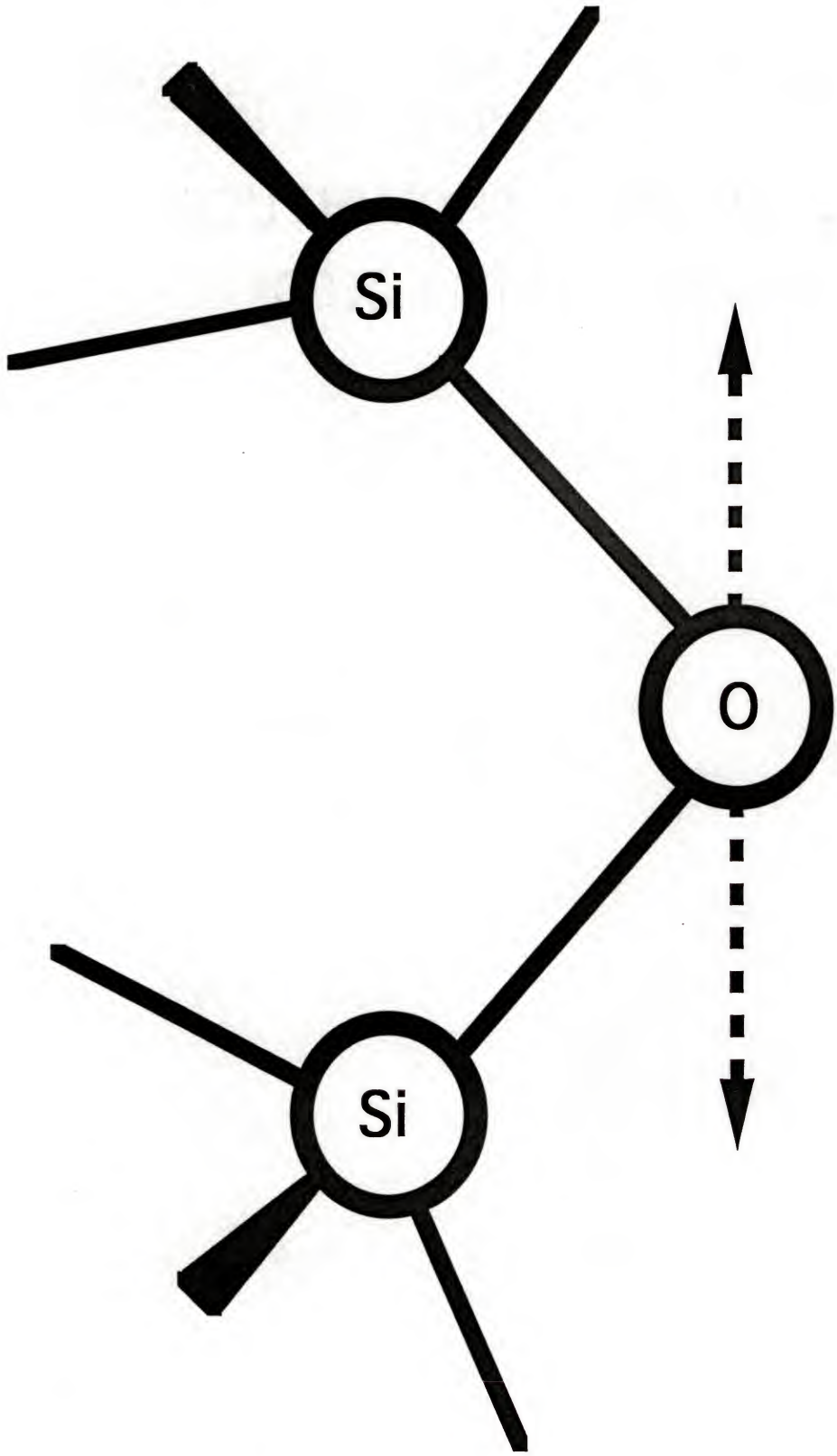

Figure 5.9 : High-frequency vibration thought to produce the FTIR peak located in the range from 1060 cm^{-1} to 1190 cm^{-1}

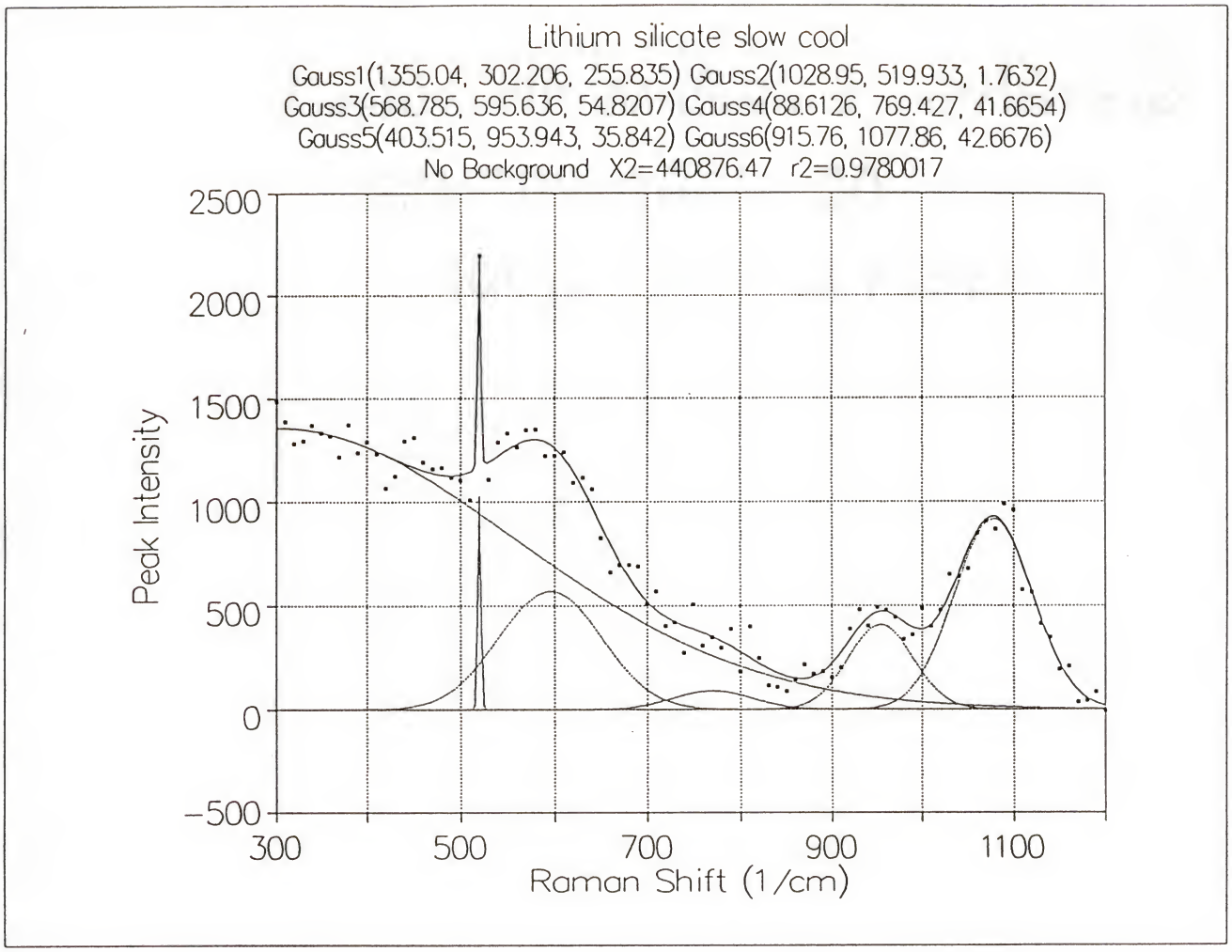

Figure 5.10 : Raman spectrum for lithium disilicate cooled slowly from the melt temperature. The sharp peak detected is due to crystalline structures within the glass.

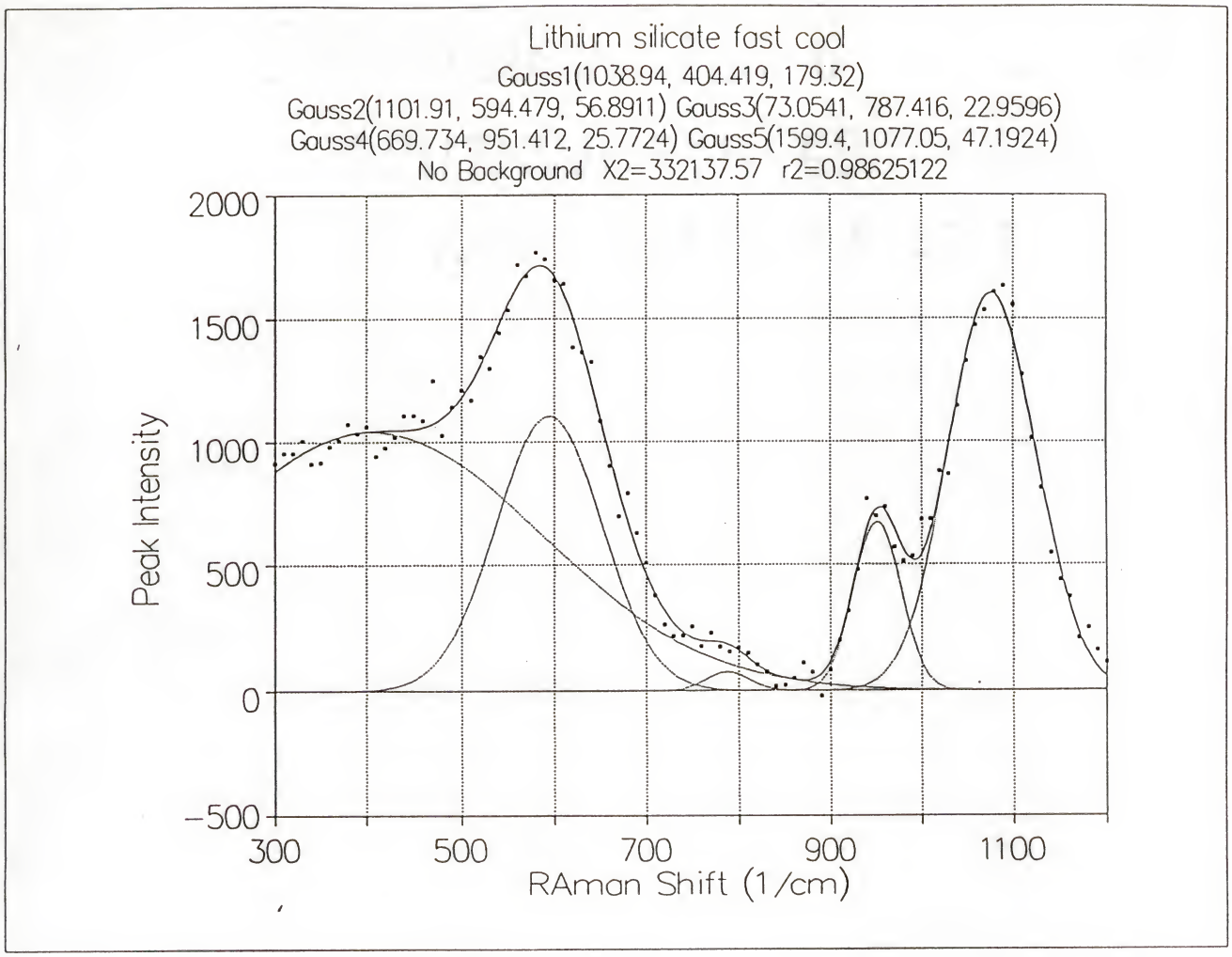

Figure 5.11 : Raman spectrum for lithium disilicate rapidly cooled from the melt temperature. The sharp peak detected in the slow cooled sample is absent from the fast cooled sample.

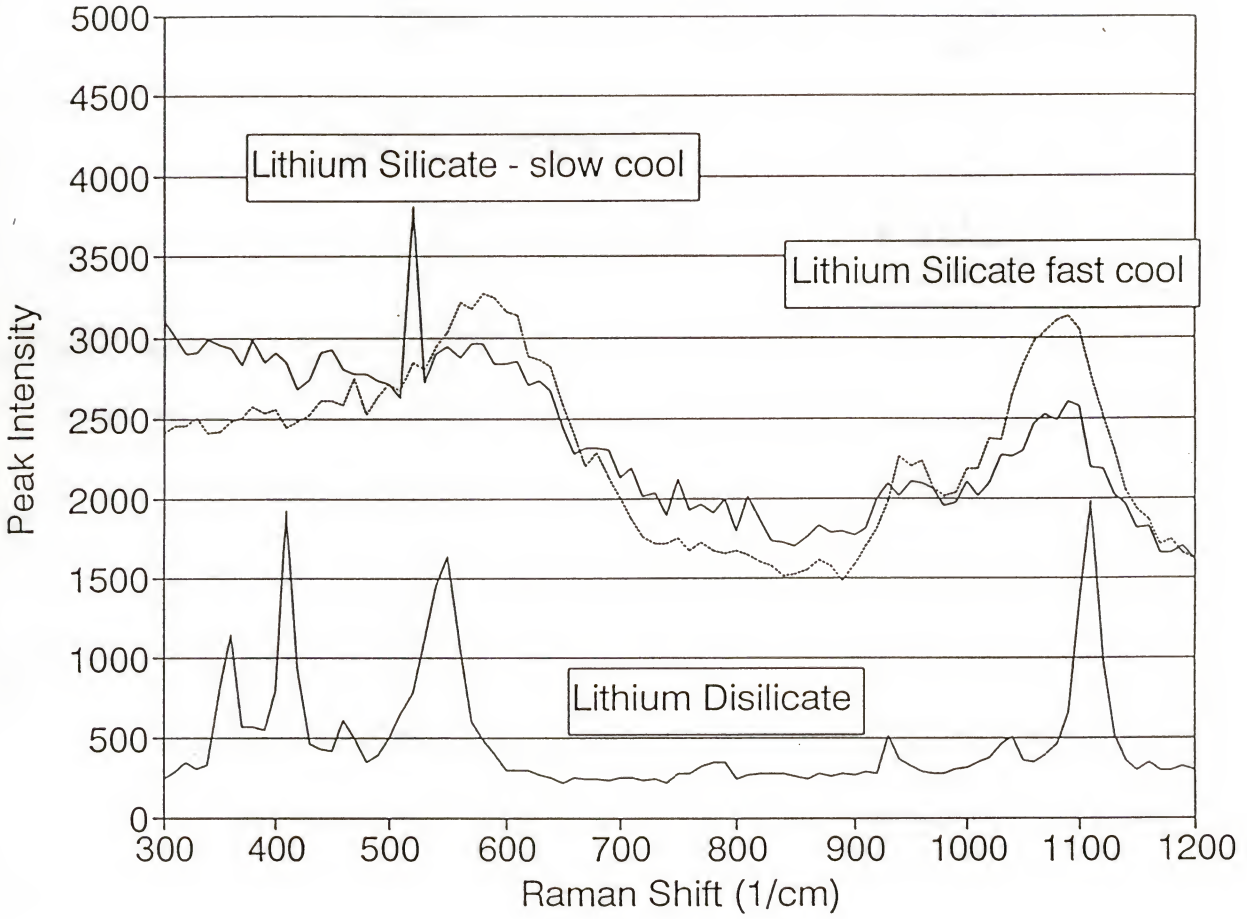

Figure 5.12 : Raman spectra for crystalline lithium disilicate compared to that for the fast and slow cooled samples. The correlation between the peak in the slow cooled sample spectra and the crystalline spectra can be seen.

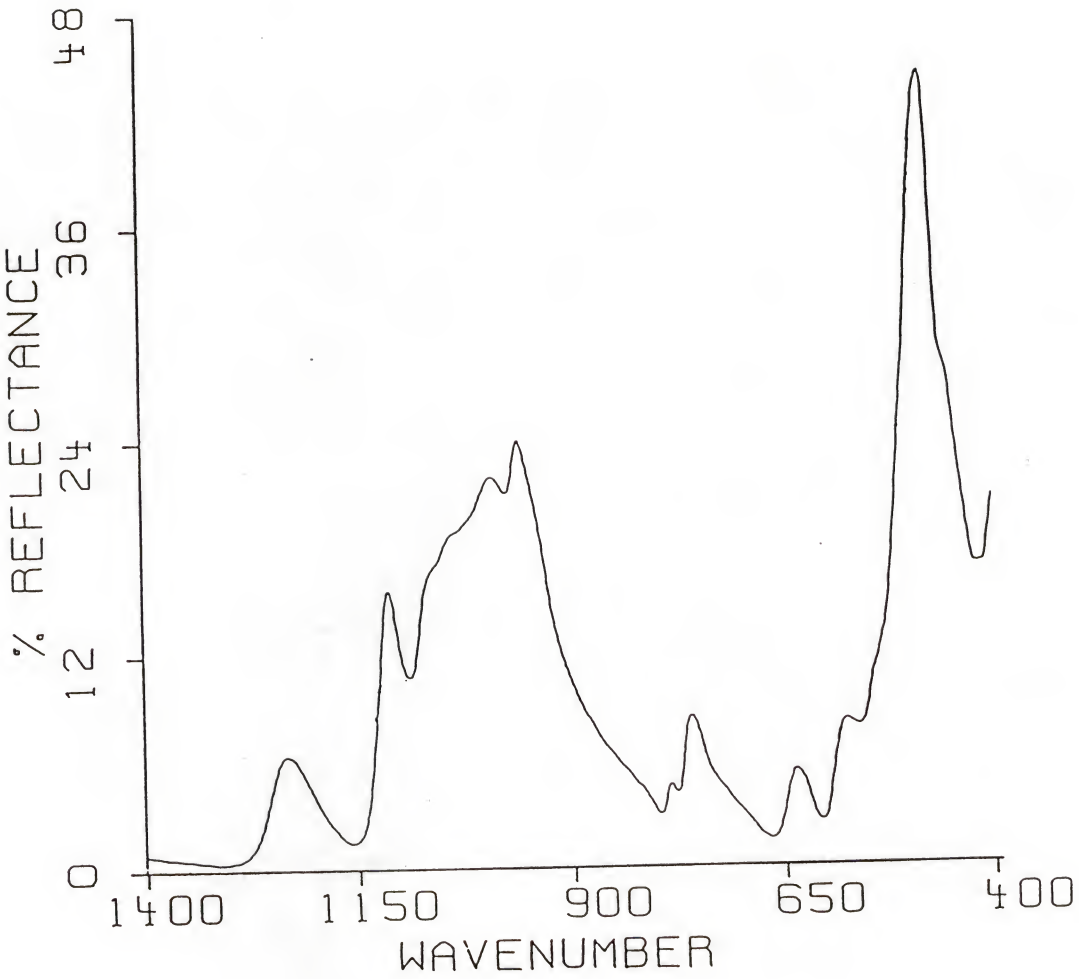

Figure 5.13 : FTIR spectrum from a fully crystallized lithium disilicate bulk sample.

Table 5.1 : Results of analysis on the lithium disilicate glass used for this study. Analysis was performed by Corning Incorporated (Corning, New York).

Quantitative Chemical Analysis

Li2O	33.03 (mol%)
SiO2	66.97 (mol%)

Semi-Quantitative Spectrographic Analysis

Range (wt%)	Element
>30	Si
10-30	Li
3-10	-
1-3	-
.3-1	-
.1-.3	Al+
.03-.1	B , Na+
.01-.03	Ba , Ca , Zn
.003-.01	Mg-
.001-.003	Fe , Sr-
<.001	Cu , Mn , Ti
<.0005	Be

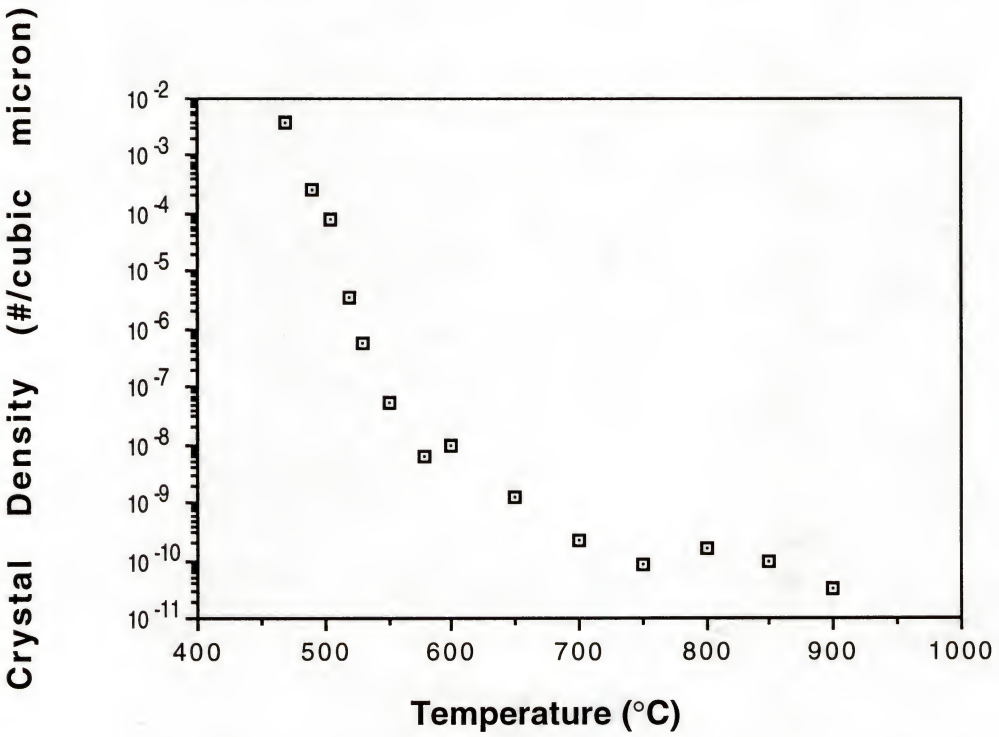

Figure 5.14 : Population density of crystals measured in fully crystallized samples of lithium disilicate as a function of isothermal heat treatment temperature.

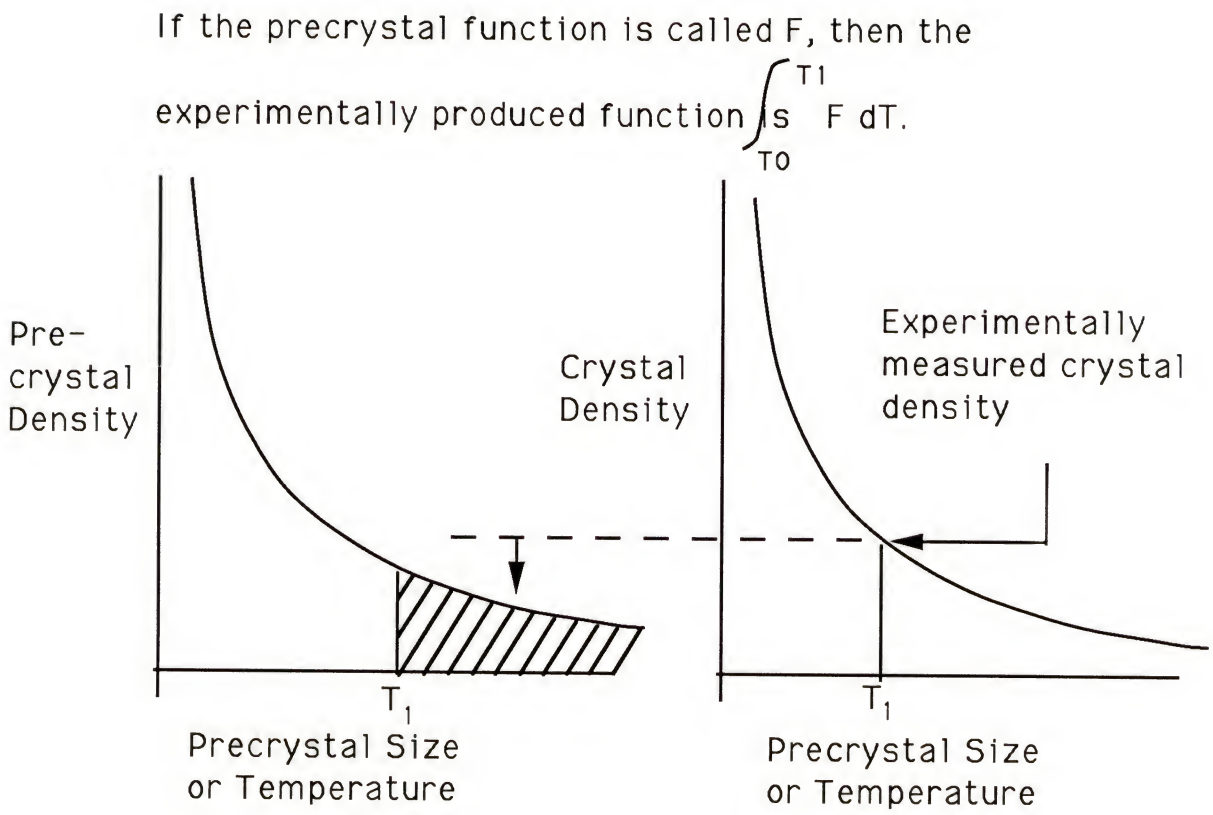

Figure 5.15 : Mathematical relationship between experimentally measured crystal density and the precrystal density as a function of temperature.

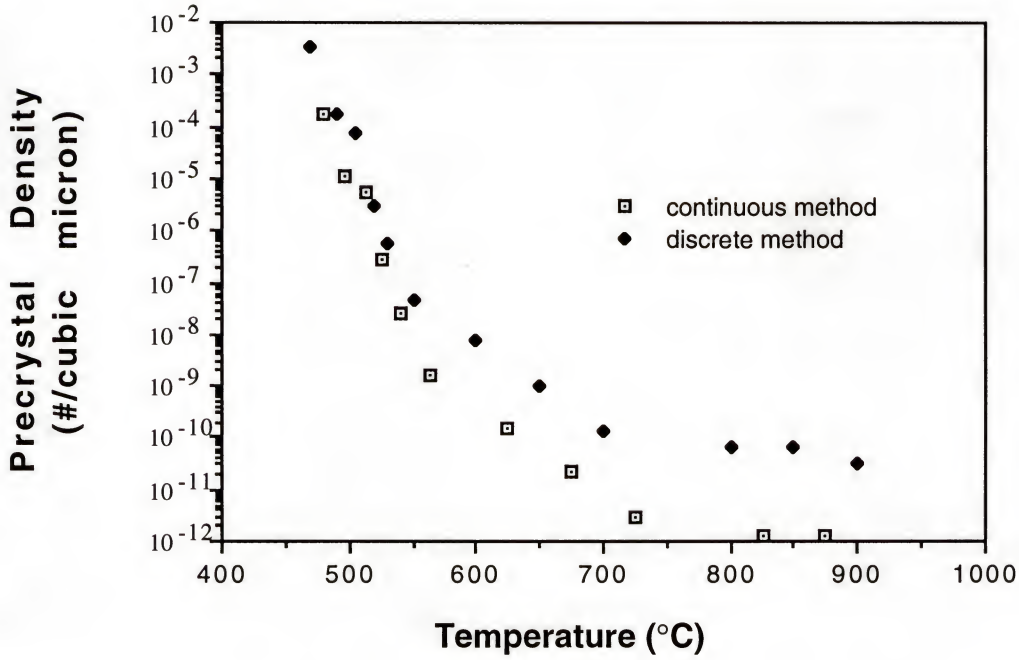

Figure 5.16 : Precrystal distribution map for lithium disilicate as calculated by the continuous method and the discrete method.

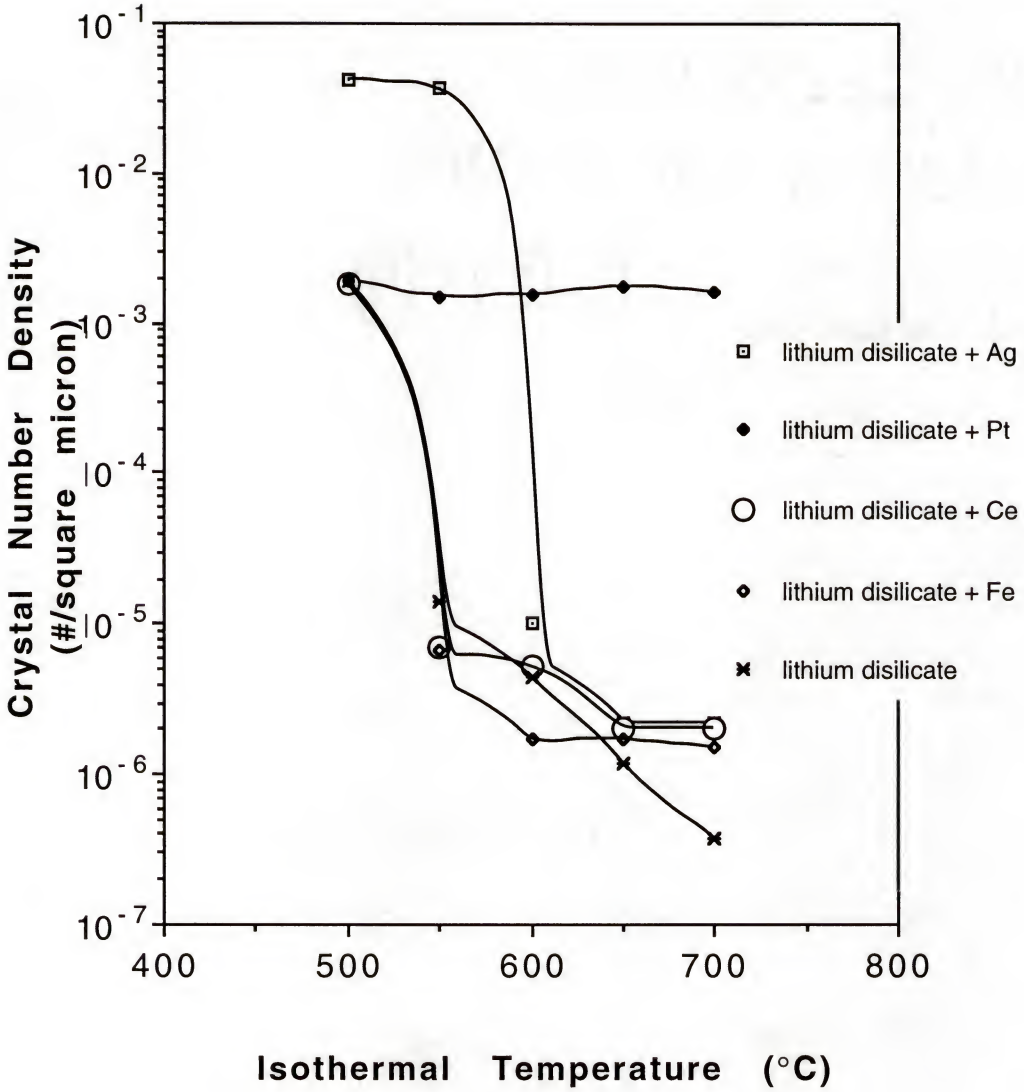

Figure 5.17 : Precrystal site map for lithium disilicate with various heterogeneous additions

CHAPTER 6
EXPERIMENTALLY DETERMINED OPTIMUM HEAT TREATMENT SCHEDULES

6.1: Introduction

Achieving the desired microstructural characteristics of the processed material in the shortest period of time is the goal of an optimum heat treatment schedule. The heat treatment schedule is the processing path which will links the precrystal distribution within the glass to the finished glass-ceramic material. An experimental approach for the generation of the most efficient heat treatment schedule will be developed and demonstrated in this chapter. The effectiveness of the novel schedule compared to the traditional two-stage schedule will be confirmed through comparison of the resulting microstructures.

For this method, a series of constant heating rates are used to heat samples from an initial temperature until the fastest rate is determined which yields a crystallized material of equivalent crystal number density as the precrystal site density map predicts for that temperature. A series of ideal heating rates is established for a series of temperatures which span the regions traditionally thought of as the nucleation and growth regions. The data is in the form of applied heating rate (Δtemperature/Δtime) versus initial heat treatment temperature. To convert this into the form

associated with traditional heat treatment schedules (time versus temperature) the integral of the inverse of the heating rate versus temperature function must be taken. The resulting heat treatment schedule is optimum for that particular glass. The scale of the final microstructure (i.e., the number of crystals per volume) determines the starting point on this heat treatment schedule. The precrystal map for the material predicts the optimum initial temperature.

This type of optimum schedule is also useful to determine the heat treatment needed for a modified system of the base glass plus the addition of heterogeneous phases. The one criterion is that the heterogeneous additions do not affect the growth kinetics of the glass-crystal transformation. In order words, the heterogeneous additions act as supplementary precrystal sites (usually of large size), but do not alter the kinetics of the crystallization process. For such modified systems, the original heat treatment schedule which was generated for the base glass is used in conjunction with a precrystal map of the new glass (base glass plus heterogeneous additions). The precrystal map of the modified glass shows a peak in the number of precrystals of a certain size which corresponds to the sites generated by the heterogeneous addition. The location of this peak corresponds to the starting temperature for the crystallization heat treatment.

6.2: Materials and Methods

Lithium disilicate of molar composition 33.3% Li_2O and 66.7% SiO_2 (Specialty Glass Inc., Oldsmar, FL.) was melted from a powder

frit in air at 1300°C for 18 hours to ensure homogenization. The glass was cast at a temperature of 1330°C onto room temperature blocks of graphite to form small discs approximately 15 mm in diameter. The small sample size produced a cooling rate for the glass which was sufficient to prevent any crystal formation as detected by 400x optical observation and x-ray analysis.

The precrystal data was collected by heat treating a series of discs over a range of isothermal temperatures. The length of the heat treatments was determined by the time needed to obtain a fully crystallized sample. Once crystallized, a section of material was cut from the interior of the sample with a diamond saw. The cross-section was mounted to a polishing stud with a resin wax and the sample was polished through 1μm-grit abrasive. The polished surface was etched with a dilute (2%) HF solution for approximately 5 seconds. For improved image resolution, the etched surface was sputter-coated with a Au/Pd layer. Six optical micrographs were taken from a series of sample locations for each sample. The effectiveness of the heat treatment was evaluated by measuring the number of crystals per cross-sectional area. It was calculated that to achieve crystal number density values which are representative of true bulk values a sampling area should contain at least 200 crystals. This criterion was satisfied for all temperature values used with the exception of the very coarsest crystallized samples produced by temperatures in excess of 675°C.

The optimum heat treatment curve for lithium disilicate was selected by determining the most rapid heating rate from the initial precrystal temperature until the sample is fully crystallized

without decreasing the initial nuclei population. The poulation density values from the precrystal plot controls the crystal population density which must be preserved for each temperature evaluated. The same experimental protocol was used as with the precrystal work to determine crystal population densities for the various heating rate runs at each temperature. It was expected that the crystal population density versus heating rate plots for each temperature would take the form of a plateau region for the slowest heating rates. As heating rates further increased, the plateau leads into a region of decreasing crystal population density. The optimum heating rate, for that particular temperature, corresponds to the fastest heating rate which remained on the plateau region. The plot of heating rate versus temperature can be converted into the form of a traditional heat treatment schedule (i.e., time versus temperature) by integrating the inverse of the function with respect to time.

When there exist processing time constraints, the heat treatment schedule can be compressed along the time axis to produce the needed crystal volume fraction within a given time period. Whether a linear or nonlinear compression should be applied to the time axis to maximize heat treatment efficiency is discussed later.

6.3: Results

The precrystal distribution plot for lithium disilicate is shown in Figure 6.1. Because the crystal population density values cover many orders of magnitude, the y-axis is a log scale.

Figures 6.2 through 6.4 are composed of six plots, one for each temperature where the optimum heating rate was investigated. In these plots, the x-axis is the heating rate and the y-axis is the resulting crystal population density. The chosen heating rate for each temperature plot is designated by the dashed line.

Figure 6.5 is the inverse heating rate versus temperature plot which can be generated from the series of optimum heating rates derived from Figure 6.2, 6.3 and 6.4.

Figure 6.6 is the optimum heat treatment schedule for lithium disilicate glass. It is generated by the integration of the inverse heating rate versus temperature plot (Figure 6.5).

To test the significance of the new heat treatment schedule, samples were prepared using the best two-stage heat treatment schedule and the newly generated optimum heat treatment schedule. Comparisons were made using total heat treatment time periods of 20 hours and 4 hours. The nucleation isotherm for the two-stage schedule was determined using the thermal analysis method. The results were shown in Figure 4.3. From this data, a nucleation temperature of 468°C was selected. The two-stage schedules consisted of an 18.5 hour nucleation segment for the 20 hour schedule and a 2.5 hour nucleation segment for the 4 hour schedule. A temperature of 630°C was used for the growth stage for time periods of 1.5 hours for both schedules. To fit the imposed time constraints, the optimum schedule was linearly compressed along the time axis. Figures 6.7 and 6.8 show the two-stage schedule and the optimum schedule for the 20 hour and the 4 hour cases.

The results for the 20 hour time limit show an average crystal population density for the two-stage schedule to be $8.1 \times 10^{-5}/\mu m^3$ and $1.2 \times 10^{-4}/\mu m^3$ for the optimum schedule. The standard deviations were $2.0 \times 10^{-7}/\mu m^3$ and $1.1 \times 10^{-7}/\mu m^3$, respectively. The optimum heat treatment schedule showed a 50.2% improvement over the two-stage schedule in terms of crystal density.

The results for the 4 hour time limit show an average crystal number density for the two-stage schedule to be $8.7 \times 10^{-6}/\mu m^3$ and $1.3 \times 10^{-5}/\mu m^3$ for the optimum schedule. The standard deviations were $7.9 \times 10^{-8}/\mu m^3$ and $2.6 \times 10^{-7}/\mu m^3$, respectively. The optimum heat treatment schedule showed a 44.2% improvement over the two-stage schedule in terms on crystal population density.

6.4: Discussion

6.4.1: Time Compression of the Optimum Heat Treatment Schedule Generated for the LS System

The optimum schedule for crystallization produces a glass-ceramic material containing the maximum number of crystals per volume for the selected initial temperature. The schedule produced a material having a crystal population density equal to that which is generated by isothermally treating a sample at 470°C until fully crystallized. Such a heat treatment results in a crystal number density of approximately $3 \times 10^{-2}/\mu m^2$. For production applications, the 800+ hour processing time associated with the schedule makes it impractical. Another aspect of this schedule which should be noted, a sample will reach 100% crystalline phase long before the entire schedule can be executed. For these reasons, the compression

of the schedule was performed to produce more useful 4 hour and 20 hour schedules. These schedules were superior to the comparative two-stage schedules. However, it is uncertain if the linear compression of the time axis produces the optimum heat treatment schedule for the desired processing time period. To evaluate this, it is necessary to plot the crystal population density lost due to application of increasingly rapid heating rates (greater than the optimum rate) for a range of temperatures. Figure 6.9 shows this data. The units for the x-axis are in terms of the number of minutes saved during one degree of temperature increase due to the accelerated heating rate and the y-axis is in terms of the crystal number density lost due to the faster-than-optimum heating rate. The number density lost data is the difference between the precrystal density value for that temperature and crystal density value resulting from the accelerated heating rate. The time savings data is the difference between the inverse of the optimum heating rate and the inverse of the accelerated heating rate. From Figure 6.9 it can easily be seen that acceleration of the optimum schedule in the lower temperature regions results in a much greater loss of nuclei than does a similar acceleration in the higher temperature regions. Therefore, a linear compression does not result in the most efficient heat treatment schedule for limited time processing. To produce the most effective heat treatment schedule, the reduction in processing time should be done with the guiding principle of maximum time savings with minimal loss of nuclei. Figure 6.9 shows that the most efficient time savings are made by reducing the time spent at higher temperatures and preserving the optimum heating

rate for lower temperature regions. Using these guidelines, a modified 20 hour schedule was generated. Figure 6.10 shows a comparison between the linearly compressed 20 hour schedule and the modified 20 hour schedule. Samples processed with the modified 20 hour schedule had an average crystal density of $2.35 \times 10^{-4}/\mu m^3$ with a standard deviation of $5.43 \times 10^{-6}/\mu m^3$, as measured by quantitative microscopy. The modified schedule produced crystal density improvements over the linearly compressed schedule of 96% and improvements over the two-stage schedule of 190%.

6.4.2: A Hypothetical Crystal Growth Rate Distribution that is Independent of Temperature and Crystral Size

The observation that a time compressed optimum schedule produces a finer-grained product than does the optimum schedule using the same amount of time (and therefore starting at a higher initial temperature) complicates the previously developed precrystal approach. According to the precrystal approach, an accelerated optimum schedule should lose all of the nuclei associated with the initial temperature. As the schedule progresses, it will continue to produce heating rates more rapid than the smallest nuclei in the population can withstand and the population will continue to decrease. The final microstructure consists of crystals which originated from significantly large precrystal sites.

There is a possible explanation, which is consistent with the precrystal idea, for the observation that accelerated heating rates generate a final product with a microstructure consisting of a significant fraction of the total precrystal population. Since the heat treatment starts at a low initial temperature, precrystals

above this temperature will experience some amount of growth before the rapid heating rate produces temperatures equal to these site's stability temperature. If this amount of pre-growth was large enough, it might explain the increased population density measured in the final product.

A more likely explanation for the unexpected effectiveness of the accelerated schedules is that for the population of precrystals associated with a given temperature there exists a range of growth rates as a function of temperature. If this were true, the experimentally determined optimum rate is the rate needed to develop the slowest growing site in the precrystal population for that temperature. Physically, the idea of a range of growth rates is plausible. By the same argument that assumes atypical sites within the glass act as precrystals and that the range of precrystal sizes is continuous due to slight influences from a host of features, the growth rate of a precrystal could be affected by these same unaverage features as the nuclei grow and feel the influence of new glassy regions. The merging of several nuclei very early in their development could also produce a site which grows at a rate more rapidly than its initial size would predict. Therefore, it would be capable of surviving a heating rate faster than the optimum heating rate for that initial precrystal size.

6.4.3: A Hypothetical Influence of Crystal Size on the Significance of the Growth Rate Distribution Effect

If the hypothesis of a growth rate distribution for each

precrystal size because of the influence of anomalies in the surrounding matrix is accepted, then the significance of these anomalies to influence the growth rate of the crystal should be a function of the crystal size. Intuition suggests that the smaller the crystal, the more significant will be the influence of these growth stimulating regions. Once a crystal approaches the size termed "bulk", the growth rate is not significantly affected by any further increase in the size of the crystal. The growth rate is only a function of temperature. Most likely, the significant influence of matrix anomalies ends before a crystal reaches a size which can be assumed to approximate a bulk crystal size.

The idea that the significance of accelerated growth producing regions are a function of crystal size suggests a form for an effective heat treatment schedule. Considering the experimentally determined optimum heat treatment schedule in terms of the hypothesized growth rate distribution effect, the schedule proceeds slow enough as to maintain the slowest growing sites for each precrystal size. Therefore, the derived optimum schedule could be approximately divided into two temperature regions: region 1) small crystals are growing and a distribution of growth rates for each crystal size exists, region 2) "bulk"-like crystals are growing whose growth rates are equal for each crystal size. The optimum schedule should be the most effective schedule for region (2), while the amount of optimum schedule acceleration imposed in region (1) should dictate the fraction of the initial precrystal distribution to be developed. Figure 6.11 shows the variations in the heat treatment schedule suggested by this hypothetical approach. The idea of such a

two-region heat treatment schedule and the experimentally found relationship for nonlinear schedule time compression are compatible. Maximum efficiency should be obtained when the ideal nonlinear compression of the optimum schedule is applied to region (1) while region (2) is left unaltered.

6.4.4: Process Sensitivity to Heat Treatment Schedule Deviations

To investigate the significance of oven and controller accuracy in executing the desired heat treatment schedule and any resulting effects on the microstructure of the processed material, a sample was given the 20 hour compressed optimum heat treatment using a DTA (Seiko TG/DTA320) as a heat treatment oven. Deviations from the ideal schedule temperatures produced by the thermal analysis equipment are at least one half of those produced by a conventional laboratory box oven. When the microstructure of a DTA heat treated sample was compared to that of a conventionally heat treated sample no significant improvement was found. The relatively large thermal mass of the conventional oven is thought to buffer the larger controller fluctuations such that the sample experiences a smooth heat treatment. The importance of this effect might be significant if complex heat treatment schedules such as these are to be used on a larger, commercial scale.

6.5: Conclusion

An improved approach for the production of glass-ceramic

materials has been developed. Glass-ceramic materials produced from the optimum schedules showed a significant improvement in their crystal number density as compared to materials produced by using traditional two-stage heat treatment schedules. The best method for compression of the optimum heat treatment schedule to meet processing time limitations was found to be non-linear. The higher temperature regions of the schedule can be compressed more without a significant effect on the final glass-ceramic microstructure. The form of the compressed schedules approaches that of the traditional two-stage schedule. The significant difference in the number density of crystals measured when comparing the similar schedules (compressed optimum and two-stage) shows the large influence of the heating rate during the first few degrees of the heat treatment schedule. The idea of a distribution of growth rates for a given temperature and nucleus size was proposed and its implications discussed.

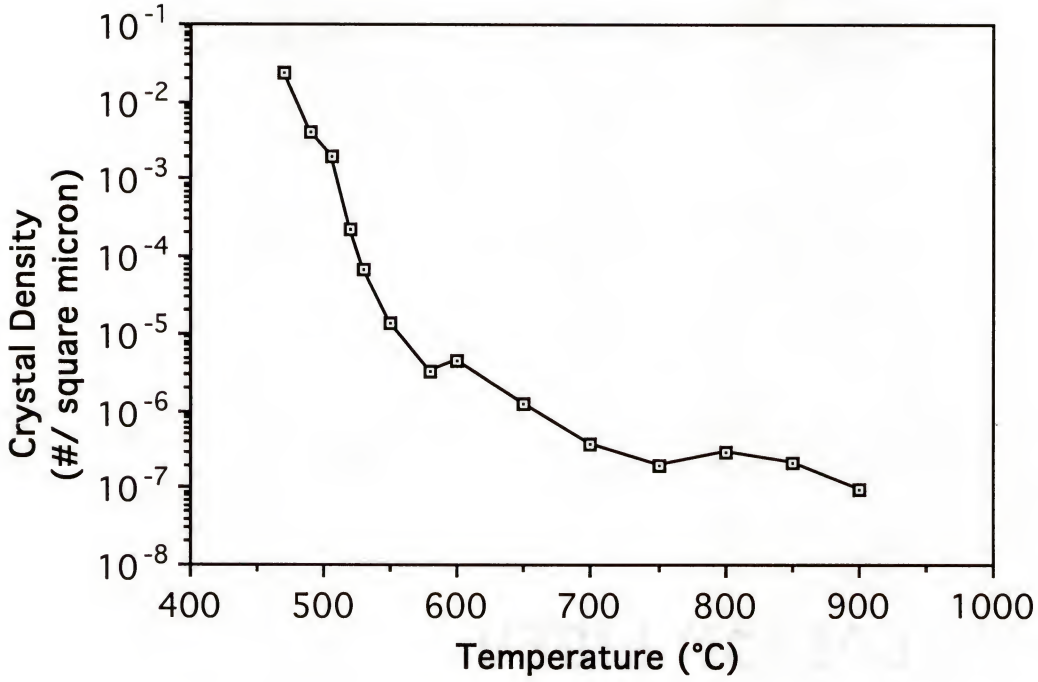

Figure 6.1 : Population density of crystals measured in fully crystallized samples of lithium disilicate as a function of isothermal heat treatment temperature.

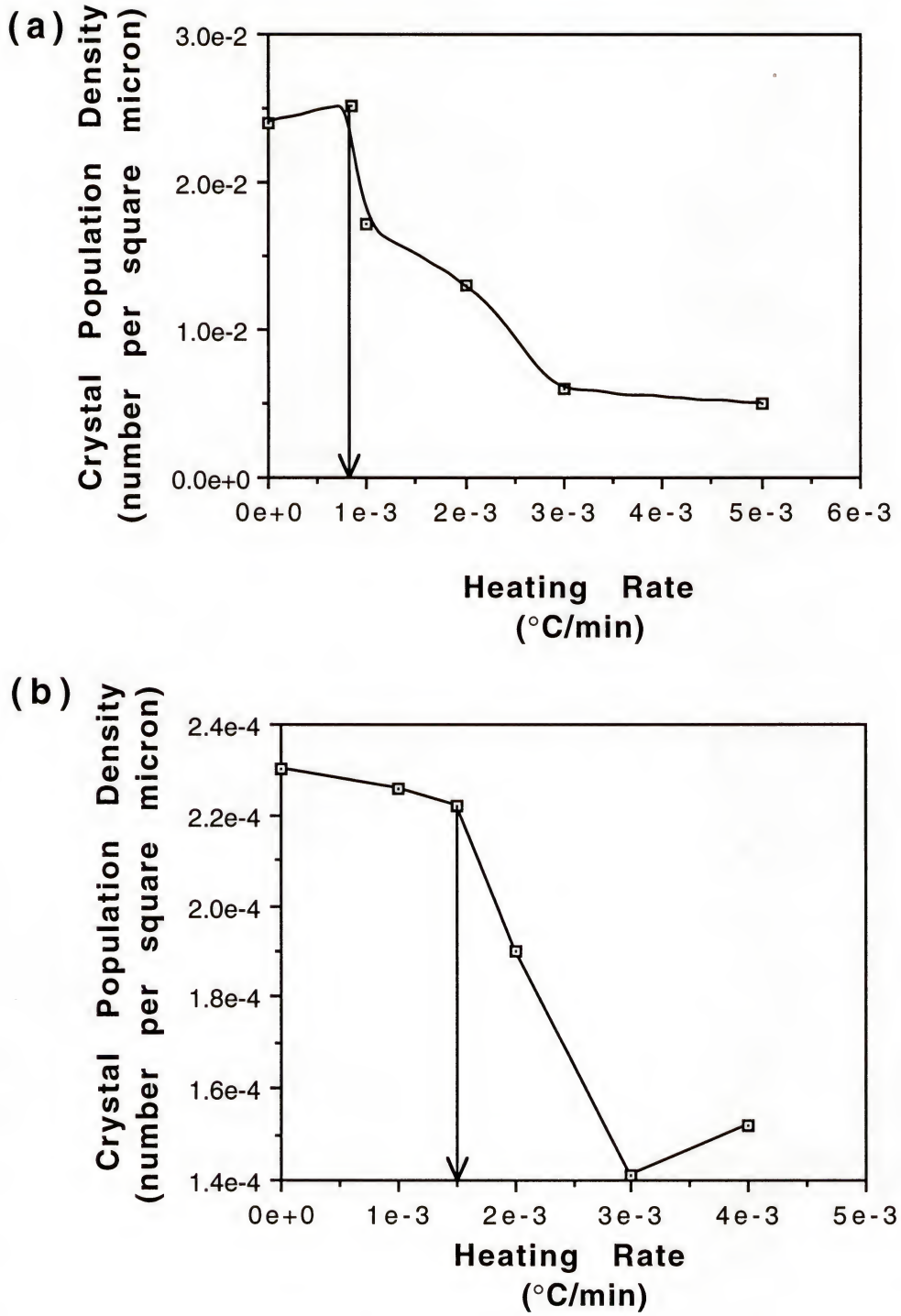

Figure 6.2 : Effect of heating rate variation on the resulting crystal number density; (a) 470°C initial temperature, (b) 520°C initial temperature

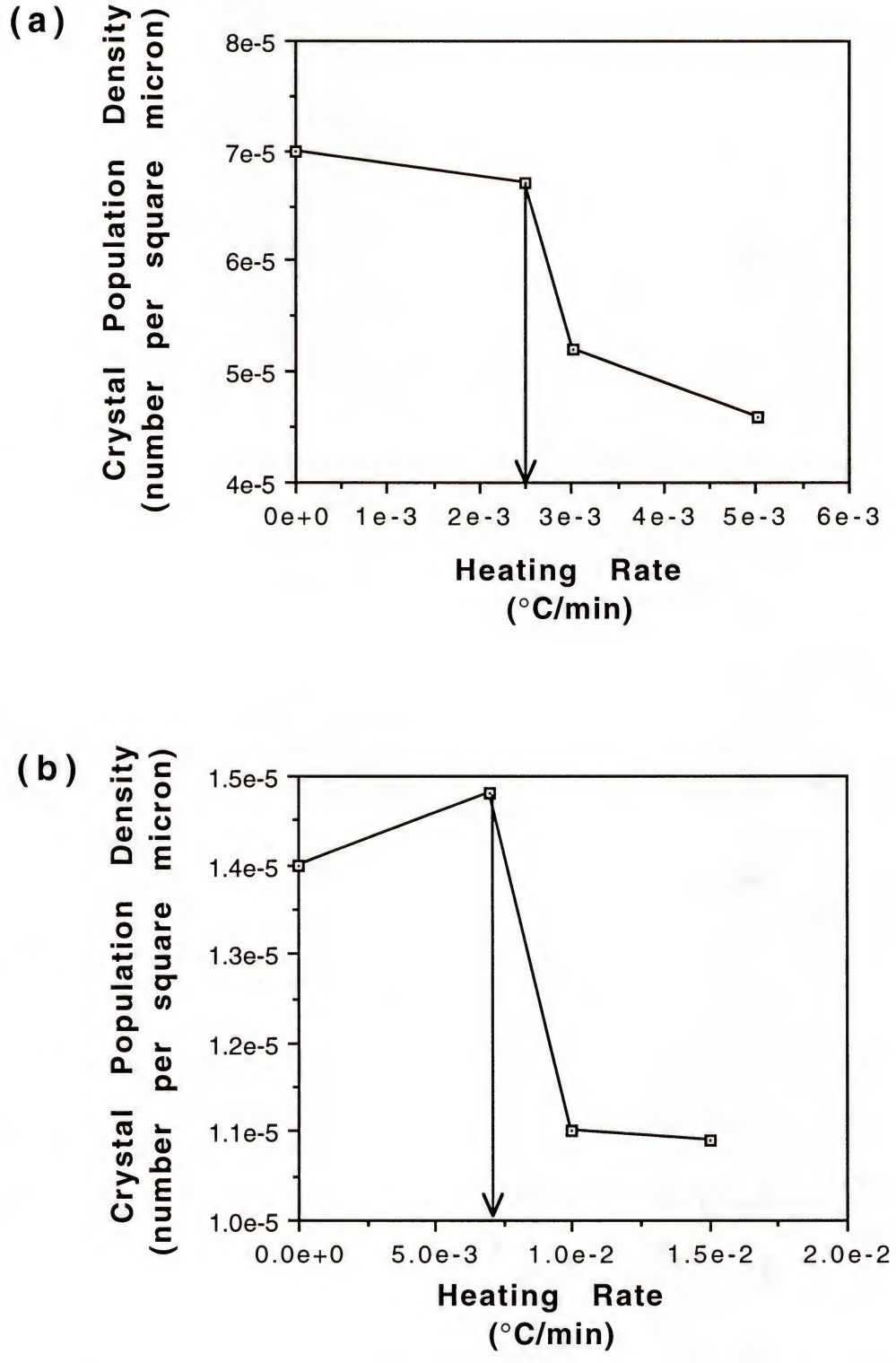

Figure 6.3 : Effect of heating rate variation on the resulting crystal population density; (a) 530°C initial temperature, (b) 550°C initial temperature

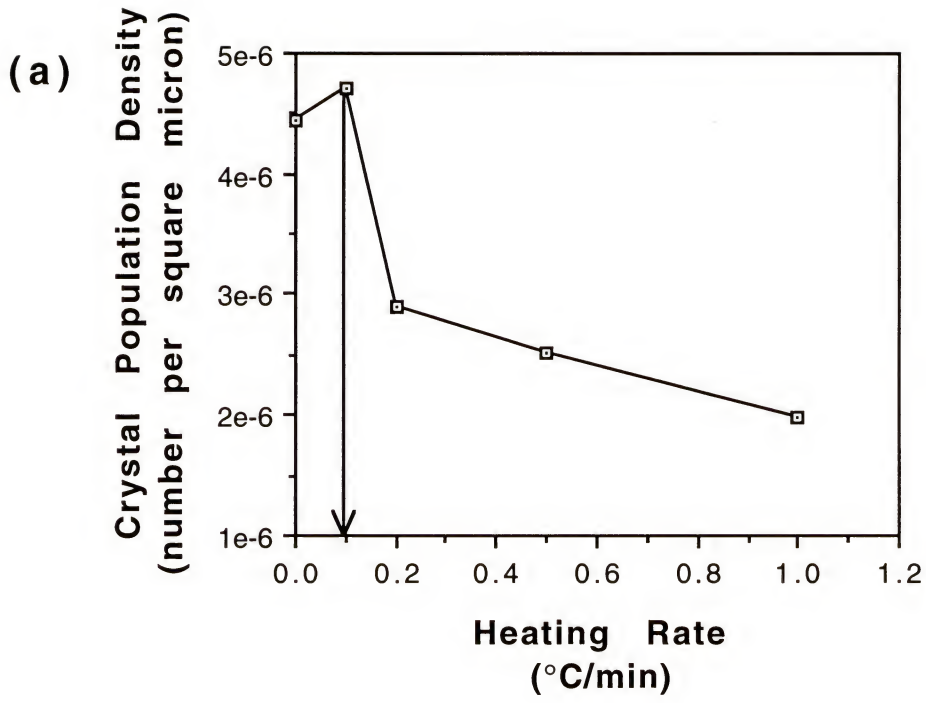

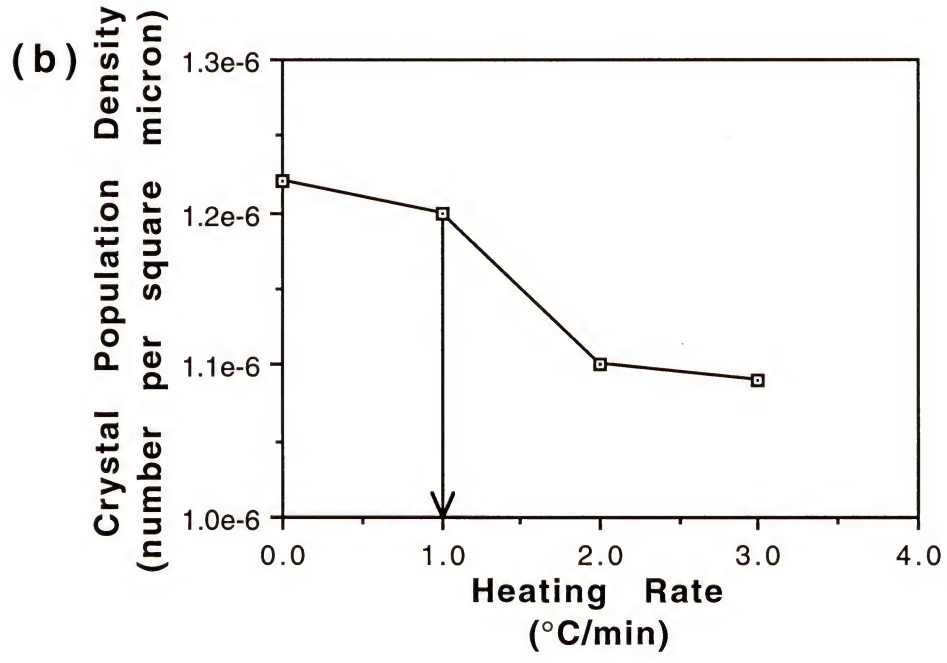

Figure 6.4 : Effect of heating rate variation on the resulting crystal population density; (a) 600°C initial temperature, (b) 650°C initial temperature

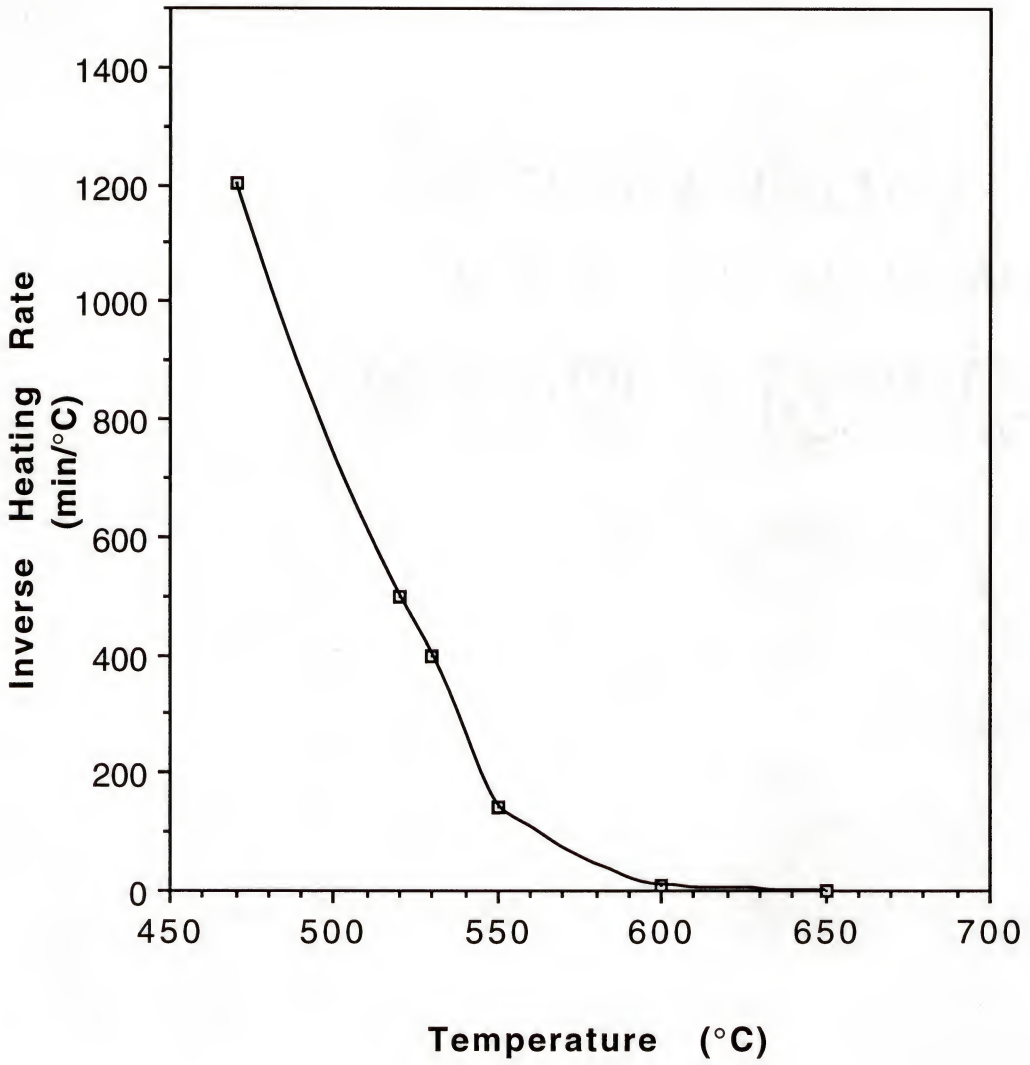

Figure 6.5 : Optimum heating rate (shown as an inverse) as a function of temperature. Data derived from plateau decline points from Figures 6.2, 6.3 and 6.4.

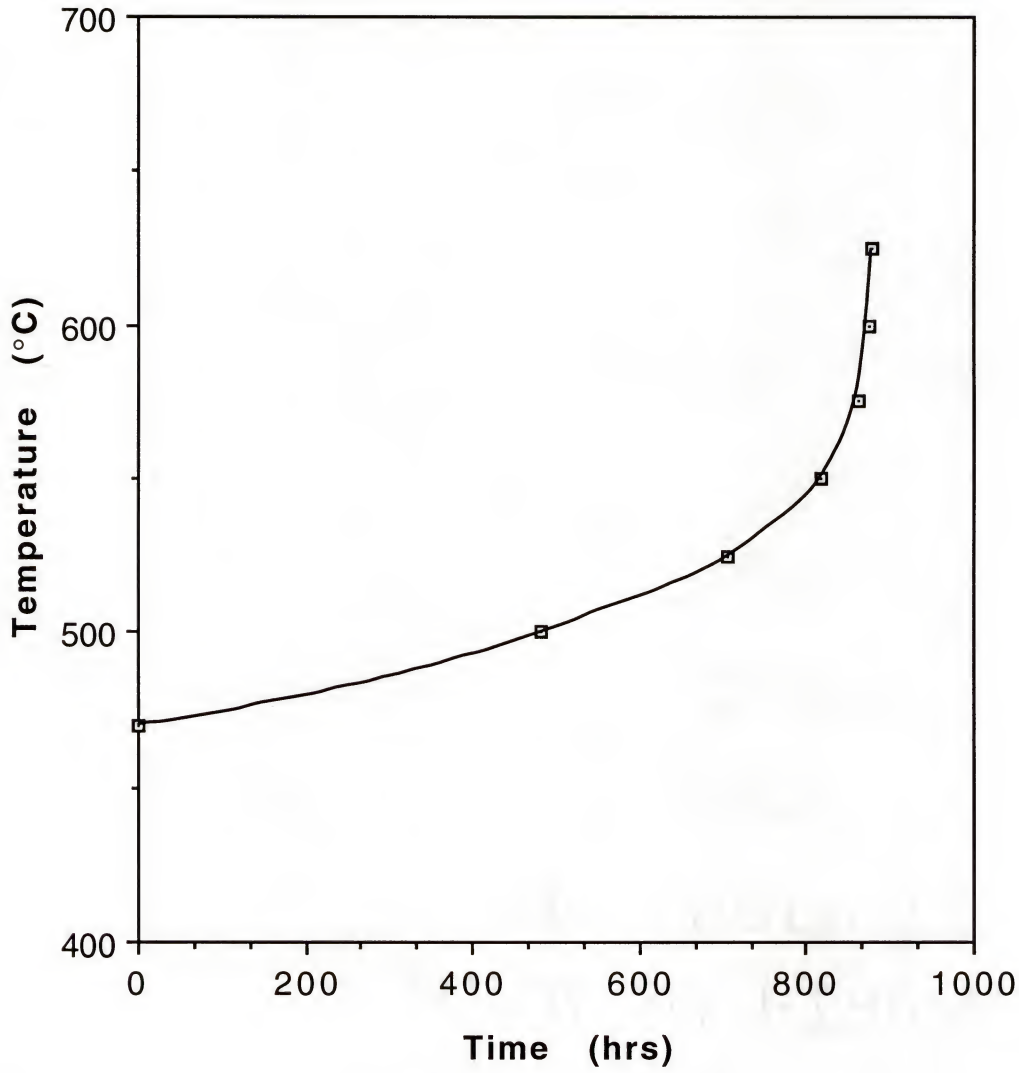

Figure 6.6 : Experimentally derived optimum heat treatment schedule for lithium disilicate

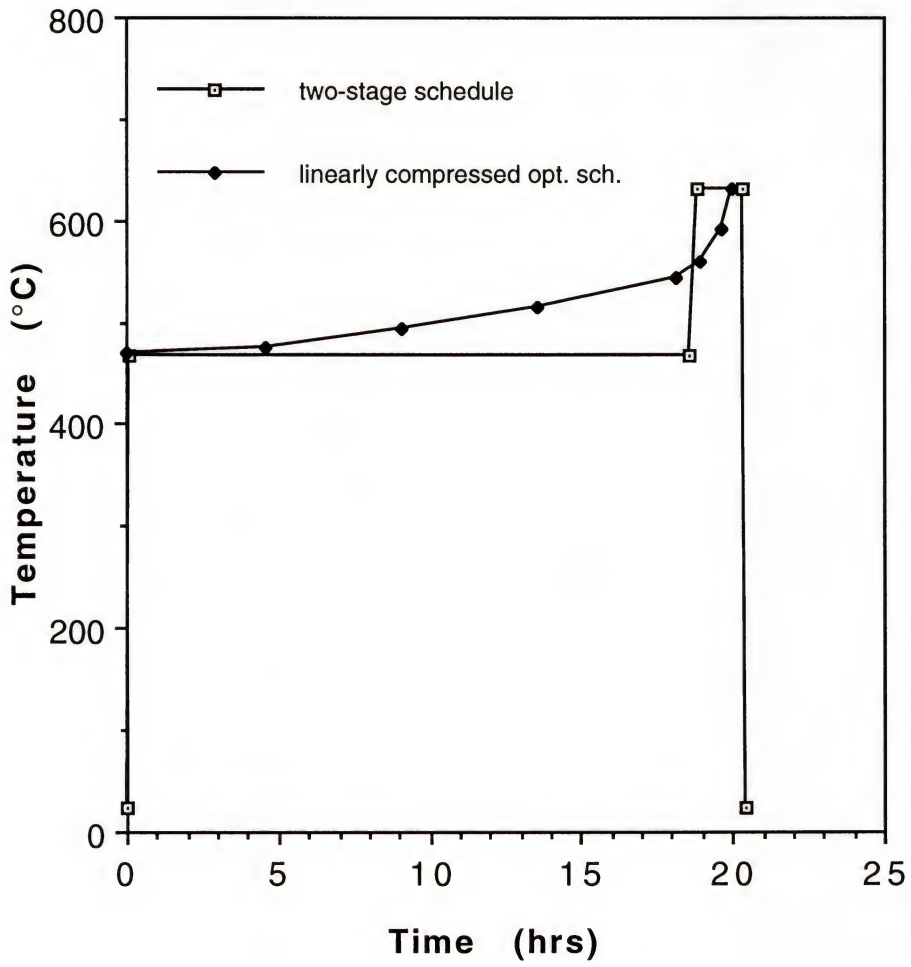

Figure 6.7 : Comparison of a two-stage schedule and a linearly-compressed optimum schedule for lithium disilicate, given a 20 hour processing limit.

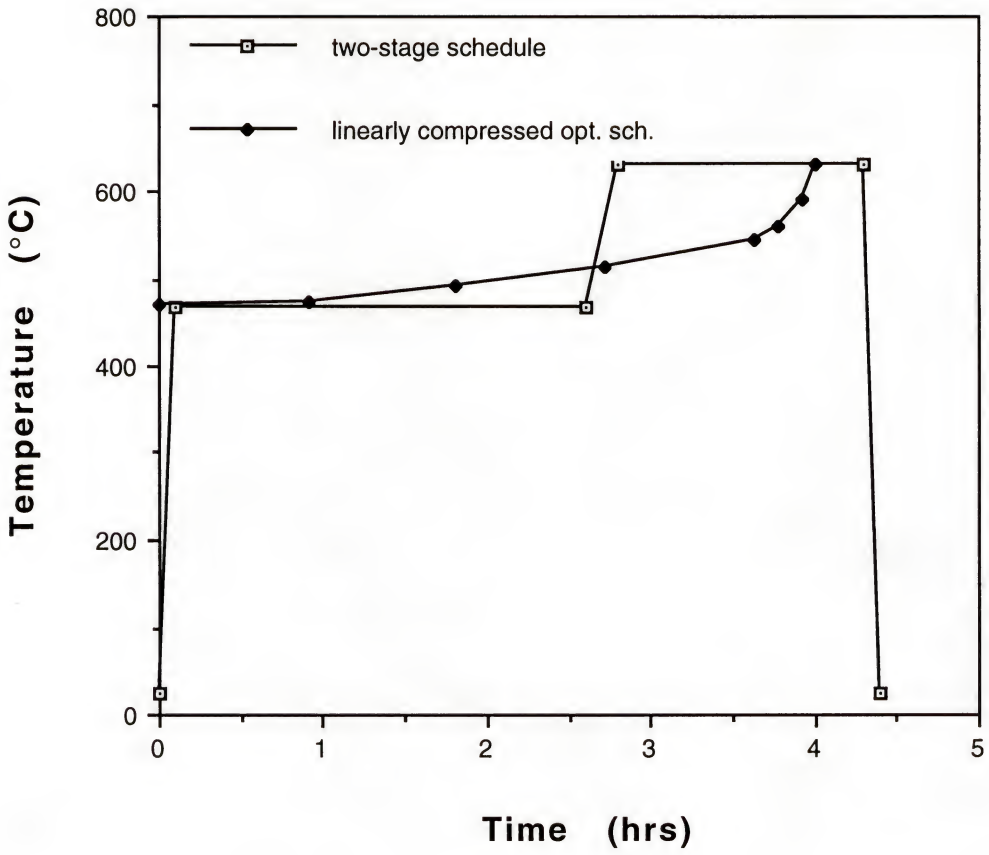

Figure 6.8 : Comparison of a two-stage schedule and a linearly-compressed optimum schedule for lithium disilicate, given a 4 hour processing limit.

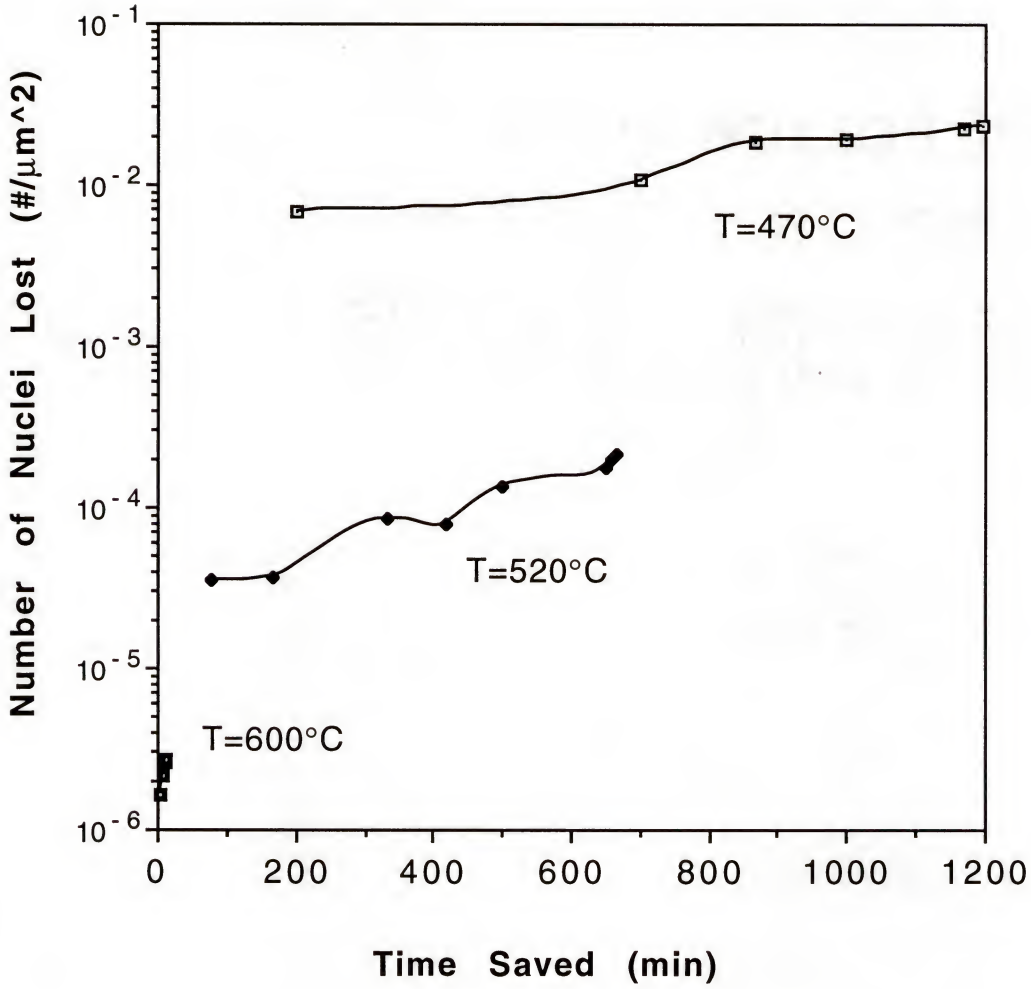

Figure 6.9 : Number of nuclei lost because of accelerated optimum heating rates as a function of the resulting processing time savings. The material is lithium disilicate. Data is shown for a series of initial temperatures.

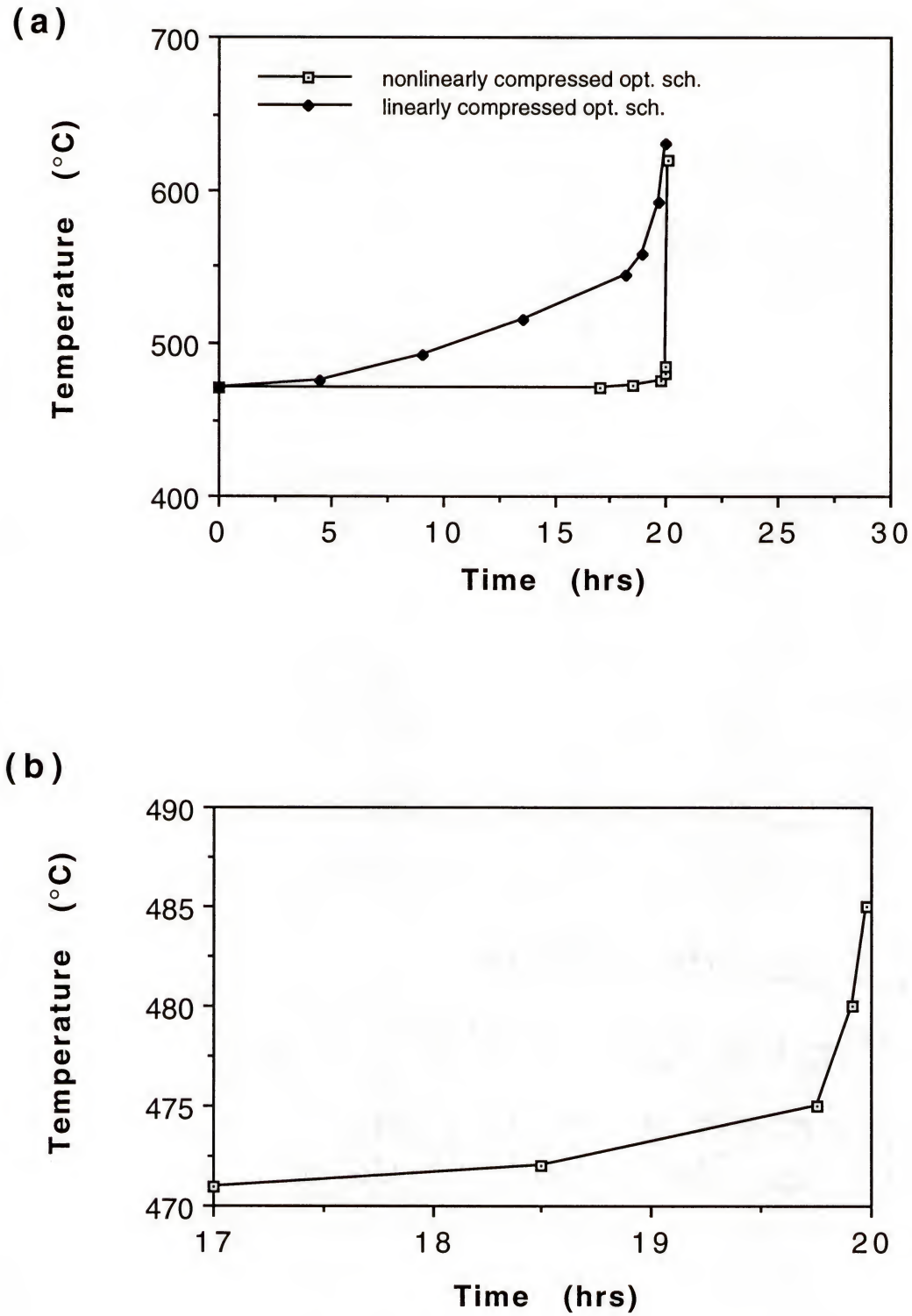

Figure 6.10 : Comparison of linearly compressed optimum schedule and nonlinearly compressed optimum schedule, for lithium disilicate: (a) full 20 hour schedule (b) expanded view of nonlinearly compressed schedule

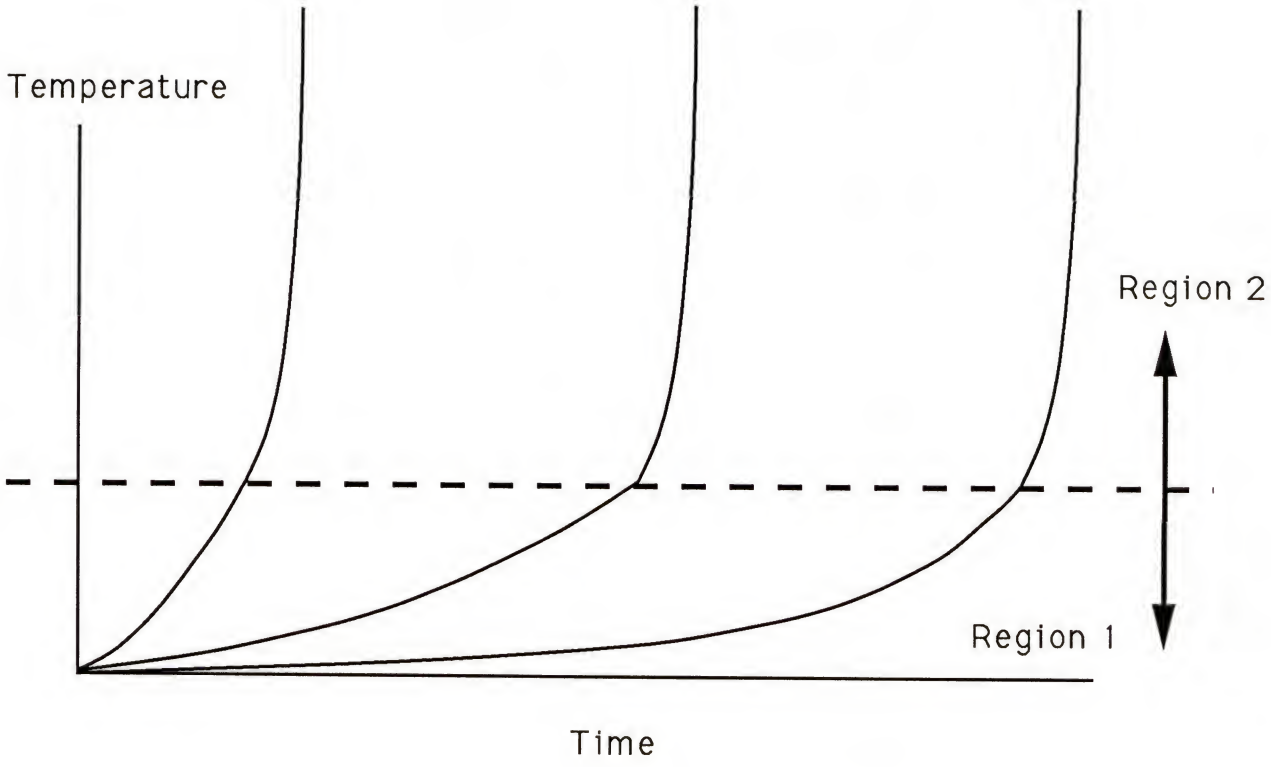

Figure 6.11 : Most effective form for heat treatment schedule time reduction, as predicted by the growth rate distribution idea. Below the dashed line, crystal growth rates are affected by their local environment. Above the dashed line, all crystals of equal size at equal temperature grow at the same rate.

CHAPTER 7
EXPERIMENTAL AND THEORETICAL DEVELOPMENT OF THE CRYSTAL GROWTH RATE EQUATION

7.1: Introduction

It has been emphasized throughout this work that no delineation exists between what has classically been termed the nucleation regime and the growth regime. Experimental data can be explained through the conceptual use of a precrystal site density map subject to the given heat treatment. Because of the continuous nature of this approach through both the nucleation regime and the growth regime, it is reasonable to assume that a single growth equation can predict the development of crystals from precrystal size to micron size. This growth equation would be the link between the precrystal site density map and experimental measurements of the developing microstructure.

The growth rate equation, for the simplest systems, needs to be in terms of the sample temperature and a characteristic crystal dimension, which is representative of the crystal size. Because the kinetics of the glass-ceramic phase transition are rather slow, it is a good assumption that the average sample volume and the glass/crystal interface have equal temperatures. This assumption is necessary due to the technical difficulties involved in accurately measuring the interfacial temperature during crystallization.

Development of reasonably accurate growth equations is significant from both a scientific and a commercial viewpoint. Scientifically, a growth rate equation would function as a critical test for the validity of mechanistically derived growth ("nucleation" and/or "growth") equations. Commercially, a growth equation can be used to generate the heat treatment schedule to take a precrystal population to microstructural maturity in the shortest amount of time, i.e. the optimum heat treatment schedule.

7.2: Materials and Methods

7.2.1: Development of Experimentally Derived Growth Rate Equations

The growth rate equation can be formulated by two different approaches. One approach is to gather growth rate data in terms of temperature and crystal size and then attempt to fit an appropriate equation to the data. Growth data can be collected via transmission electron microscopy (TEM) or small angle x-ray scattering (SAXS). For the system used primarily in this study, lithium disilicate, SAXS was unusable due to a lack of sufficient electron density difference between the glass phase and the crystal phase. A TEM study should be able to yield the needed data, however, the time demands of a TEM study are extensive. A TEM study requires cold stage sample preparation techniques in order to prevent alteration of the nuclei population.

As an alternative to the more traditional techniques mentioned above, the growth rate equation can be formulated by simulating the development of the crystals from the precrystal state to the

observable microstructural state. Experimental data has been collected which maps out the precrystal distribution for lithium disilicate (Figure 5.14) and experimental data, for a range of isothermal temperatures, has also been collected which documents the arrival of lithium disilicate crystals to an optically observable size (Figure 5.6). The equation which uses the precrystal distribution data as input data and can successfully reproduce the experimentally observed outcome, for a range of isothermal temperatures, should be a reasonably good approximation of the true growth rate equation. This method does not attempt to attach any mechanistic significance to the function which translates one data set to the other data set. Rather, this function is only used as a tool to approximate the characteristics of the true growth rate function.

In order to test potential growth rate equations, it was necessary to write a computer program to simulate the development of the lithium disilicate microstructure given the initial precrystal distribution and an isothermal temperature (Appendix C). The program grows the crystal distribution by assigning the appropriate number density value (number of crystals per cubic micron) for each initial precrystal size. This number density value remains constant as the group of crystals of that particular size grows. To be able to make such number density assignments the function relating precrystal size to number density needed to be fitted. The experimental data was of a form characteristic of a modified Weibull distribution. Utilizing this observation, the precrystal distribution data was fit using a statistical analysis program (SAS). The following equation was the best fit obtained and is compared to

the experimental data shown in Figure 7.1 .

number density (number/cubic micron) = 10^(-11.65*(1-exp(-1*((1125.95-1.2267e11*b)/(-6.2909e10*b-2288.68))^6.77))) (7.1)

For each iteration of the program, the amount of growth during that increment of time is calculated for each group of crystal sizes. Each group of crystals is then assigned a new characteristic length equal to their previous length plus the growth length. The growth length is the output of the experimental growth rate equation using the previous characteristic crystal length and the isothermal temperature as input data. To simulate the experimentally collected data, as in Figure 5.6, the program notes the number of crystals and the associated time for crystals surpassing the limit of optical observability (one micron). The program was arbitrarily written using "b" as the characteristic crystal length dimension. "b" is the length of the orthorhombic lithium disilicate crystal along its [010] axis (Figure 7.2). The growth direction parallel to the "b" direction has been shown by TEM to be the slowest growth direction.[63] Since experimental observations cannot be made exclusively along the "b" direction, the "b" length needs to be multiplied by a factor to make it more experimentally representative or, equivalently, the limit of observability needs to be divided by a factor. A term is needed to account for the deviation from orthorhombic structure to the spherulitic structure experimentally observed at larger crystal sizes (i.e. one micron size). A term is also needed to take into account the effect of making measurements on three dimensional

microstructures using two dimensional cross-sectional micrographs. Multiplying these factors together yields a value which translates "b" into the crystal dimension measured by optical micrographs. The relationship between the core crystal orthorhombic dimensions and the overall spherulitic dimensions depends upon the branching of the original orthorhombic crystal during growth. Figure 7.3 shows how the lithium disilicate spherulite form the original orthorhombic lithium disilicate crystal.[64] From this structural relation, it can be seen that the "c" dimension of the orthorhombic crystal is equivalent to the diameter of the spherulitic crystal. The "c" dimension is approximately 4.5 times the magnitude of the "b" dimension.

Assuming the spherulitic crystal to be spherical (it is actually shaped more like a football), the average cross-section of a randomly located plane of intersection is that of a plane located half the distance between the pole and the equator of the sphere. The diameter of such a plane is 0.7071 times the actual sphere diameter. Therefore, applying these translational factors to the one micron limit of observability results in a simulated crystal being detected when the following is true.

$$0.7071 * 4.5 * \text{"b"} > 1 \text{ micron} \qquad (7.2)$$

$$3.182 * \text{"b"} > 0.0001 \text{ cm} \qquad (7.3)$$

$$\text{"b"} > 3.143\text{e-}5 \text{ cm} \quad (\text{ the relative limit for observability }) \qquad (7.4)$$

It was noted that the number of crystals reaching the observable size limit (approximately one micron) as a function of

time is a relatively constant value. This observation held true for most of the 470°C isothermal temperature data. Using this observation, the experimental growth rate equation is based on the previously fit number density function. Because for every incremental time segment an equal number of crystals cross over the one micron size limit, it is assumed that the growth rate for each incremental precrystal size segment is proportional to the number density of the largest precrystal segment divided by the number density of that segment. This approach depends upon the assumption that the largest precrystal segment exhibits growth rates equivalent to that of bulk crystals. This assumption was supported when it was found that to reproduce what was observed experimentally it was necessary to increase the crystal growth rate to that of bulk crystals for the large crystals of the precrystal distribution.

To produce the experimentally observed response, the growth rate equation based upon the above approach needed to be multiplied by an additional temperature dependent factor called the "V" factor. V values were found for the three experimental isothermal temperatures; 470°C, 490°C, and 550°C. The equation

$$V = \exp(93.105 - 0.18112*\text{Temperature}(°C)) \qquad (7.5)$$

was found to fit the temperature dependence of this data (Figure 7.4).

The temperature dependence of the bulk crystal growth rate was described by the following equation (Figure 7.5).

Bulk
Growth = exp(-1.1419e10*Temp(°C)^-3.2523) [cm/sec] (7.6)
Rate

The bulk growth rate data was generated using the stoichiometric lithium disilicate composition. Samples were made by cooling droplets approximately 15-20 mm in diameter from the melted glass (1320°C) on a block of room-temperature aluminum. The growth-rate data were obtained by heat treating pieces of the lithium disilicate glass at an isothermal temperature until an optically measurable (at 400X) layer of surface crystallization was observed. The average thickness of the surface crystallized layer was found and then the same piece was exposed to the isothermal temperature for a measured time period. The change in the surface crystalline layer thickness divided by the exposure time results in the bulk crystal growth rate for that temperature. Exposure time periods were limited such that no impingement occurred between surface crystals and bulk crystals or between surface growth fronts originating from opposite sides of the sample. This procedure was used for a series of isothermal temperatures to find the temperature dependence of the bulk growth rate function.

The growth rate of a certain crystal face for a crystal of a given "b" length and isothermal temperature was calculated by multiplying together the size dependent growth rate factor, the "b" translating factor, the V factor, and the bulk sized crystal growth rate.

7.2.2: Determination of the Theoretically Derived Growth Rate Equation

It is believed that the main controlling force in the early development of a new phase is the difference between positive and negative free energy. In most systems, the primary driving force behind the evolution of a new phase is the overall free energy reduction. This reduction in free energy is a result of the generation of a new volume phase in respect to the mother phase. Therefore, the volume free energy change is assigned a negative magnitude. The free energy associated with a volume of lithium disilicate in its crystalline form has a lower value than the free energy associated with an equal volume of lithium disilicate glass. The relatively high free energy term associated with the initiation of a new phase comes from the planes of interface between the new and the old phases and from any strains associated with the development of the new phase. These free energy terms will be greater than similar terms (if comparable terms exist) in the matrix phase.

The competition between the free energy terms is generally a function of the size of the developing phase. The ratio of surface area to volume increases as the size of the body decreases. As mentioned previously, this is the reason for "critically sized nuclei". Crystals must pass over this free energy maxima which is produced by their own surfaces. Most previous growth theories centered around surmounting this obstacle and ignored the influence of the negative free energy surplus resulting from further crystal growth (Figure 7.6). The theory developed here, the surplus ledge growth theory, depends on this free energy surplus to predict the growth

rate of the crystalline phase.

The surplus ledge theory is based on the concept that a growing crystalline phase will generate a surface which is roughened to a degree which compensates for the excess free energy of this developing crystal. As the crystal grows, the surface-to-volume ratio decreases and the surplus free energy builds. Therefore, the amount of thermodynamically allowable ledge surface area increases as the crystal grows. The crystal growth rate is measured in a direction perpendicular to the plane of the crystal/glass interface. The growth rate is measured by assuming that all ledge surface area perpendicular to the ledge growth direction acts as an active growth front. The ledge growth velocity can be calculated and therefore the volume transformed per time can be determined. This value is then divided by the overall interfacial area to yield the growth rate in a direction perpendicular to the crystal/glass interface.

The surplus free energy approach implies the influence of an effect akin to atomic communication from one region of the crystal to another. The existence of one ledge will influence the probability of existence of another ledge elsewhere on the crystal. It is proposed that when the bulk of the crystal can accommodate or redistribute the higher free energy generated at the interface, the surface ledge units will be more likely to remain stable and grow. This effect is a function of both the size of the crystal and the free energy of the surface. The free energy of the surface is a function of the number of ledge units per interfacial area. Figure 7.7 shows schematically how crystal size and surface ledge density determine

whether new ledge units are likely to survive or dissociate.

The surplus free energy approach is now applied to the orthorhombic crystal structure of lithium disilicate in an attempt to theoretically predict the crystal growth rate as a function of a characteristic crystal length and temperature. There are several reasons why the lithium disilicate composition is one of the most often used glasses for crystallization studies. Lithium disilicate readily crystallizes internally at a relatively low temperature and without the need for significant amounts of diffusion. For this thermodynamic approach to predict growth rates, lithium disilicate is also ideal because of the wealth of existing thermodynamic data on the glass. Volume free energy values used were those determined by Takahashi[65] through the use of a continuous high-temperature calorimeter. The volume free energy as a function of temperature (in units of erg/cm^3) is shown in Figure 7.8 and can be expressed as follows.

$$\Delta G_v = 6.5807e8\ (5.1141 - (4.8334e\text{-}3 * T)) \qquad (7.7)$$

The surface free energy values used were those determined by Rowlands and James[63] for an orthorhombic cluster. The temperature dependence of these values was assumed to scale similarly as the relationship Rowlands and James used to fit the classically derived pre-exponential factor to the experimental nucleation data for temperatures above the maximum nucleation rate temperature. This temperature range corresponds well with that used for this work. The surface free energy relations for the corresponding crystal

faces are as follows, in units of ergs/cm^2.

face (1) : $\sigma_1 = 54 + (0.109 * T)$ (temperature is in °K) (7.8)

face (2) : $\sigma_2 = -59.5 + (0.109 * T)$ (7.9)

face (3) : $\sigma_3 = 173 + (0.109 * T)$ (7.10)

It was observed by TEM that the orthorhombic crystal maintains relatively fixed relationships between the lengths of the crystal axes.[63] The observed ratios of a/b/c = 2.7/1.0/4.5 are shown in Figure 7.2. Using this information the surplus ledge growth rate theory was developed.

As was previously outlined, the available surplus (negative) free energy is found by subtracting the surface free energy from the volume free energy .

$$\text{Surplus } \Delta G = (abc\ \Delta G_V) - ((2bc\ \sigma_1) + (2ac\ \sigma_2) + (2ab\ \sigma_3)) \quad (7.11)$$

The surplus free energy is consumed by high energy ledge surfaces which grow perpendicular to the overall crystal growth direction. Figure 7.9 shows the arrangement of the hypothesized ledges. The ledge shapes are assumed to be in proportion to the dimensions observed experimentally on the orthorhombic lithium disilicate crystal. For example, a square crystal face would be expected to have square surface ledges while an elongated crystal face would have surface ledges elongated in proportion to the overall crystal face shape.

The average surface free energy for a ledge surface on one of the crystal faces is calculated by assuming it to be proportional to the shape of the ledge (Figure 7.9) and to the temperature dependent surface free energy of that particular ledge surface. Using this approach, the average surface free energy per area for ledges on each of the orthorhombic faces can be calculated as follows:

$$\sigma_{ledge\ 1} = 2.7((4.5\ \sigma_2)+(1.0\ \sigma_3))/2.7(4.5+1.0)$$

$$\sigma_{ledge\ 1} = 0.818\ \sigma_2 + 0.182\ \sigma_3 \qquad (7.12)$$

$$\sigma_{ledge\ 2} = 1.0((4.5\ \sigma_1)+(2.7\ \sigma_3))/1.0(4.5+2.7)$$

$$\sigma_{ledge\ 2} = 0.625\ \sigma_1 + 0.375\ \sigma_3 \qquad (7.13)$$

$$\sigma_{ledge\ 3} = 4.5((2.7\ \sigma_2)+(1.0\ \sigma_1))/4.5(2.7+1.0)$$

$$\sigma_{ledge\ 3} = 0.730\ \sigma_2 + 0.270\ \sigma_1 \qquad (7.14)$$

The calculations involved in the development of the growth rate equation can be simplified if the relative amount of ledge surface area per crystal face is known with respect to the other crystal faces. The comparative ratio of ledge surface area per face is calculated by initially assuming that the crystal faces grow at rates proportional to the experimentally observed orthorhombic dimensions. Growth rates for each face can be defined in terms of the available ledge surface area (SA_n), the ledge velocity parallel to the crystal face (V_e), and the crystal face surface area as follows:

$$GR_1 = ((SA_1)*(V_e)) / 2bc \qquad (7.15)$$

$$GR_2 = ((SA_2)*(V_e)) / 2ac \qquad (7.16)$$

$$GR_3 = ((SA_3)*(V_e)) / 2ab \qquad (7.17)$$

The growth rates of faces 2 and 3 can be expressed in terms of face 1 as follows.

$$GR_1 = GR_1 \tag{7.18}$$

$$GR_2 = GR_1\ (1.0/2.7) = 0.3704\ GR_1 \tag{7.19}$$

$$GR_3 = GR_1\ (4.5/2.7) = 1.6667\ GR_1 \tag{7.20}$$

Substitution of these terms into the previously defined growth rate equations allows for the amount of ledge surface area for faces 2 and 3 to be defined in terms of face 1.

$$SA_1 = SA_1 \tag{7.21}$$

$$SA_2 = (2*ac*0.3704\ GR_1)/(V_e) = SA_1(0.3704*a/b) = SA_1 \tag{7.22}$$

$$SA_3 = (2*bc*1.6667\ GR_1)/(V_e) = SA_1(1.6667*a/c) = SA_1 \tag{7.23}$$

Therefore, $SA_1 = SA_2 = SA_3$

The term representing the ledge velocity parallel to the crystal face is also temperature dependent. (The other temperature dependent terms involved in the formulation of a growth rate equation are the volume free energy and the surface free energy.) The equation used to calculate the ledge velocity is one that has previously been established in the field of metallurgy.[32]

$$V_e = (3DL\Delta T)/(hRTT_m) \quad (7.24)$$

In this equation, D is the self-diffusion coefficient (defined below), L is the heat of fusion (7.3 Kcal/SiO_2) [66], ΔT is the degree of undercooling, h is the ledge height, R is the gas constant, and T_m is the melting temperature. The ledge height is assumed to be the lithium disilicate unit cell height for the orientation of that given crystal face.[67]

h_1 = 6 Å

h_2 = 15 Å

h_3 = 5 Å

The self-diffusion term is also a function of temperature.

$$D = D_o \exp(-E / k_B T) \quad (7.25)$$

In this equation, D_o is the pre-exponential diffusivity coefficient (2×10^9 m^2/sec), E is the activation energy for diffusion (440 KJ/mole) and k_B is the Boltzman constant.[68] From this data, the temperature-dependent V_e values for each crystal face are calculated as follows:

$$V_{e1}=(4.5E20)(1033-T)(1/(T+273))(\exp(-5.292E4/(T+273))) \quad (7.26)$$

$$V_{e2}=(1.12E21)(1033-T)(1/(T+273))(\exp(-5.292E4/(T+273))) \quad (7.27)$$

$$V_{e3}=(3.75E20)(1033-T)(1/(T+273))(\exp(-5.292E4/(T+273))) \quad (7.28)$$

For temperature in degrees Celsius, the above expression yields V_e in terms of cm/sec.

Using the above information, the equation for the temperature and size dependent growth rate equation can be calculated. The available ledge surface area for any of the orthorhombic crystal's faces is shown below.

$$SA=((3.8515E10-39.123\ T)\ b^3\ -(1125.8+4.218\ T)\ b^2)/(52.58+0.327\ T) \quad (7.29)$$

Using this equation, the growth rate equations can be calculated. The growth rate equation is assigned the number corresponding to the crystal face which is perpendicular to the growth vector.

$$GR_1 = (SA\ V_{e1}) / 2bc \quad (7.30)$$

$$GR_2 = (SA\ V_{e2}) / 2ac \quad (7.31)$$

$$GR_3 = (SA\ V_{e3}) / 2ab \quad (7.32)$$

7.3: Results

The growth rate equations are used to generate data which can be compared to equivalent experimental data. The first comparisons are made between data generated using the experimentally derived growth rate equation and experimentally measured data. The goal of this test is to show the validity of the experimentally derived equations. Once this is established, it is reasonable to use the experimentally derived equation as a good approximation of the

actual ("true") growth rate equation in comparison with the theoretically derived growth rate equation.

As previously stated, data for the number of crystals optically observable (> 1 μm) as a function of time was measured for three different isothermal temperatures: 470°C, 490°C, and 550°C. Figs. 7.10, 7.11 and 7.12 show these data sets with the corresponding data set derived from the experimental growth rate equation. Because the computer simulation of the growing precrystal distribution involves a series of discrete sizes compared with a continuum of precrystal sizes, it was expected that the number of crystals formed per unittime by simulation does not equal that seen experimentally. To account for this, the simulated values are scaled in terms of a constant needed to make the maximum derived crystal popluation density equal to the maximum experimental crystal population density.

A good match is seen between the equation derived data and experimentally measured data for all three temperatures. However, the calculated data tends to overestimate the number of crystals measured during the intermediate portion of the microstructural development. This trend increases as the isothermal temperature is increased.

Since it has been observed that the simulation using the experimentally derived growth rate equation is a reasonably good predictor of experimentally measured data, the experimentally derived growth rate equation is now used in comparison to the theoretically derived growth rate equation. This comparison is shown for the 470°C isothermal temperature in Fig. 7.13. The growth

rates shown are for orthorhombic crystal face 1. The thermodynamically derived growth equation is also shown with a ledge surface area limit imposed. The theoretically predicted maximum growth rate matches the experimental rate when a surface saturation factor (n) of 4.5 is used. The significance of this will be discussed later. Figure 7.13 shows the correlation between the experimental growth rate equation and the thermodynamic growth rate equation. A significant difference between the two equations exists only for the smallest sized crystals. For crystal sizes below that associated with thermodynamic stability, the thermodynamically derived growth rate equation predicts a negative growth rate while the experimentally derived growth rate equation predicts a positive growth rate.

7.4: Discussion

7.4.1: Experimentally Derived Growth Rate Equation

The reason for developing the experimentally derived growth rate equation is to use it as an approximation of the true growth rate equation for comparison with theoretically derived growth rate equations. The functions which drive the experimental equation are based on mathematical curve fitting of experimental data. The interpretation of these mathematically produced equations in terms of their atomistic relevance was not attempted. Rather, they are used as a simulator of the true growth rate equation.

As shown in the results section, the data produced through the use of the experimental equation in the growth simulation program

matches well with the experimentally measured glass crystallization, especially at the lower temperatures investigated. As the temperature is increased, the experimental values increases in magnitude faster than the experimentally measured data. This is due to the experimental equation being based on the concept of the evolving precrystal distribution such that a steady-state flux of growing crystals is produced. Since lower temperatures at longer times produce microstructures which are dominated by crystals originating from the smaller sized precrystal sites and the experimentally derived equation tends to fit best the linear portions of the lower isothermal temperature data, it can be concluded that the experimentally derived equation models the growth of the smaller sized crystals adequately but increasingly overestimates the growth rates for larger sized crystals as the temperature increases.

7.4.2: Theoretically Derived Growth Rate Equation

The thermodynamically derived equation was shown to match the experimentally derived equation adequately in terms of magnitude and location. Because of the validity of the experimental equation, the good correlation observed with the thermodynamic equation supports to the methodology used to develop the thermodynamic equation.

For crystals in the size range 9.1e-8 cm to 1.2e-7 cm the thermodynamically derived equation overestimates the experimental values and therefore it is assumed to also overestimate the true growth rates. Overestimation of the growth rate can be ascribed to

the lack of a delay factor in initiation of new ledge sites. The theory was formulated by assuming instant ledge nucleation once conditions were such that the ledge would be thermodynamically stable if it were in existence. A delay period for the formation of ledges would appear to help the theory coincide with the true function. Potentially, statistical mechanics could be used to predict the time period that might precede each surface nucleation event.

Once the crystal size has become sufficiently large, further increases in size do not affect the measured isothermal growth rate. Crystals in this size range will be termed bulk size crystals. A growth rate equation should account for this effect. It is logical to assume that the surface of the growing crystal will reach a maximum ledge density at a certain crystal size. For the thermodynamic model, the ledge density needed to yield the experimentally observed bulk size crystal growth ratecan be calculated.

Using an isothermal temperature of 470°C, the observed growth rate (1.8E-10 cm/sec), and the crystal face 1:

$$GR_1 = (8.2651E\text{-}4)(b) - 6.6696E\text{-}11 \text{ [cm/sec]} \qquad (7.33)$$

solving for b : b = 2.98E-7 cm

$$SA_{1\ max} = (n)(2bc) = (1.867E8)(b\text{^}3) - (15.071)(b\text{^}2) \qquad (7.34)$$

solving for n : n = 4.5

The maximum allowable ledge surface area is calculated by

multiplying the crystal face surface area by a term (n) which accounts for the topography of the surface. Making the simplifying assumption of cubic surface units, a three level ledge surface structure would have an n value of 1.44, a two level structure has an n of 1.78, and a single level structure has an n of 4.0. Fig. 7.14 shows these hypothetical ledge structures. The calculated value of n=4.5 suggests that the surface of the crystal evolves towards a single level ledge structure as the crystal grows and the growth rate approaches a maximum. The concept of a single level ledge structure is synonymous with that of a normal growth mechanism. This implies that once a crystal reaches bulk size, "nucleation" on surface sites occurs at a rate roughly equal to the ledge growth rate. The idea of a crystallization front decreasing in ledge complexity as the growth rate increases parallels Cahn's work[32] which suggests a transition from a ledge growth mechanism to a normal growth mechanism as a function of crystal size.

It has been shown that the theoretically derived growth rate equation is very similar in shape and magnitude to the experimentally derived growth rate equation. Because the experimentally derived equation was able to predict the observed evolution of the lithium disilicate microstructure, it is assumed to be a good approximation of the true growth rate equation. It is of interest to compare, in a similar manner, a growth rate equation based on classical homogeneous nucleation theory. Kelton and Greer[68-70] developed such a growth rate equation by modeling the dynamics of cluster formation through a series of bimolecular reactions. Kelton and Greer used this simulation to investigate the

formation and growth of crystalline nuclei during a quench from melt temperatures. The resulting equation predicts the crystal growth rate as a function of temperature and crystal size, the same terms used in the thermodynamically derived growth rate equation. The equation is shown below.

$$\frac{dr}{dt} = \frac{16D}{\lambda^2}\left(\frac{3V}{4\pi}\right)^{1/3}\sinh\left[\frac{V}{2K_BT}\left(\Delta G_v - \frac{2\sigma_A}{r}\right)\right] \qquad (7.35)$$

where D = diffusion coefficient

V = molar volume

λ = jump distance

Figure 7.15 compares the data generated from the classically derived growth rate equation and from the experimentally derived growth rate equation. The values are growth rates as a function of crystal size for lithium disilicate at 470°C. It can be easily seen that significant differences exist between the classically predicted growth rate equation and the approximate true growth rate equation. The introduction of the precrystal idea to the classically derived approach would result in a shift of the growth rate curve towards smaller crystal sizes. Such a shift would improve the comparison of this theory with the experimentally derived equation.

7.4.3: Surface-to-Volume Ratio Growth Rate Equation

The main concept behind the thermodynamic development of a crystal growth rate equation is the competition between volume free energy and surface free energy. The balance between these two

factors was shown to be a function of the crystal size. The most common parameter to characterize this competition is the surface to volume ratio. A very simplistic analysis was performed for the growing lithium disilicate crystals. Referring back to the orthorhombic crystal (Fig. 7.2), the surface-to-volume ratio can be calculated as follows:

volume = (4.5n)(2.7n)(1.0n)

surface = (4.5n)(2.7n)(2) + (4.5n)(1.0n)(2) + (2.7n)(1.0n)(2)

n is a unitless linear dimension of crystal size

$$\text{surface-to-volume ratio} = 3.18518/n \tag{7.36}$$

Therefore, as the crystal grows (n increases), the ratio of surface area to volume decreases. This ratio can then be used to control the effect of crystal size on the crystal growth rate. A simplistic growth rate equation based on this ratio is shown below.

$$\text{growth rate} = (\text{large crystal growth rate})(1-(3.18518/n)) \tag{7.37}$$

Fig. 7.16 is a plot of this equation. The plotted shape from the equation is very similar to that generated from the thermodynamically derived equation (Fig. 7.13). Since, as was mentioned earlier, the basis for the thermodynamic derivation is the competition between surface and volume energies, it is expected that the two equations should generate similar plots. Note that, as with the thermodynamically derived equation, the surface-to-

volume equation does not predict the tail seen in the very small crystal region of the experimentally derived equation. This very small region, however, has little physical significance because it is in the size range of a single silica tetrahedron and smaller. If every tetrahedron is considered a crystal site then the glassy state is already 100% crystallized and the only modification to the microstructure would be a result of a coarsening process.

7.4.4: A Method for Deriving the Optimum Heat Treatment from the Growth Equation

If the growth rate of a crystal is known as a function of temperature and crystal size, it should be possible to mathematically derive the optimum heat treatment schedule from the growth rate equation. An optimum heat treatment schedule must continuously predict the unique temperature which produces the maximum growth rate for the smallest crystal of microstructural importance to the final microstructure at that point in time. A hypothetical true growth rate equation is plotted against temperature and crystal size in Fig. 7.17. For a certain size crystal, the temperature which produces the maximum growth rate is found by setting the first derivative of the growth rate equation to zero. The derivative is taken in terms of temperature while crystal size is held constant. This is shown graphically in Fig. 7.18. A plot of the temperature that results in maximum growth rates versus crystal size can be constructed. Such a plot is shown in Fig. 7.19a. Note that this curve should approximate that produced by plotting the highest temperature for stability versus crystal size. Since the heat treatment schedule is traditionally formulated in terms of time

versus temperature, it is necessary to convert the information in Fig. 7.19a to this form. The information in Fig. 7.19a can be used to plot the maximum growth rate versus crystal size by converting the temperature data to the growth rate at each temperature. This is shown in Fig. 7.19b. Now that the maximum growth rate is expressed as a function of crystal size, the amount of time required to produce a crystal of a given size (using the defined growth rates) can be determined by integrating the inverse of the function shown in Fig. 7.19b from the smallest precrystal size reasonable to the crystal size b. In this case, the smallest precrystal size would be that of a unit cell of lithium disilicate. A plot of the calculated time values versus the associated crystal size values is shown in Fig. 7.19c. Comparison of Figs. 7.19a and 7.19c reveals that the temperature and the time needed for an optimum heat treatment schedule have both been defined as a function of crystal size. For each b value these plots yield a unique temperature and time which is the optimum heat treatment schedule. The schematic plot for such a derived schedule is shown in Fig. 7.19d.

Converting a growth rate equation to the form of a heat treatment schedule should serve as a test of the equation's accuracy. Accuracy could be evaluated through comparison of the mathematically derived heat treatment schedule with an experimentally found schedule. Such an approach was taken using the experimentally derived growth rate equation. The results of this approach showed that differences exist between a true growth rate equation and that developed experimentally. These differences were not large enough to significantly affect the number of crystals

observed as a function of time but are significant enough as to make transformation of this equation into a realistic optimum heat treatment schedule impossible.

It is important to note that of the four components of the experimental growth rate equation, two are size dependent and two are temperature dependent. Of the two temperature dependent factors, V and bulk growth rate, V decreases with increasing temperature while bulk growth rate increases with increasing temperature. It was found that as temperature is increased, initially the bulk growth rate term dominates and the resulting growth rate increases. However, at temperatures above 460°C the V term will dominate over the bulk growth rate term, producing the net effect of a decreasing growth rate as a function of temperature. The hill-shaped growth rate curve produced is similar in form to that seen experimentally. This is shown schematically in Fig. 7.20. While it is predicted that the magnitude of the growth rate is dependent upon crystal size, Fig. 20 conflicts with the experimentally observed trend because the location of the growth rate maximum is predicted to be dependent upon crystal size. Because of this inconsistency, the simplicity of the V term is thought to be a source of error in the growth rate equation.

Taking the first derivative of the experimental growth rate equation in terms of temperature and setting it to zero results in the maximum growth rate temperature being independent of crystal size. This maximum occurs at approximately 460°C. However, this result is independent of crystal size is not realistic and is derived from the error in the V term. Refinement of the V term may be able

to produce an equation which can be transformed into an optimum heat treatment schedule. It can be seen through comparison of Figs. 7.17 and 7.20 that modification of the V term or addition of another term is needed to push the maximum growth rate towards higher temperatures as the crystal size increases. Improvement in the V term could come by more accurately reproducing the increasing slope measured experimentally in the plot of the number of crystals versus time, compared to the current V term which produces a more constant slope. An improved V term should also be influenced by b as well as by temperature. It should be noted that this technique for experimentally determining the growth rate equation may not be precise enough to produce an equation which can be reliably transformed into an optimum heat treatment schedule. If this is true, the best alternative for this system would be a TEM study to improve the precision of the data.

To demonstrate the transformation method the following example is presented. Because of the lack of a sufficiently accurate experimental growth rate function, approximate functions are used. Therefore, the heat treatment schedule generated is not the optimum schedule, but if the schedule produced approximates the schedule derived experimentally, the transformation method is would be given credibility. It can be seen in Fig. 7.17, the temperature for crystal stability is greater than the maximum growth rate temperature for all crystal sizes, but it should approximately parallel the maximum growth rate temperature. It is possible to then use the thermodynamically defined temperature/crystal size relationship as the starting point for the mathematical transformation to yield a

heat treatment schedule. The resulting schedule will not be an optimum schedule but should have the same general form as an optimum schedule. For this reason, it will be termed a mock-optimum schedule. The stability relationship is shown in Fig. 7.21 and can be expressed as follows:

Stability T[°C] = ((2.044e10*b^1)+12.825)/((1.932e7*b^1)+2.11) (7.38)

The above equation predicts a maximum temperature for stability which matches well with the experimentally found value. The lower stability temperatures and the crystal size region where the most significant changes in stability temperature occur do not match experimentally determined values. To make this equation more realistic, a slightly modified version of this equation will be used.

$T_{stability}$=((2.044e10*b^1.5)+(12.825*72.7))/((1.932e7*b^1.5)+2.11) (7.39)

Using the previously defined stability temperatures, a growth rate can be associated with each crystal size. The relationship between temperature and bulk crystal growth rate will be used to yield growth rate values for each crystal size. Because a bulk size growth rate is being used as opposed to a more accurate size dependent growth rate, it was necessary to multiply the bulk growth rate equation by a factor of 0.01 to account for the slower growth rates experienced by the smaller-sized crystals.

$$GR = \exp[(-1.142e10)(T_{stability})^{-3.2523}]*0.01 \quad (7.40)$$

This relationship is shown graphically in Fig. 7.22. Growth rate versus crystal size must now be converted to the time required to reach a given crystal size versus that crystal size. As was stated previously, this is accomplished through integration of the inverse of the growth rate/crystal size function over the range of crystal sizes. This was done numerically using an algorithm based on Simpson's rule. The plot of time versus crystal size is shown in Fig. 7.23. Now that both the optimum processing temperature and the optimum processing time have been defined in terms of a common parameter, i.e.,the crystal size, the two sets of information can easily be combined to yield the mock-optimum heat treatment schedule. The resulting schedule is shown in Fig. 7.24. In Fig. 7.24, the calculated schedule is plotted as well as a modified schedule which takes into account the experimentally measured temperature of maximum growth rate for bulk-sized crystals (950°C).

The above exercise demonstrates that the suggested method of generating an optimum heat treatment schedule from a growth rate equation is viable. The fact that the resulting mock-optimum schedule reasonably resembles an experimentally derived optimum heat treatment schedule establishes this validity. The transformation method can be used to generate the optimum heat treatment schedule from growth rate equations determined experimentally or theoretically.

7.5: Conclusion

The crystal growth rate equation is considered the fundamental basis for an optimum heat treatment schedule for glass-ceramic materials. An experimental method for determining the crystal growth rate equation has been developed and demonstrated. The use of this equation to predict experimentally measured microstructure evolution was shown. Because the derived equation predicted fairly accurately what was observed experimentally, the equation is assumed to be a good approximation for the true growth rate equation.

A theory has been proposed which predicts a crystal growth rate equation by allotting surplus free energy to surface ledge units which are responsible for crystal growth. Comparison of plots of crystal growth behavior based on the theoretically derived equation and the experimentally derived equation show enough correlation to accept the theoretical approach for further study.

A transformation method was developed to convert a growth rate equation into an optimum heat treatment schedule. The transformation was unsuccessfully attempted on the experimentally derived equation. The main reason for the flaw in the experimentally derived equation was the insufficient temperature dependence of the V term. A mock-optimum heat treatment schedule was successfully generated using the transformation method and a modified growth rate equation. The form of the heat treatment generated corresponds with that which was constructed experimentally. This good correlation gives credibility to the transformation technique.

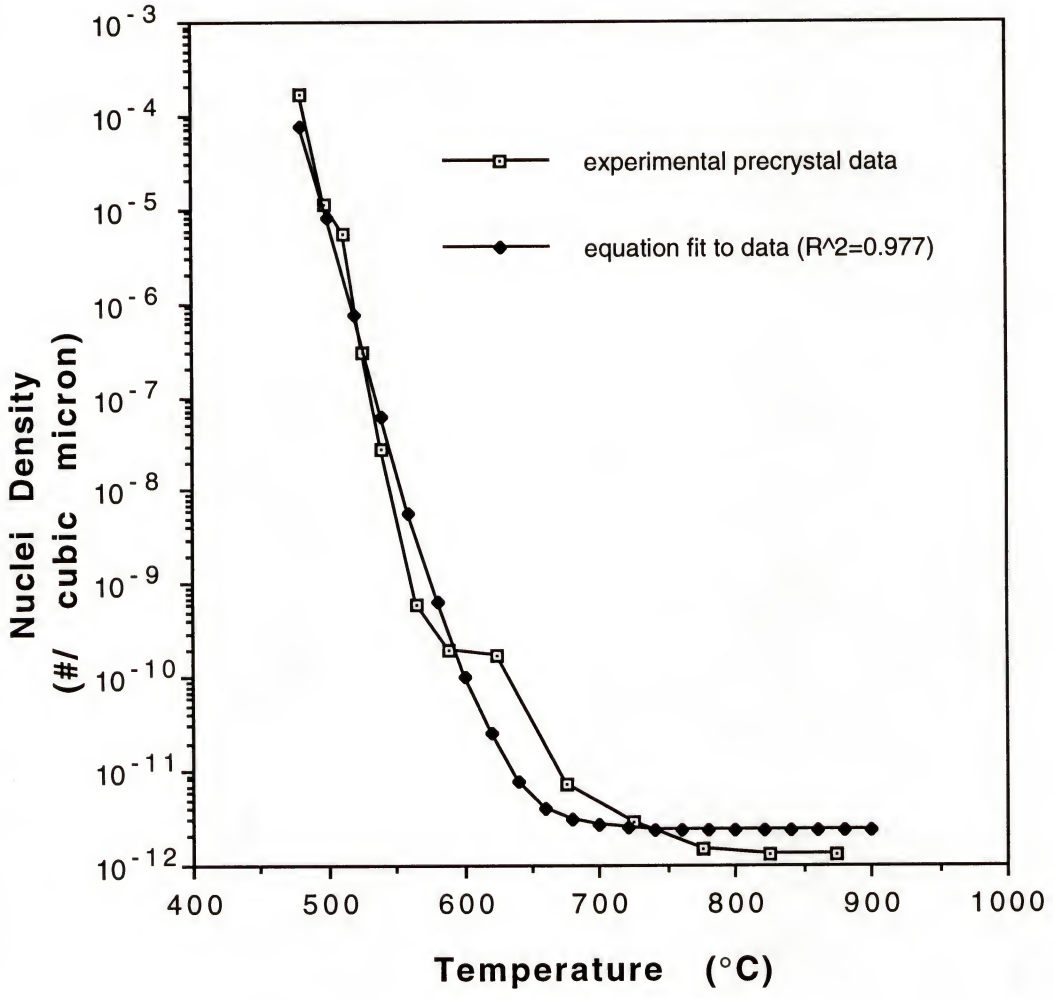

Figure 7.1 : Precrystal density data and the equation fit to the data for lithium disilicate

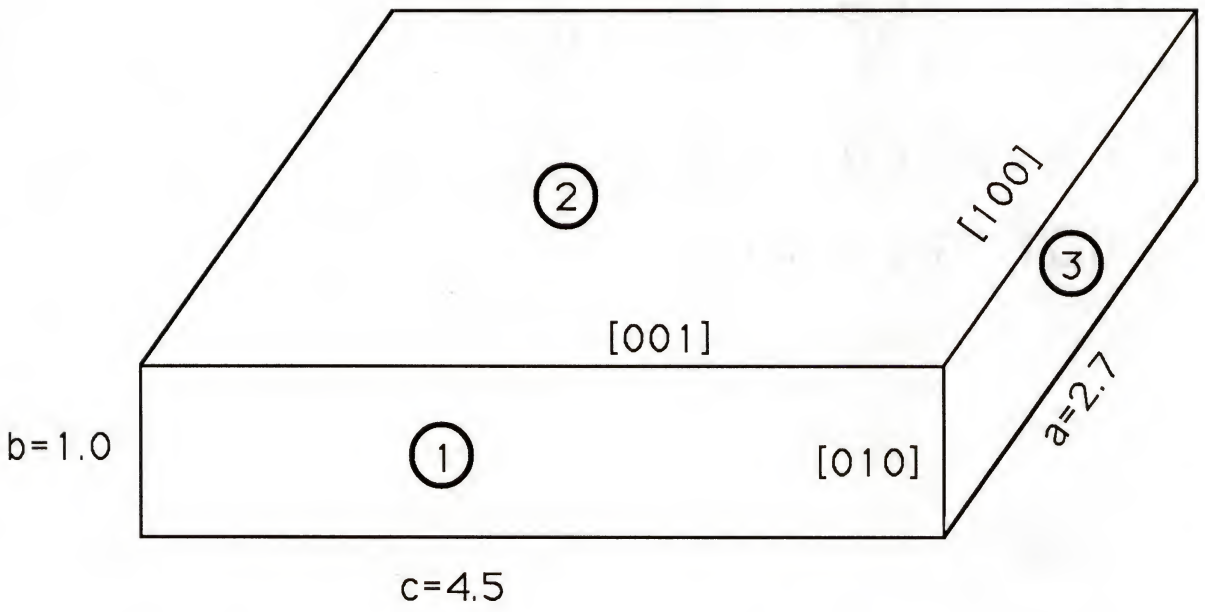

Figure 7.2 : Orthorhombic shape of lithium disilicate nuclei as measured by TEM observation.

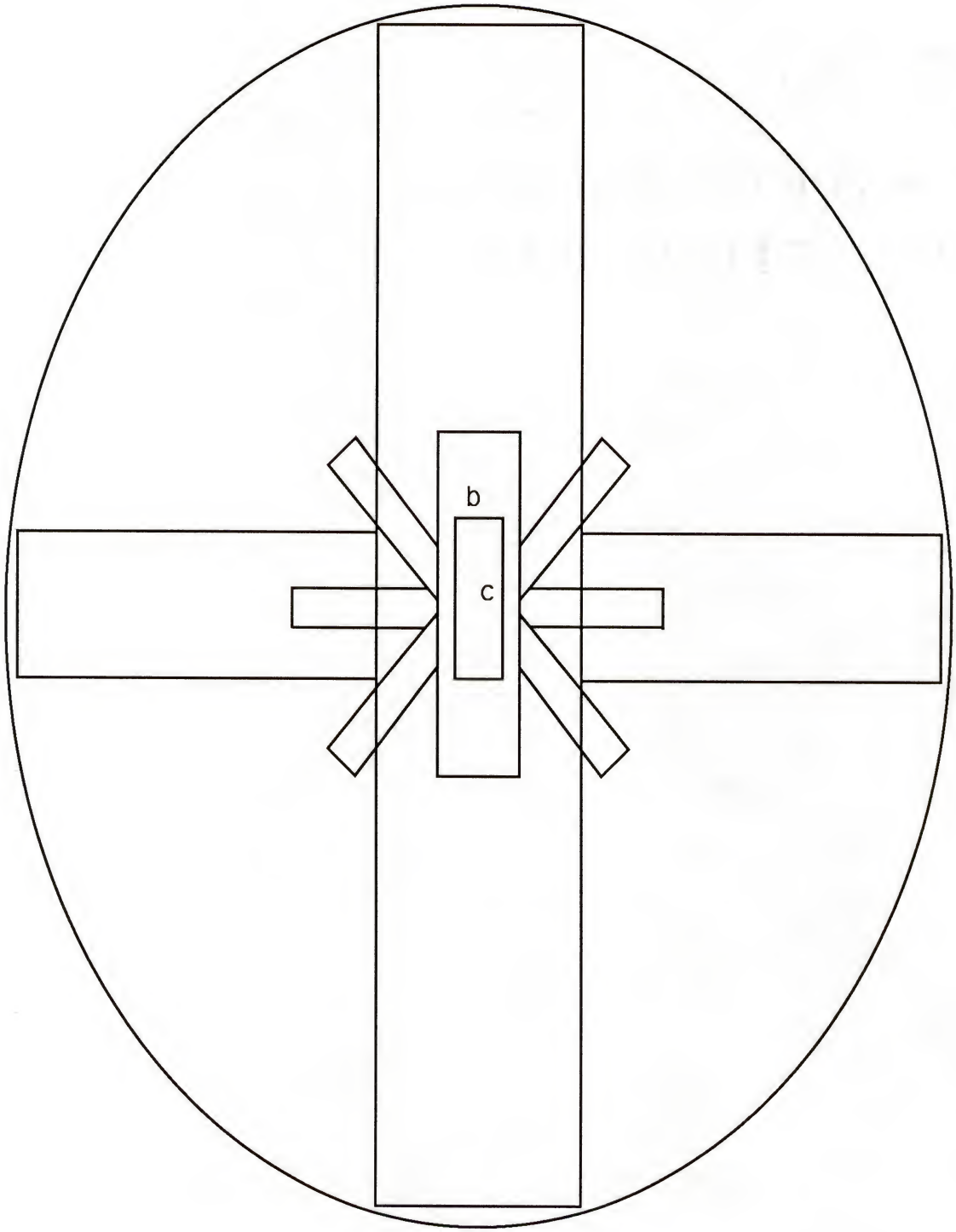

Figure 7.3 : Shape of lithium disilicate spherulite formed from twinning of orthorhombic lithium disilicate nuclei.

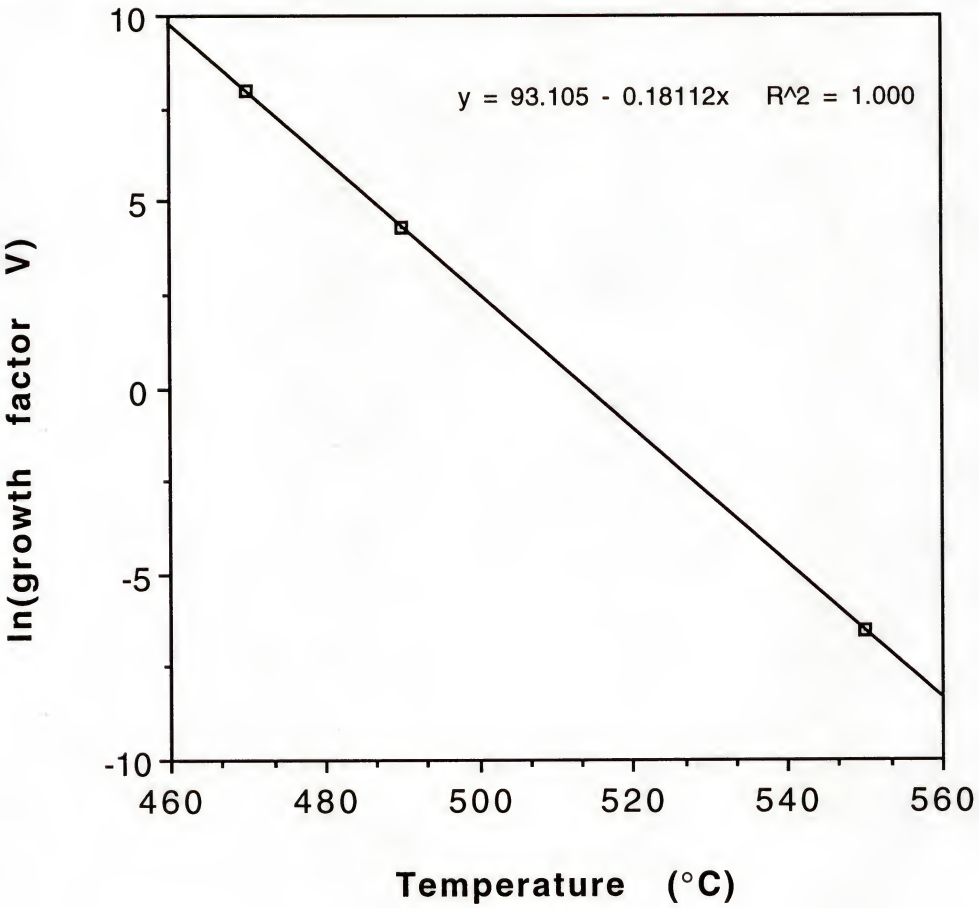

Figure 7.4 : Experimentally derived growth equation factor (V) as a function of growth temperature, for lithium disilicate

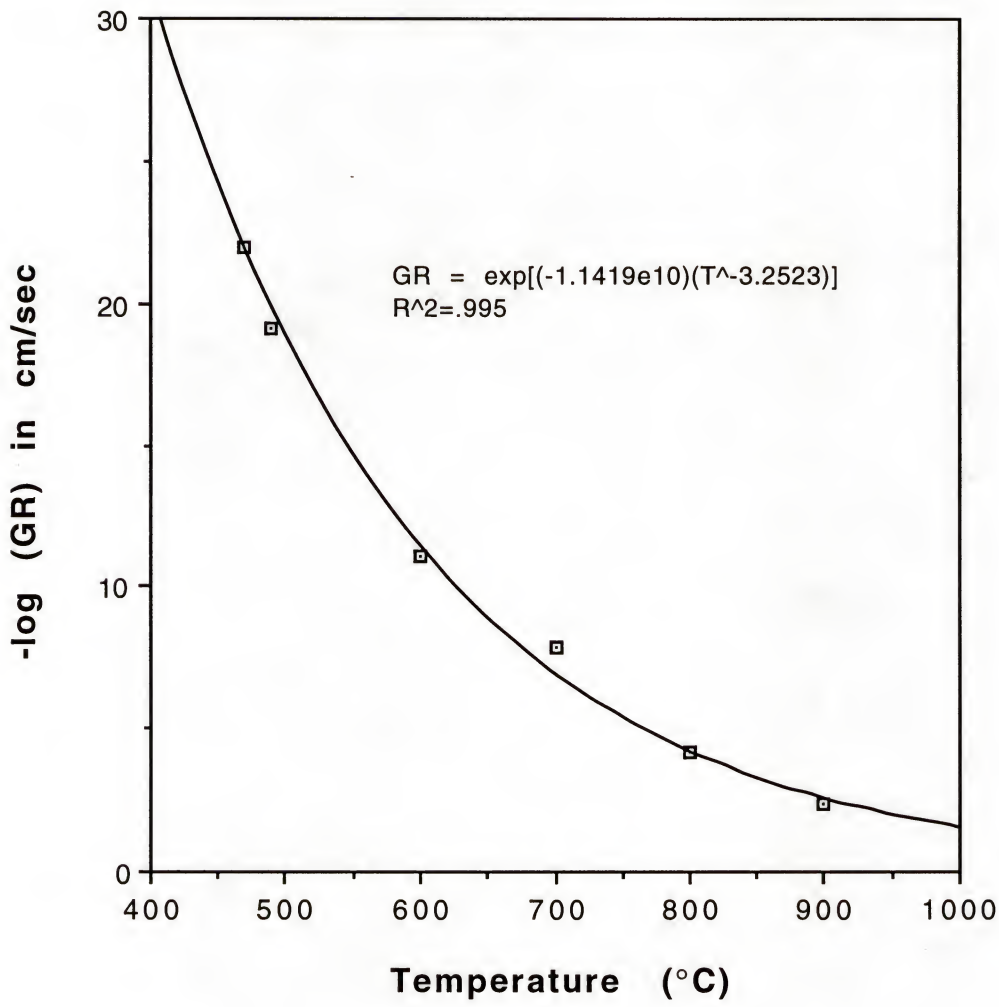

Figure 7.5 : Lithium disilicate bulk crystal growth rate as a function of temperature.

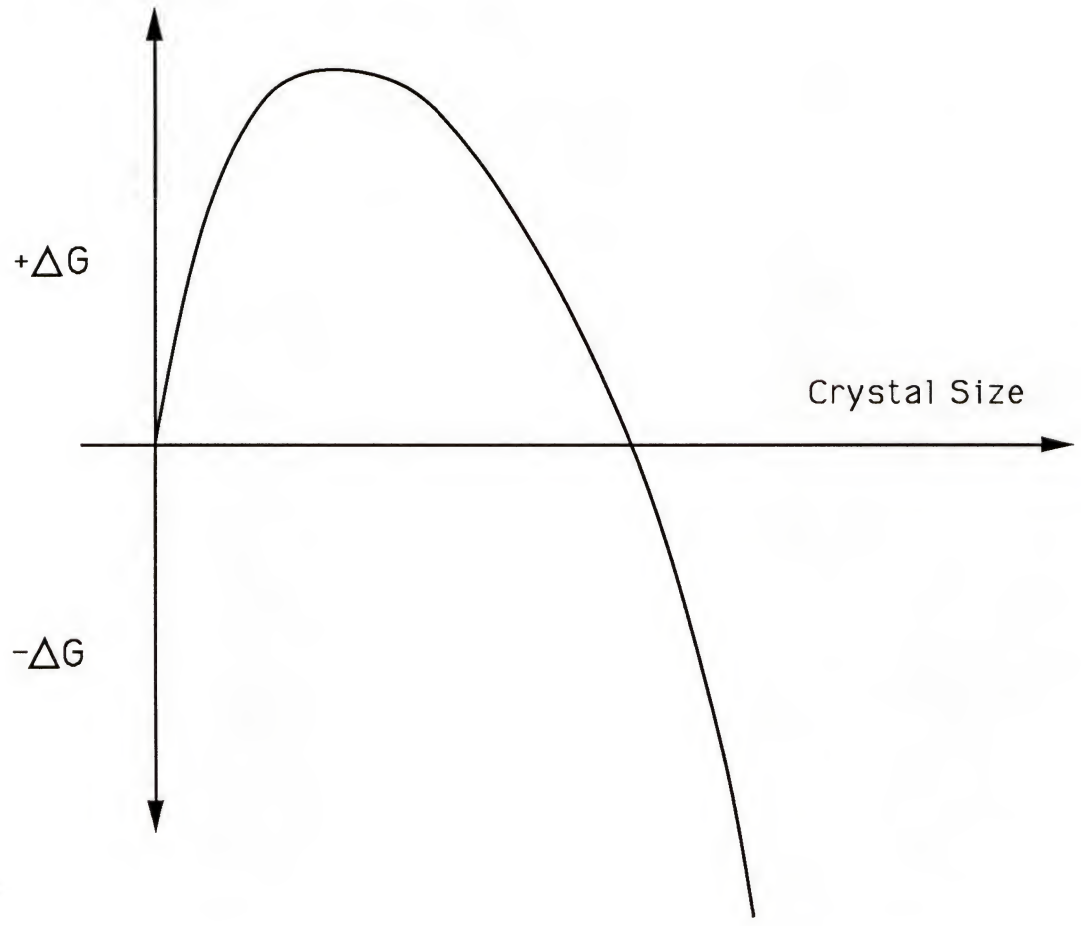

Figure 7.6 : Total free energy of a crystal (volume plus surface) as a function of the crystal size. Crystal shape is assumed to be spherical.

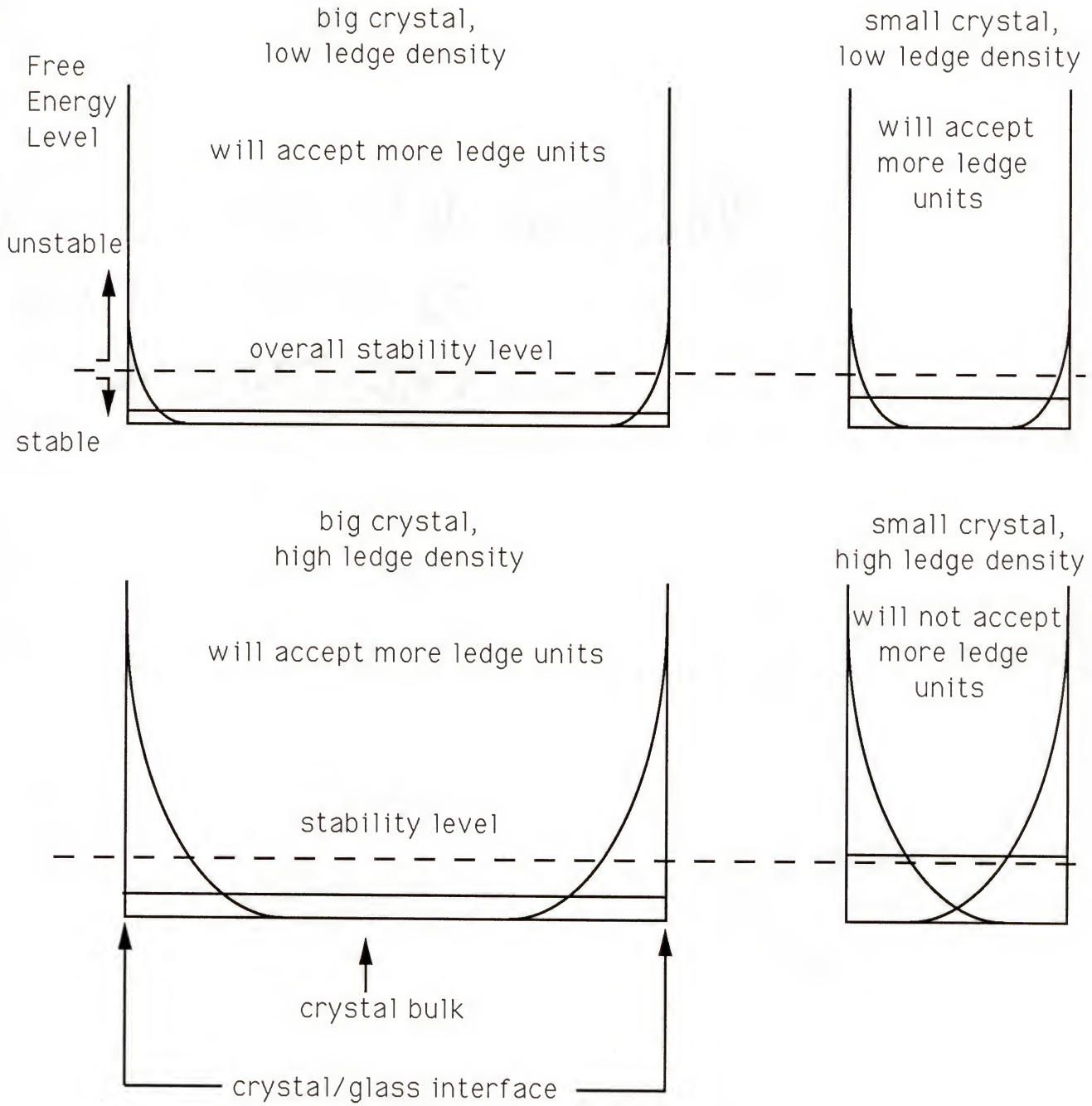

Figure 7.7 : Schematic representation of the effect of crystal size and ledge number density on the stability of newly formed ledges.

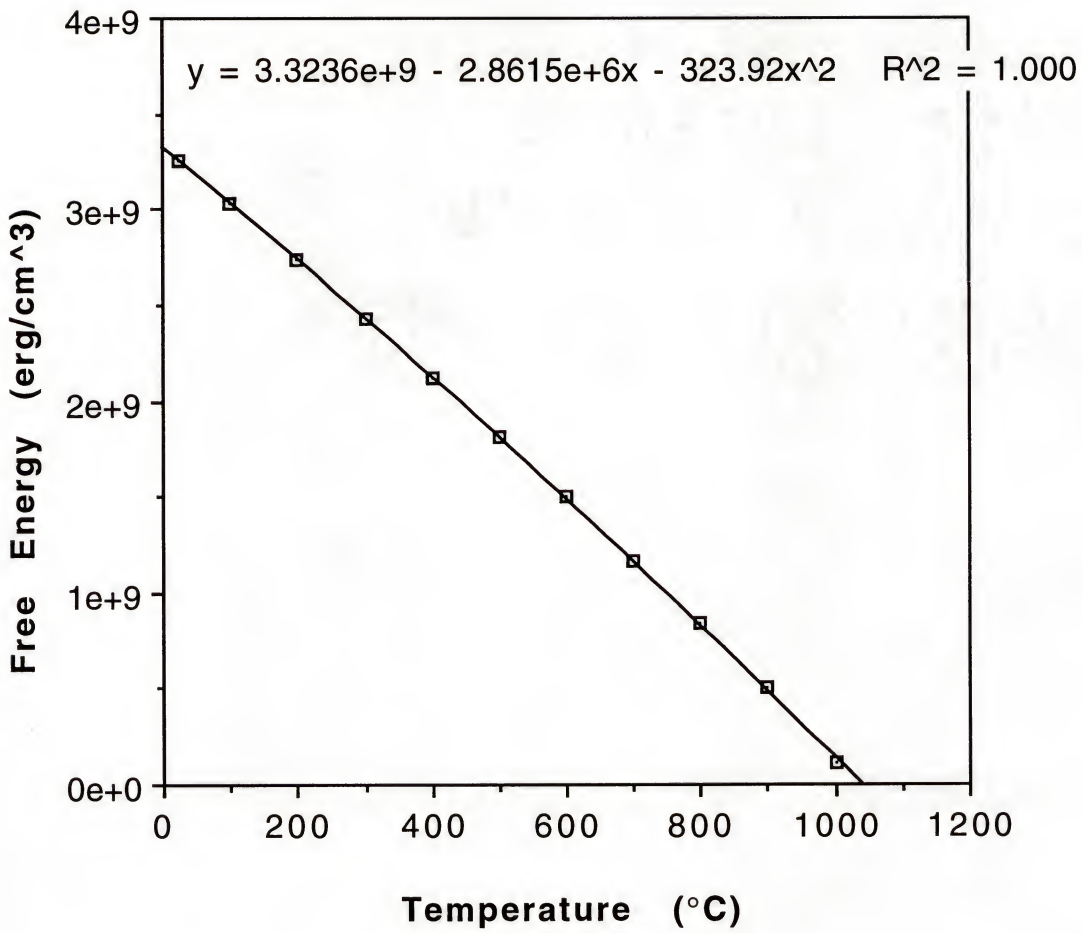

Figure 7.8 : Volume free energy data for the crystallization of lithium disilicate, from reference #65.

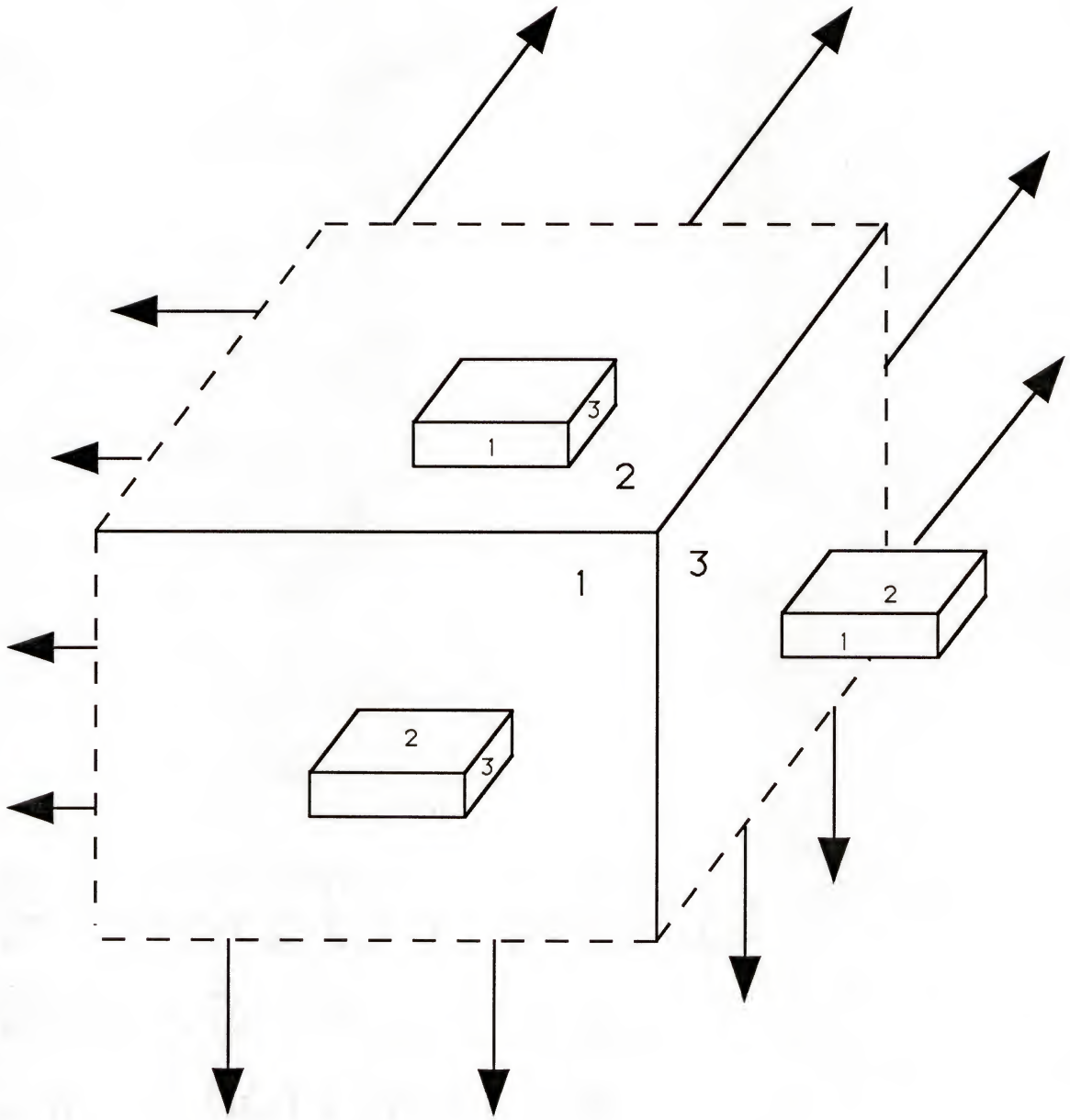

Figure 7.9 : Schematic of orthorhombic surface ledges on the faces of an orthorhombic lithium disilicate crystal. Active ledge growth surfaces are numbered.

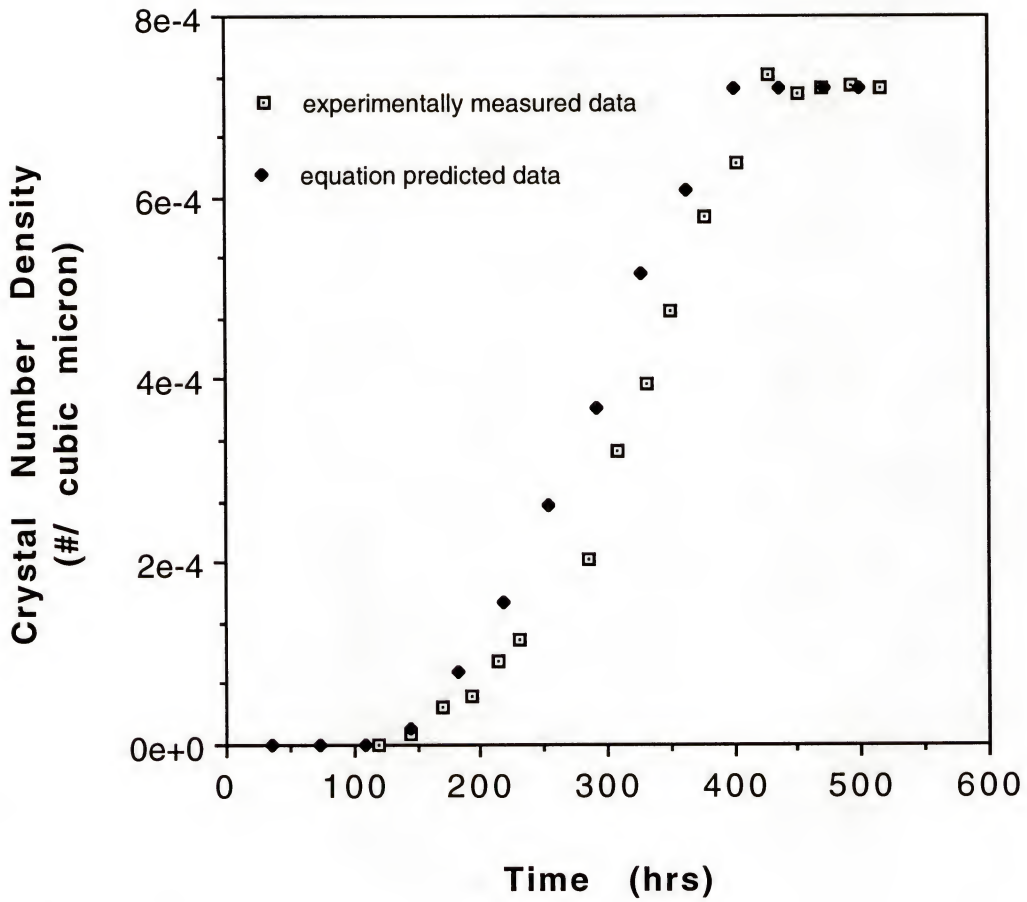

Figure 7.10 : Comparison of experimental and equation predicted data for the evolution of the number density of lithium disilicate crystals for an isothermal temperature of 470°C.

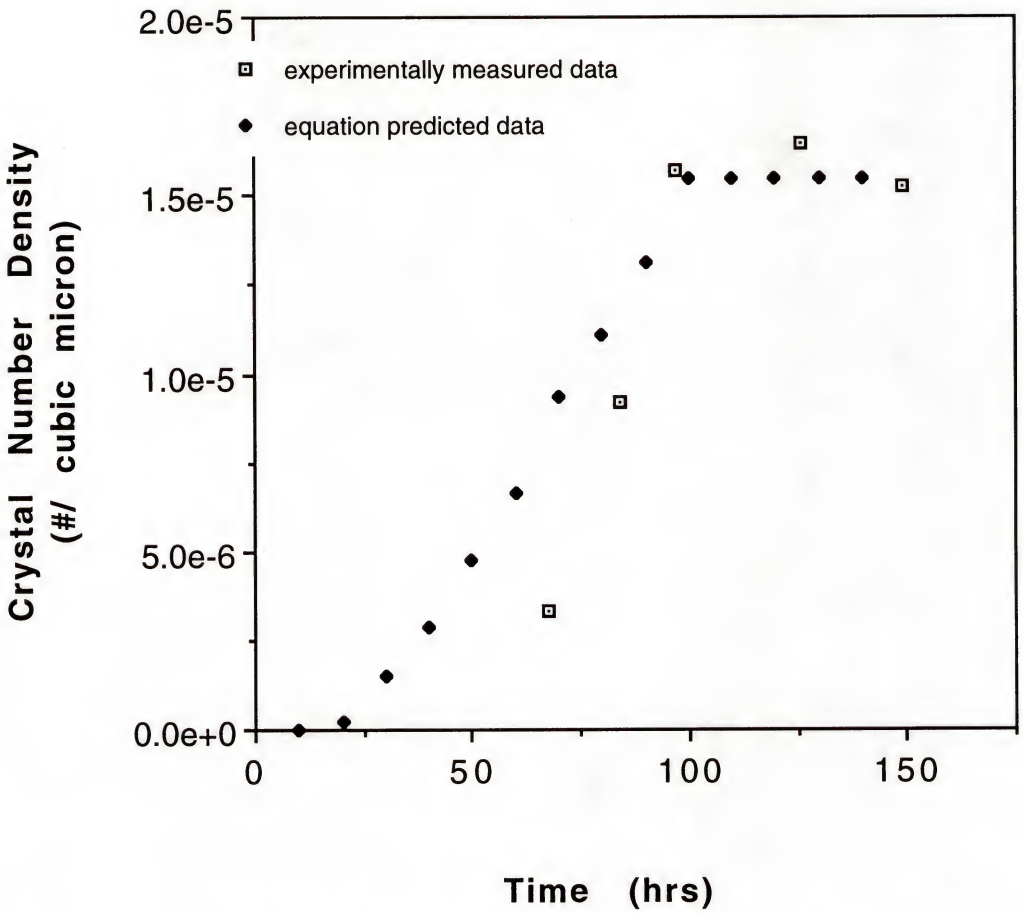

Figure 7.11 : Comparison of experimental and equation predicted data for the evolution of lithium disilicate crystals for an isothermal temperature of 490°C.

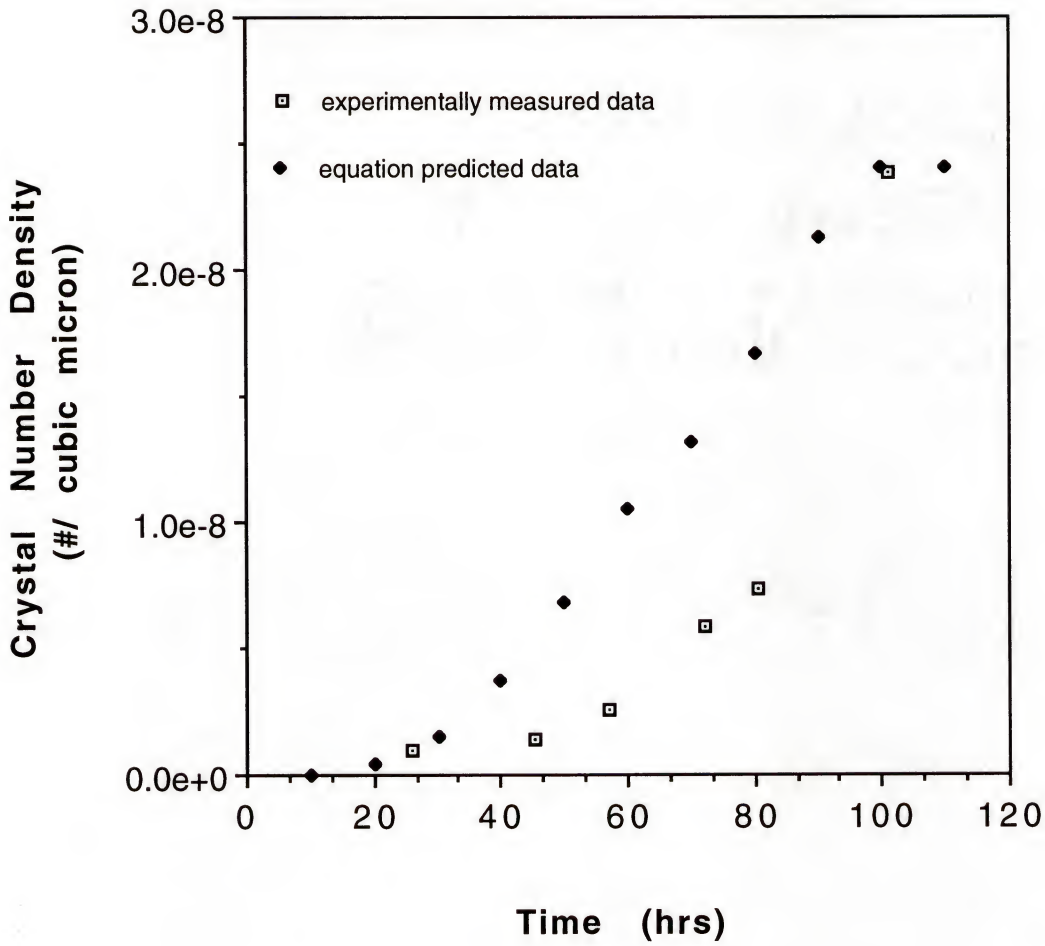

Figure 7.12 : Comparison of experimental and equation predicted data for the evolution of lithium disilicate crystals for an isothermal temperature of 550°C.

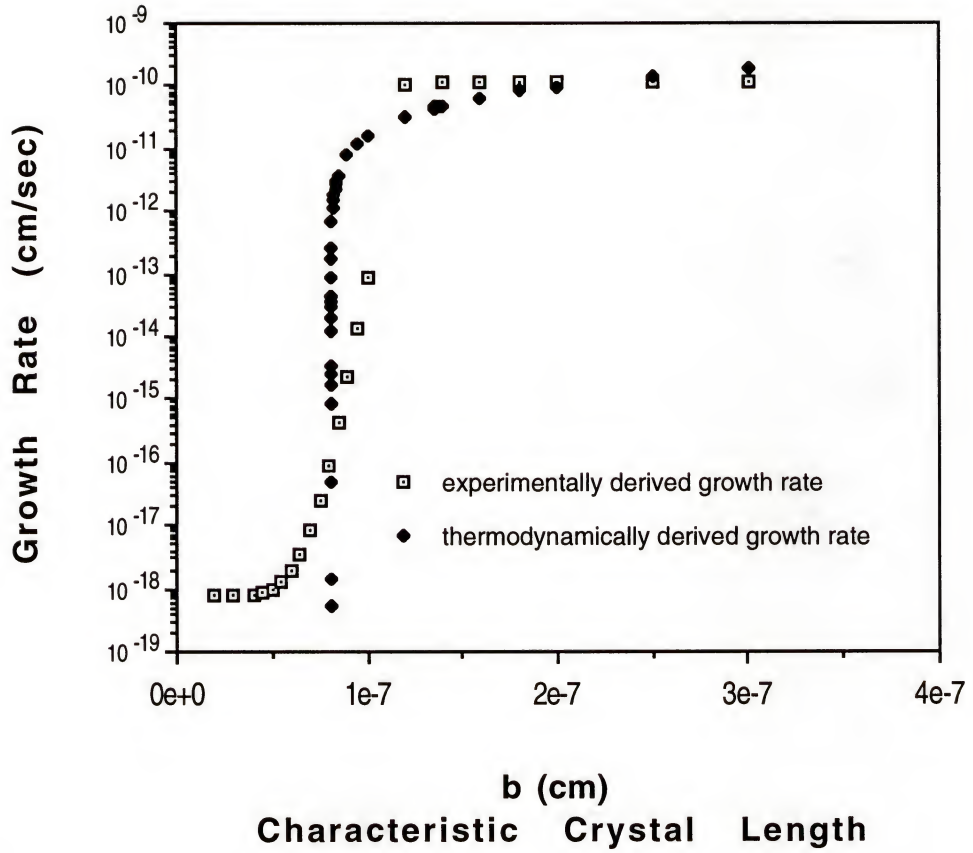

Figure 7.13 : Comparison of the predicted growth rates for the experimentally derived growth rate equation and the thermodynamically derived growth rate equation for lithium disilicate at 470°C.

single
level

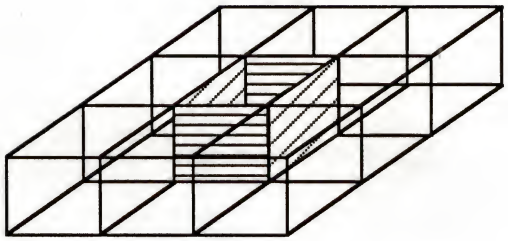

4 edge surfaces / 1 top surface

n = 4

two
levels

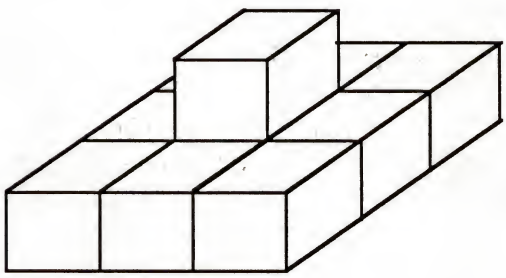

16 edge surfaces / 9 top surfaces

n = 1.78

three
levels

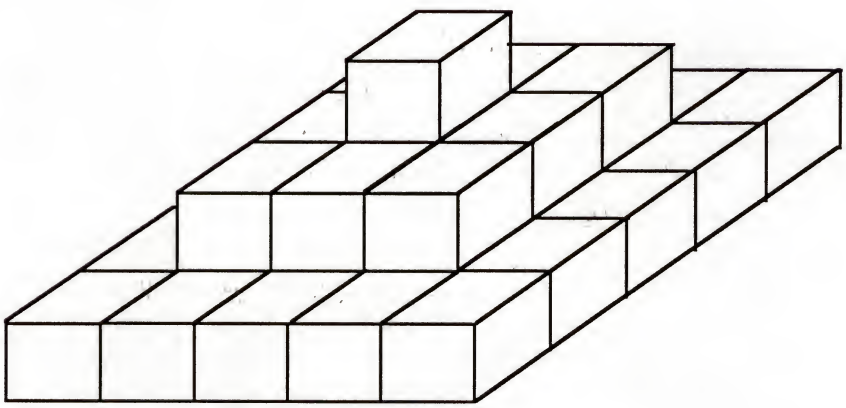

36 edge surfaces / 25 top surfaces

n = 1.44

Figure 7.14 : Various surface ledge layers and their associated n values. The n value characterizes the amount of ledge edge surface area per surface area covered.

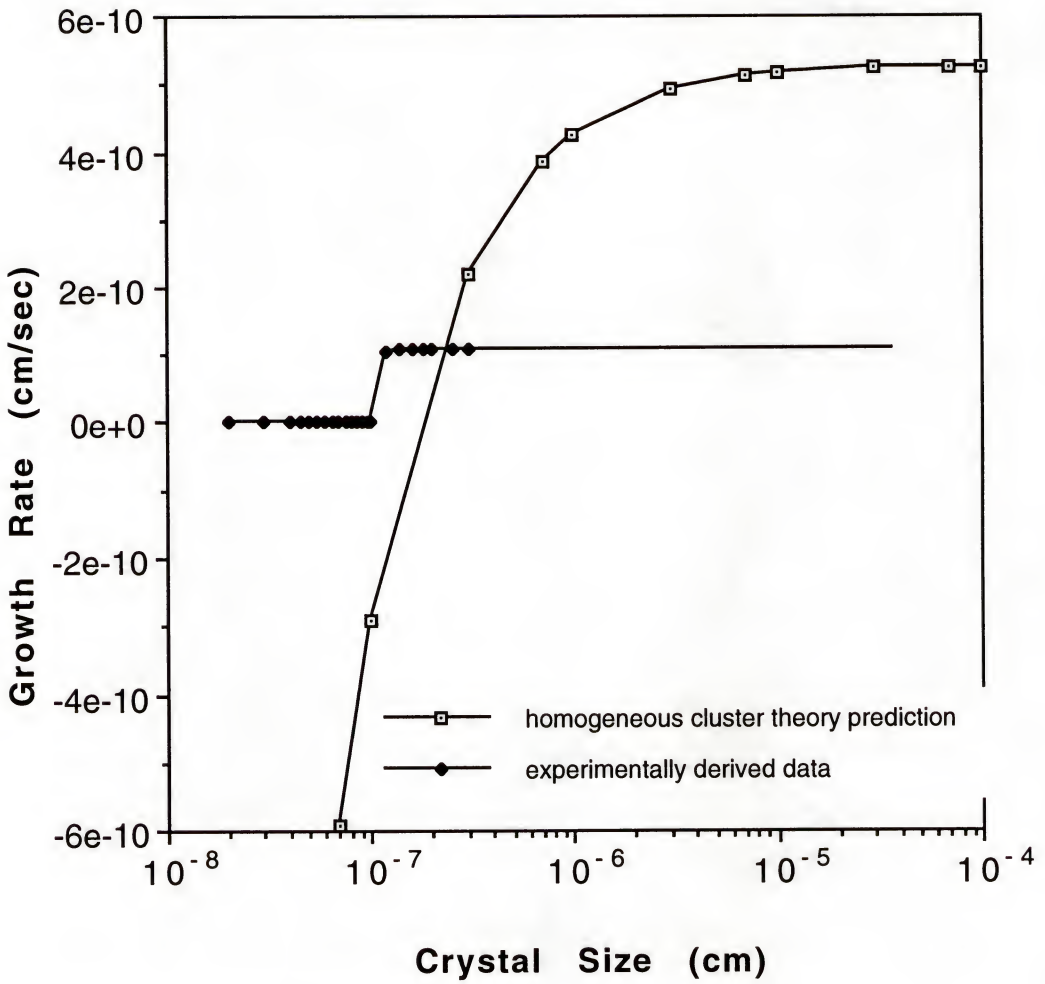

Figure 7.15 : Comparison of homogeneous classical theory based cluster growth equation to the experimentally generated data for lithium disilicate.

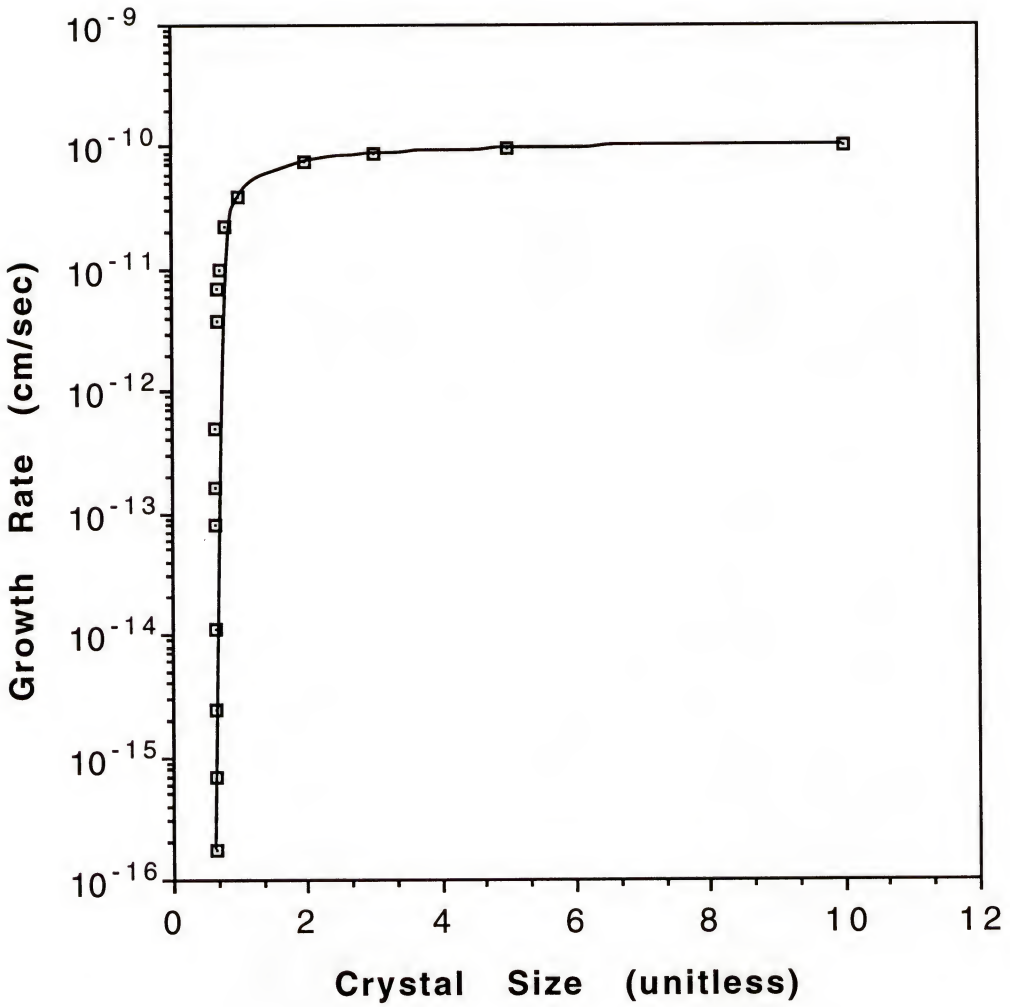

Figure 7.16 : Growth rate as a function of crystal size as predicted by the surface-to-volume ratio growth equation

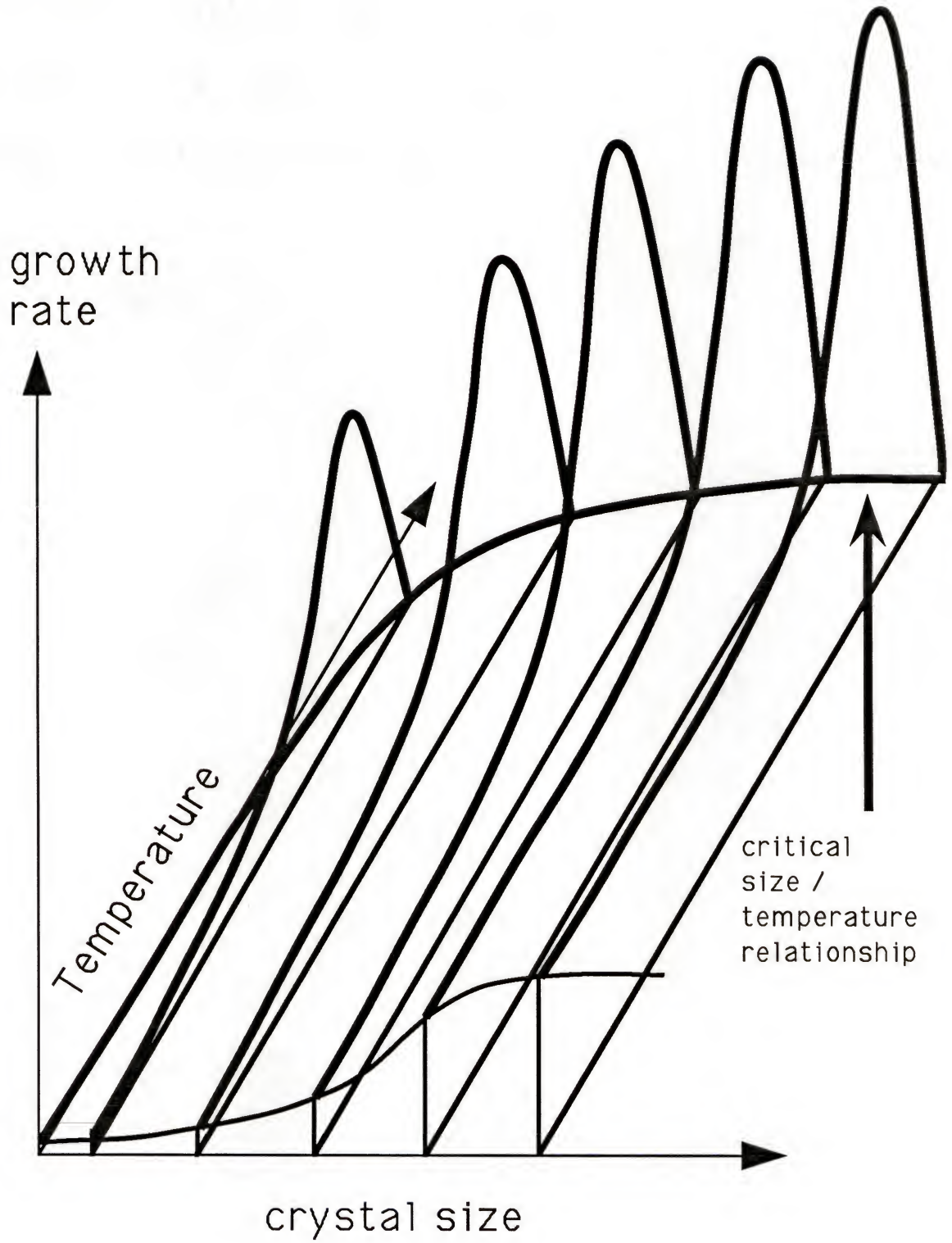

Figure 7.17 : Graphic representation of the temperature / crystal size / crystal growth rate relationship.

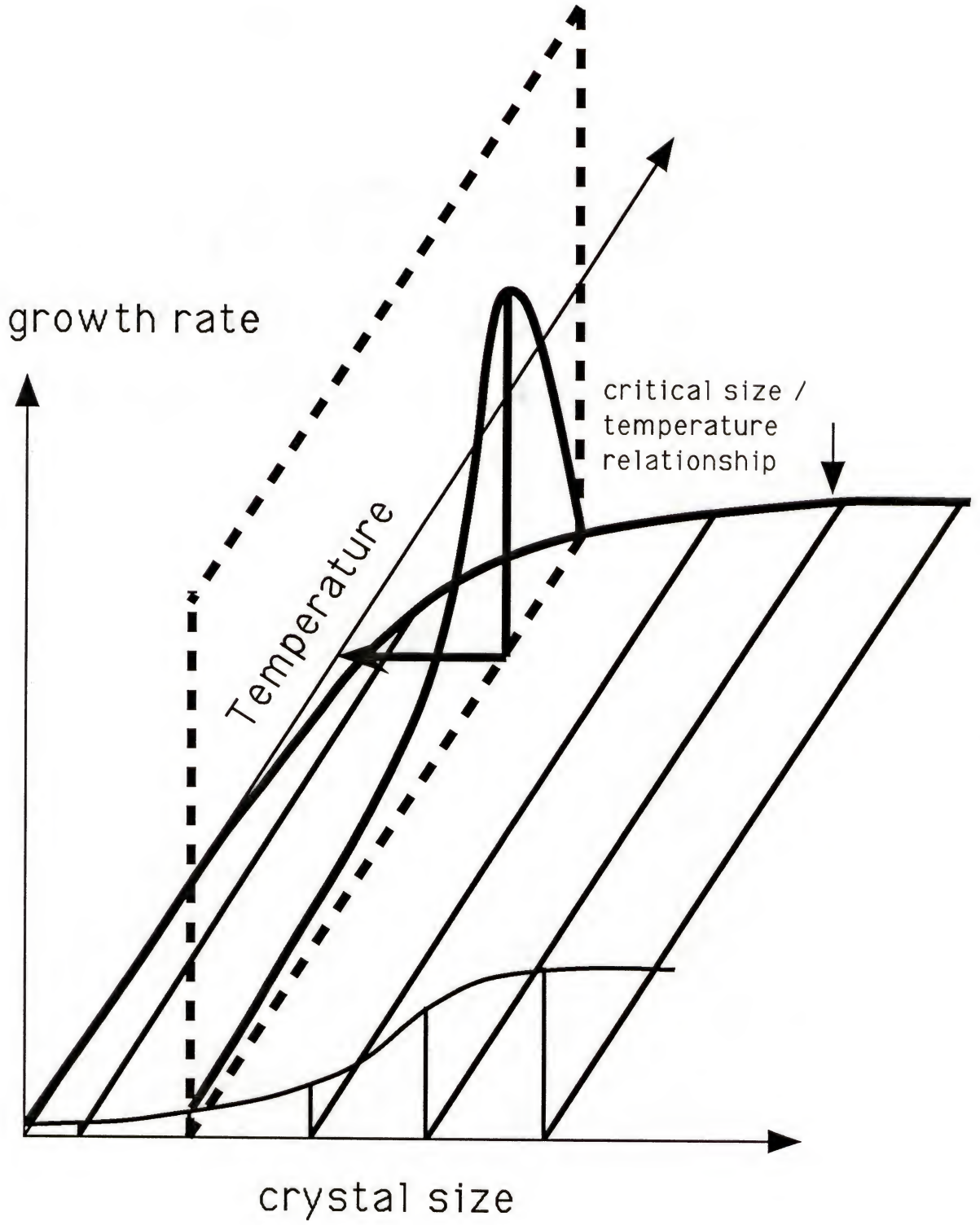

Figure 7.18 : Graphical representation of the method for determination of the temperature for maximum crystal growth rate as a function of crystal size.

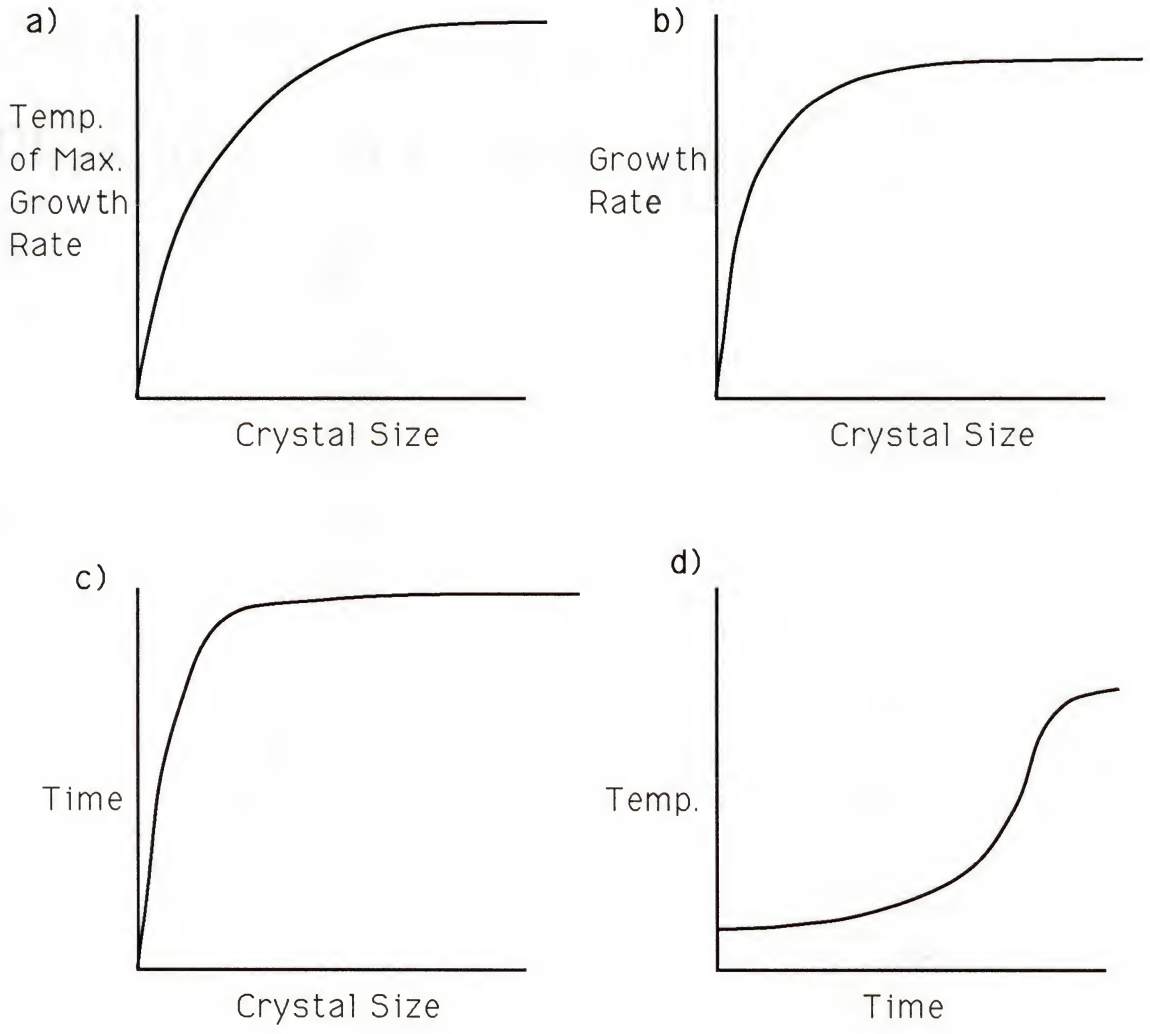

Figures 7.19 : Method for generation of the optimum heat treatment schedule from the information taken from the crystal size / crystal growth rate / temperature relationship.
a) the temperature for the maximum crystal growth rate as a function of crystal size
b) the maximum crystal growth rate as a function of crystal size
c) the minimum time required to grow a crystal to a certain size as a function of that size
d) the optimum temperature/time schedule

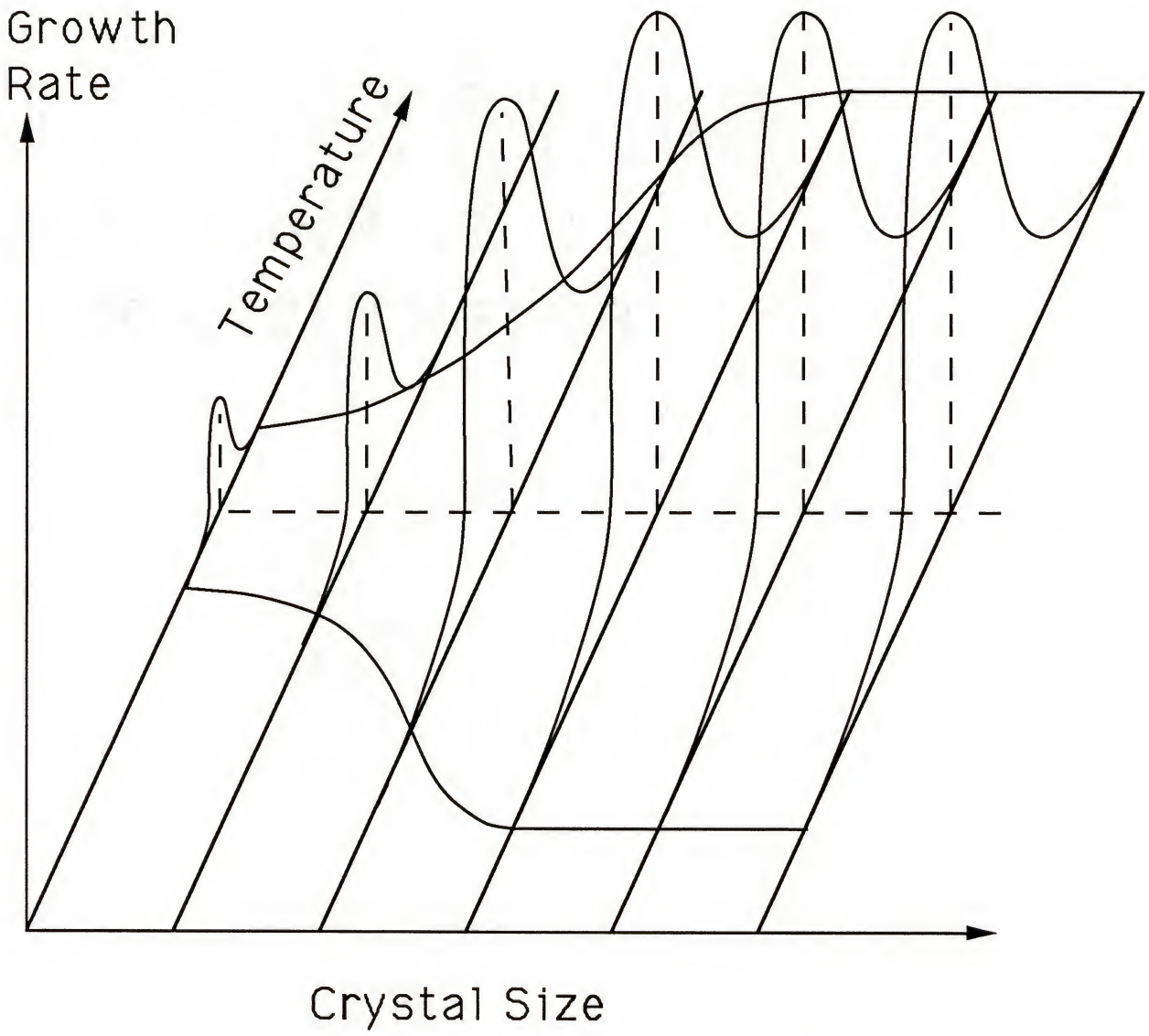

Figure 7.20 : Schematic illustration of the experimentally derived growth rate equation.

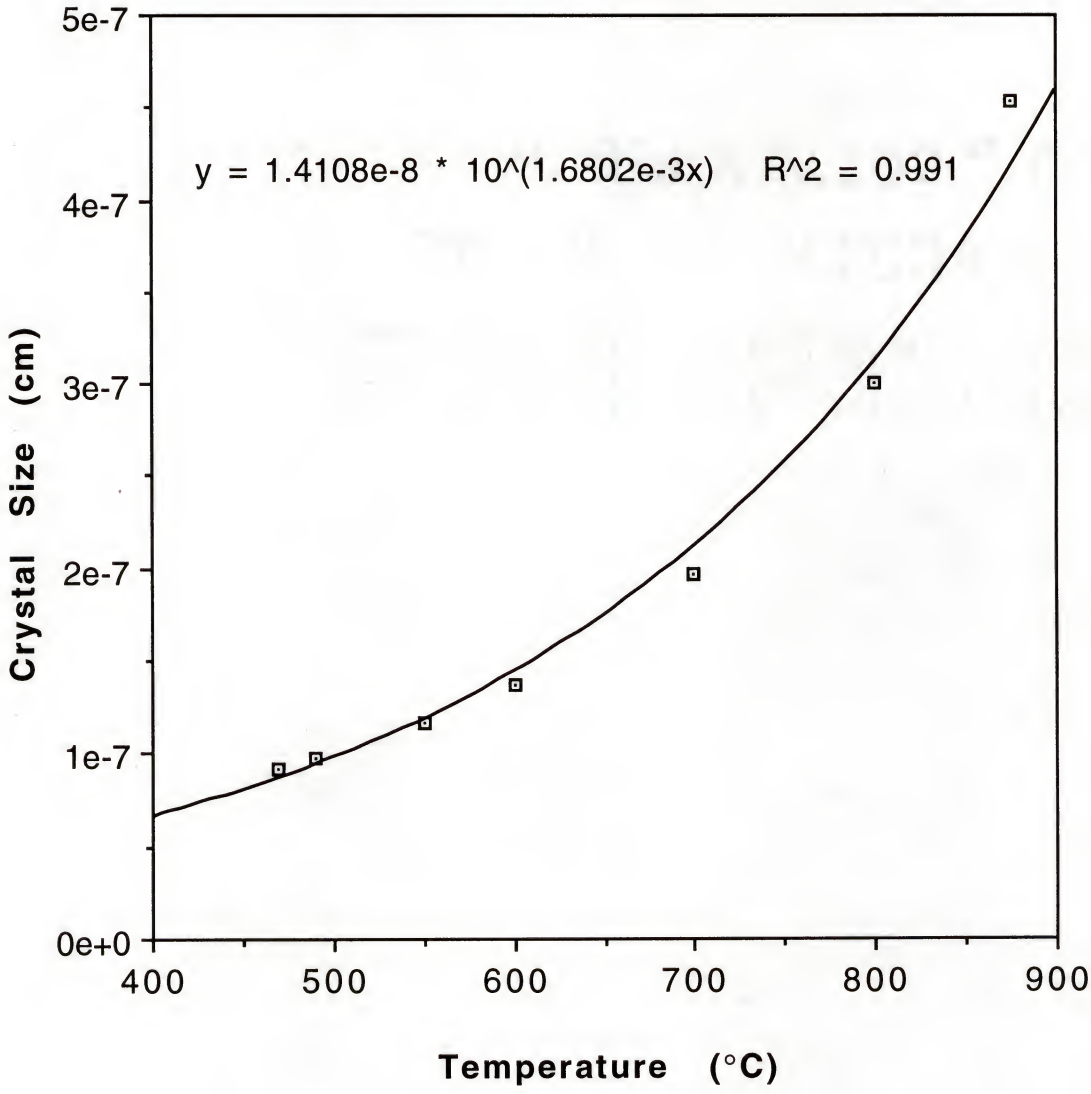

Figure 7.21 : Thermodynamically derived relationship for the maximum temperature for crystal stability as a function of crystal size

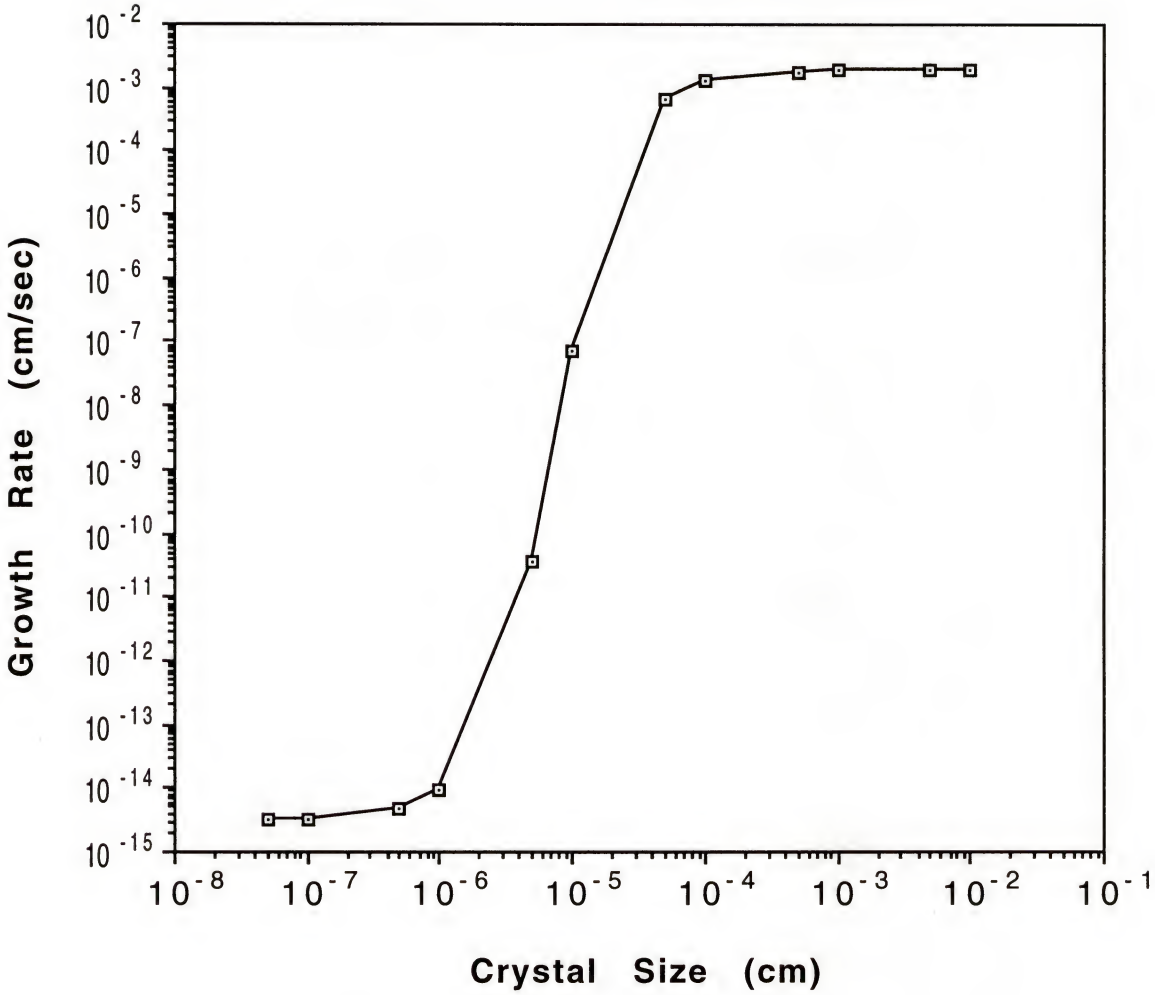

Figure 7.22 : Crystal growth rate as a function of crystal size for the mock-optimized heat treatment schedule for lithium disilicate

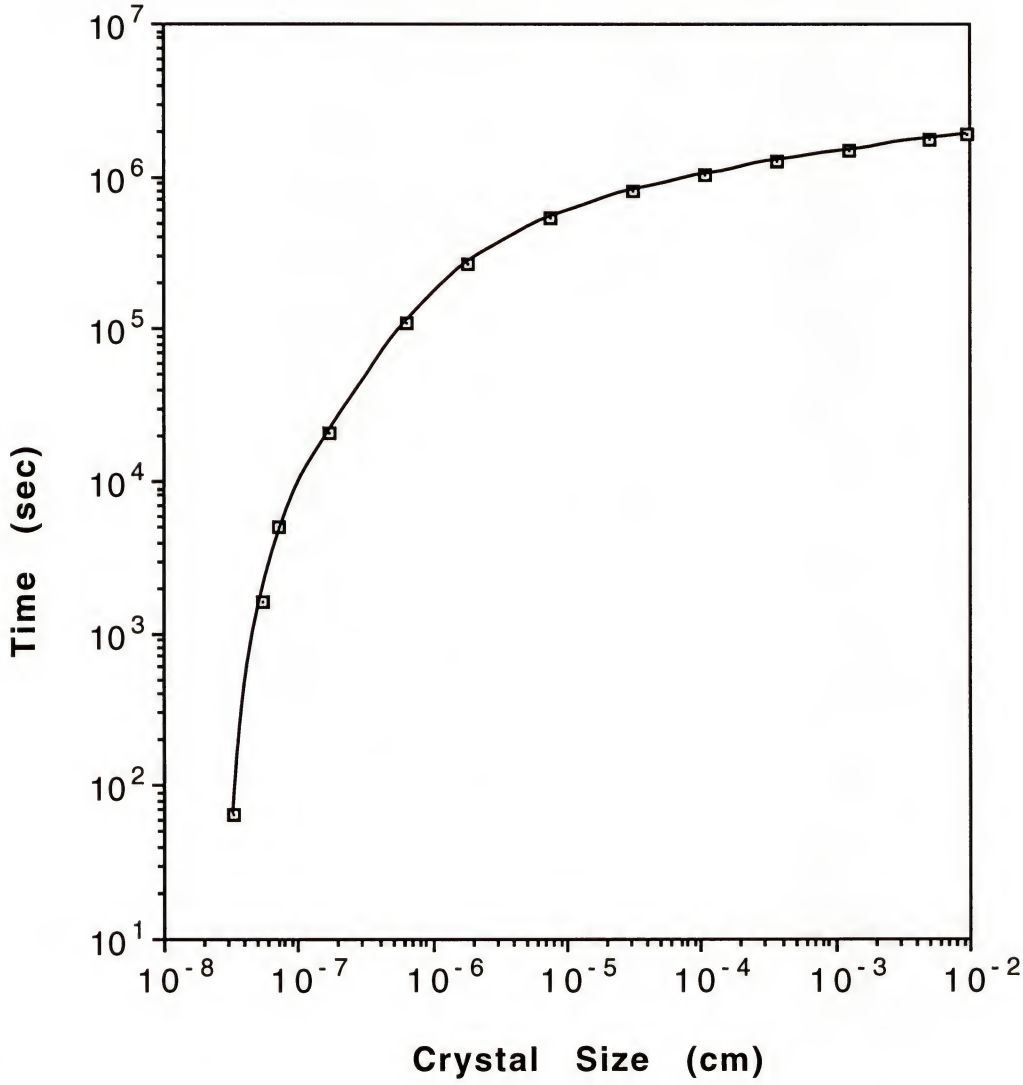

Figure 7.23 : Time to reach crystal size as predicted by the mock-optimum heat treatment schedule for lithium disilicate.

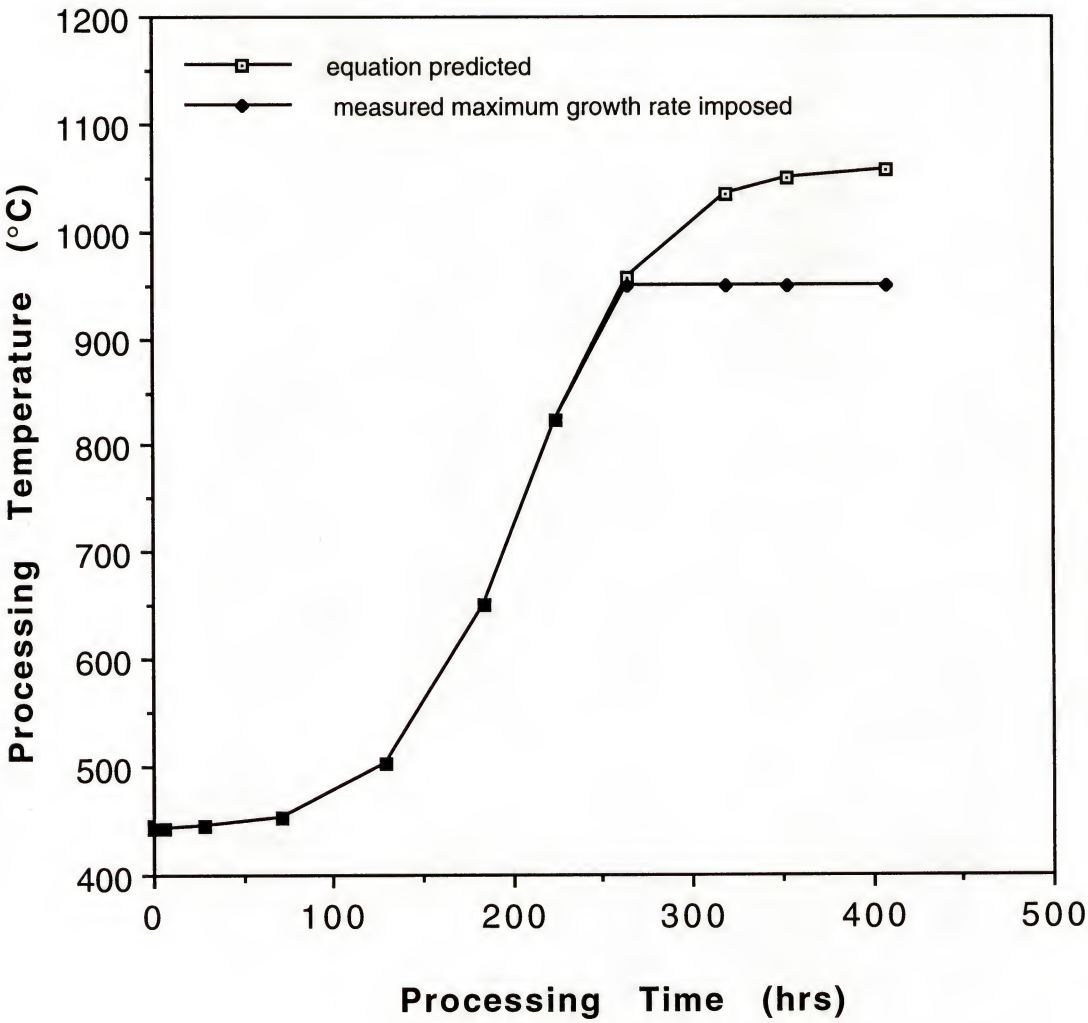

Figure 7.24 : Mock-optimum heat treatment schedule for lithium disilicate.

CHAPTER 8
CONCLUSIONS

This work has made advancements in several areas concerning the processing of glass-ceramics. This progress was made by re-evaluating the fundamentals of the crystallization process. The new perspective on the process is extremely simplistic, but may serve as a promising start for future work.

The novel points of achievement in this work are as follows. (1) A thermal analysis method was developed, modeled, tested, and validated which allows for more rapid determination of the effectiveness of heat treatment schedules. (2) The theoretical concept was proposed that crystallization in the lithium disilicate system is dominated by precrystal sites was proposed and supporting experimental evidence was presented. (3) A procedure was developed to plot these precrystal sites to create a tool to guide the generation of efficient heat treatment schedules. (4) An experimental technique was developed and demonstrated which, in conjunction with the precrystal distribution map, yields optimum heat treatment schedules. (5) The effectiveness of these schedules was evaluated through microstructural comparison of glass-ceramics produced by the optimum schedule and the most effective traditional two-stage schedule. (6) An experimental method was developed and used to generate the growth rate equation for lithium

disilicate. The experimentally derived equation predicted fairly well the experimentally observed microstructural evolution. (7) A thermodynamically-based crystal growth theory was proposed. (8) A growth rate equation was generated from this theory. Good correspondence between the growth rate plots for the experimentally verified equation and the theoretically derived equation supported the theoretical approach. (9) A mathematical transformation was developed and demonstrated to transform the growth rate equation into an optimum heat treatment schedule.

APPENDIX A
THERMAL ANALYSIS SIMULATION

```
      READ (5,*) R,RT,S,DT
      WRITE (8,400)
400   FORMAT (70('='))
      DO 100 I=1,INT((.866*((1/R)^.333)*(1/RT))+DT)
      T=I-1
      A=1.0-((((T-DT)*RT)*-.5*(1/R)^.333)/(.366*(1/R)^.333))^2
      T2=(.5*((1/R)^.333)/RT)+DT
      WRITE (8,*) T2
      IF (T .LE. T2) GOTO 1
      GOTO 2
1     A=1.0
2     SF=12.566*(S-(T*RT))^2*(1-(R*4.188*(T*RT)^3))
      BK=A*R*S^3*52.638*((S^3-(S-(T*RT))^3)/S^3)*((T-DT)*RT)^2
      HT=SF+BK
      WRITE (8,450) A,T,HT
450   FORMAT (2X,E10.3,5X,F10.2,5X,E10.3)
100   CONTINUE
      STOP
      END
```

Index of Variables :

- R = nuclei density
- RT = growth rate
- S = particle radius
- DT = lag time between initiation of bulk and surface crystallization
- SF = surface crystallization component
- BK = bulk crystallization component
- HT = thermal output

APPENDIX B
SIMULATION OF HOMOGENEOUSLY NUCLEATED CRYSTALLIZATION

```
10  DIM Q(65)
20  DIM A(65)
30  K=5
40  FOR X=1 TO 30
50  R=R+1
60   T=R*K
70    IF  X=1  THEN  A(X)=((.02882*T)^3)*4.188*K*.0000327
80  IF X=1 THEN NR=.000327
90  IF X=1 THEN 150
100     NR=.0000327*(1-A(X-1))
110     Z=((.02882*T)^3)*4.1888
120      A(X)=A(X-1)+((Z*.0000327*K)-(F+(Z*.0000327*K*A(X-1))))
130     F=F+(Z+.0000327*K*A(X-1))
140  IF A(X)>.99 THEN END
150   Q(X)=Q(X-1)+(NR*K)
160   PRINT K*X;A(X);NR;Q(X),
170  NEXT X
180  END
```

Variable Index : NR = nucleation rate, experimentally measured value

A = volume fraction crystallized

Q = number of crystals per volume nucleated

K*X = time at temperature

APPENDIX C

PROGRAM LISTING OF PRECRYSTAL / GROWTH RATE EQUATION SIMULATION PROGRAM

```
10   V=2000
20   DIM A(810)
30   DIM C(810)
40   DIM E(810)
50   DIM Z(810)
60   FOR B=4.56E-08 TO 2.27E-07 STEP 2.267E-10
70     DEN=10^(-11.64*(1-EXP(-((1125.95-1.2267E+11*B)/(-
       6.2909E+10*B-2288.68))^6.77)
80   X=X+1
90   A(X)=B
100  C(X)=DEN
110     Z(X)=(2.290866E-12/DEN)*1.62E-10*((B/2.27E-07)^.7)
120   IF Z(X)>1.62E-10 THEN Z(X)=1.62E-10
130  NEXT B
140  FOR T=1 TO 12
150  FOR Y=1 TO 800
160     W=INT((2.27E-07-A(Y))/2.2675E-10)
170   IF A(Y)>=2.27E-07 THEN 230
180   Q=A(Y)
190    S=Z(500-W)*V
200   IF S>1.62E-10 THEN S=1.62E-10
210    A(Y)=A(Y)+(S*144000)
220  GOTO 250
230  Q=A(Y)
240    A(Y)=A(Y)+1.62E-10*144000
250  IF A(Y)>.00007 AND Q<.00007 THEN E(T)=E(T)+C(T)
260  NEXT Y
270  NEXT T
280  FOR X=1 TO 15 STEP 1
290  PRINT X;E(X);
300  NEXT X
310  END
```

Program loop 60 to 130 sets the initial precrystal distribution

Program loop 140 to 270 grows the crystal population and counts the number surpassing the size limit of observability

Program loop 280 to 300 prints the results

dimension A = crystal sizes
dimension C = number of crystals for each size
dimension E = number of crystals crossing observability limit
dimension Z = crystal growth rate
limit imposed in line 120 = experimentally determined bulk-sized crystal growth rate maximum

REFERENCES

1. R. Doremus, Rates of Phase Transformations (Academic Press, New York, 1983).

2. R. DeHoff, Thermodynamics in Material Science (McGraw-Hill, New York, 1993).

3. D. Porter and K. Easterling, Phase Transformations in Metals and Alloys (Van Nostrand Reinhold, Berkshire, England, 1981).

4. M. Volmer and A. Weber, Z. Phys. Chem., 119 (1926) 227.

5. L. Farkas, Z. Phys. Chem. A, 125 (1927) 236.

6. M. Volmer, Z. Phys. Chem., 25 (1929) 555.

7. R. Becker and W. Doring, Ann. Phys., 24 (1935) 719.

8. B. Zeldovich, Acta Physiochem. URSS, 18 (1943) 1.

9. J. Frenkel, J. Chem. Phys., 7 (1939) 200.

10. J. Frenkel, Kinetic Theory of Liquids (Clarendon, Oxford, 1946).

11. D. Turnbull and J. C. Fisher, J. Chem. Phys., 17 (1949) 71.

12. S. Glasstone, K. J. Laidler and H. Eyring, The Theory of Rate Processes (McGraw-Hill, New York, 1941).

13. D. Kashchiev, Surf. Sci., 18 (1969) 389.

14. D. Kashchiev, Surf. Sci., 14 (1969) 209.

15. M. Volmer, Kinetics of Phase Transformation (Steinkopff, Dresden, 1939).

16. D. Turnbull and B. Vonnegut, Ind. Eng. Chem., 44 (1952) 1292.

17. I. Gutzow and S. Toschiev, in: Advances in Nucleation and Crystallization in Glasses, L. L. Hench and S. W. Freiman, eds. (American Ceramic Society, Columbus, OH, 1971), p.10.

18. M. Tomozawa, in: Advances in Nucleation and Crystallization in Glasses, L. L. Hench and S. W. Freiman, eds. (American Ceramic Society, Columbus, OH, 1971), p.41.

19. G. Rindone, in: Symposium on Nucleation and Crystallization in Glasses and Melts, M. Reser, ed. (American Ceramic Society, Columbus, OH, 1962), p.63.

20. P. McMillian, Glass-Ceramics (Academic Press, London, 1979).

21. E. G. Rowlands and P.F. James, Phys. Chem. Glass, 20 (1979) 1.

22. E. D. Zanotto and P.F. James, J. Non-Cryst. Solids, 73 (1985) 517.

23. D. Turnbull, J. Chem. Phys., 20 (1952) 411.

24. P. F. James, J. Non-Cryst. Solids, 73 (1985) 517.

25. A. Hishinuma and D. R. Uhlmann, J. Non-Cryst. Solids, 95 (1987) 449.

26. S. W. Freiman, Ph.D. dissertation, University of Florida, Gainesville, 1968.

27. A. W. Vere, Crystal Growth: Principles and Progress (Plenum Press, New York, 1987).

28. H. A. Wilson, Phil. Mag., 50 (1900) 238.

29. J. Frenkel, Physik. Z. Sovjetunion, 1 (1932) 498.

30. D. Turnbull, Solid State Phys., 3 (1956) 279.

31. W. B. Hillig and D. Turnbull, J. Chem. Phys., 24 (1956) 914.

32. J. W. Cahn, W. B. Hillig and G. W. Sears, Acta Metal., 12 (1964) 1421.

33. F. C. Frank, in: Comments on Nucleation Theory, Crystal Growth and Characterization, R. Ueda and J. B. Mullin, eds. (North Holland, Amsterdam, 1975), p.1.

34. J. J. Favier and D. Camel, in: Fundamentals of Melt Growth, Crystal Growth in Science and Technology, H. Arend and J. Hulliger, eds. (Plenum Press, New York, 1989), p.73.

35. W. K. Burton, N. Cabrera and F. C. Frank, Phil. Trans. Roy. Soc., A243 (1951) 299.

36. K. A. Jackson, D. R. Uhlmann and J. D. Hunt, J. Cryst. Growth, 1 (1967) 1.

37. J. C. Brice, The Growth of Crystals from Liquids (North-Holland, Amsterdam, 1973).

38. B. Mutaftschiev, J. Cryst. Growth, 65 (1983) 50.

39. P. Bennema and G. H. Gilmer, in: Crystal Growth: an introduction, P. Hartman, ed (North- Holland, Amsterdam, 1973), p.263.

40. P. Hartman and W. G. Perdock, Acta Cryst., 8 (1955) 521.

41. C. S. Ray and D. E. Day, J. Am. Cer. Soc., 73[2] (1990) 439.

42. X. J. Xu, C. S. Ray and D. E. Day, J. Am. Cer. Soc., 74[5] (1991) 909.

43. A. Marotta, A. Buri anf F. Branda, J. Mat. Sci., 16 (1981) 341.

44. W. C. Weinberg, J. Am. Cer. Soc., 74[8] (1991) 1905.

45. P. W. McMillian, Glass-Ceramics (Academic Press, London, 1979) p.29.

46. P. F. James, J. Non-Cryst. Solids, 73 (1985) 517.

47. E. G. Rowlands and P. F. James, Phys. Chem. Glass, 20[1] (1979) 1.

48. E. D. Zanotto and P. F. James, J. Non-Cryst. Solids, 74 (1985) 373.

49. P. F. James, Phy. Chem. Glass, 15 (1974) 95.

50. J. J. Tuzzeo, Ph.D. dissertation, Ohio State University, Columbus (1976).

51. V. M. Fokin, V. N. Filipovich and A. M. Kalinina, Fiz. Khim. Stekla, 3 (1977) 129.

52. M. C. Weinberg, J. Non-Cryst. Solids, 83 (1986) 98.

53. M. C. Weinberg, J. Am. Cer. Soc., 70[7] (1987) 475.

54. M. C. Weinberg , G. F. Neilson and D. R. Uhlmann, J. Non-Cryst. Solids, 68[1] (1984) 115.

55. R. DeHoff, Quantitative Microscopy (McGraw-Hill, New York, 1968).

56. M. Avrami, J. Chem. Phys., 9 (1941) 177.

57. B. Bendow, in: Experimental Techniques of Glass-Science, Infrared and Raman Spectroscopy of Glasses, C. Simmons and O. El-Bayoumi, eds (The American Ceramic Society, Columbus, OH, 1993), p.34.

58. F. L. Galeener, Phys. Rev. B, 19[8] (1979) 4292.

59. P. N. Sen and M. F. Thorpe, Phys. Rev. B, 15 (1977) 4030.

60. B. Bendow, in: Experimental Techniques of Glass-Science, Infrared and Raman Spectroscopy of Glasses, C. Simmons and O. El-Bayoumi, eds (The American Ceramic Society, Columbus, OH, 1993), p.36.

61. G. S. Grest and M. H. Cohen, Adv. Chem. Phys., 48 (1981) 455.

62. P. F. James, B. Scott and P. Armstrong, Phys. Chem. Glass, 19[2] (1978) 24.

63. E. G. Rowland and P. F. James, Phys. Chem. Glass, 20[1] (1979) 9.

64. S. W. Freiman, G. Y. Onoda and A. G. Pincus, in: Advances in Nucleation and Crystallization in Glasses, L. L. Hench and S. W. Freiman, eds (The American Ceramic Society, Columbus, OH1971) p.141.

65. K. Takahashi and T. Yoshio, Yogyo-Kyohia-Shi, 81[21] (1973) 18.

66. F. C. Kracek, J. Phys. Chem., 34 (1930) 2645.

67. F. Liebau, Acta Crystallograph., 14 (1961) 389.

68. K. F. Kelton and A. L. Greer, J. Non-Cryst. Solids, 79 (1986) 295.

69. K. F. Kelton and A. L. Greer, in Rapidly Quenched Metals, eds. S. Steeb and H. Warlimont (Elsevier Science Publishers, Amsterdam, 1985) p. 223.

70. A. L. Greer and K. F. Kelton, J. Am. Ceram. Soc.,74[5] (1991) 1015.

BIOGRAPHICAL SKETCH

The author was born on September 3, 1965 in Clearwater, Florida. He graduated from Irondale High School, New Brighton, Minnesota. He earned his B.S. and Ph.D. in Materials Science and Engineering from the University of Florida.

I certify that I have read this study and that in my opinion it conforms to acceptable standards of scholarly presentation and is fully adequate, in scope and quality, as a dissertation for the degree of Doctor of Philosophy.

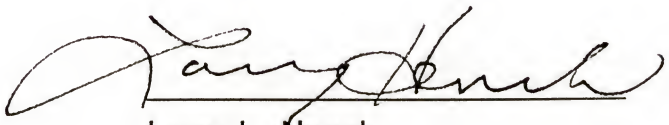

Larry L. Hench,
Chairman
Graduate Research Professor
of Material Science and
Engineering

I certify that I have read this study and that in my opinion it conforms to acceptable standards of scholarly presentation and is fully adequate, in scope and quality, as a dissertation for the degree of Doctor of Philosophy.

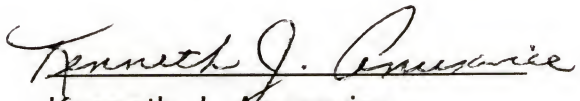

Kenneth J. Anusavice,
Co-Chairman
Professor of Dental
Biomaterials

I certify that I have read this study and that in my opinion it conforms to acceptable standards of scholarly presentation and is fully adequate, in scope and quality, as a dissertation for the degree of Doctor of Philosophy.

Joseph H. Simmons,
Professor of Material
Science and Engineering

I certify that I have read this study and that in my opinion it conforms to acceptable standards of scholarly presentation and is fully adequate, in scope and quality, as a dissertation for the degree of Doctor of Philosophy.

David E. Clark,
Professor of Material
Science and Engineering

I certify that I have read this study and that in my opinion it conforms to acceptable standards of scholarly presentation and is fully adequate, in scope and quality, as a dissertation for the degree of Doctor of Philosophy.

Anthony B. Brennan,
Professor of Material
Science and Engineering

I certify that I have read this study and that in my opinion it conforms to acceptable standards of scholarly presentation and is fully adequate, in scope and quality, as a dissertation for the degree of Doctor of Philosophy.

Kenneth B. Wagener,
Professor of Chemistry

This dissertation was submitted to the Graduate Faculty of the College of Engineering and to the Graduate School and was accepted as partial fulfillment of the requirements for the degree of Doctor of Philosophy.

December 1993

Winfred M. Phillips
Dean, College of Engineering

Karen A. Holbrook
Dean, Graduate School